# DESIGN OF COMPACT BAND PASS FILTER FOR UWB APPLICATION WITH MULTIPLE NOTCHES

*A thesis submitted to*

**DELHI TECHNOLOGICAL UNIVERSITY**

*in Partial Fulfilment of the Requirements of the Award of the Degree of*

Doctor of Philosophy

*in*

**Electronics and Communication Engineering**

*By*

**MOHD. SAZID**

**(Enrolment No.: 2K18/PHDEC/507)**

*Under the Supervision of*

**PROF. N. S. RAGHAVA**

**And**

**PROF. ASOK DE**


**Department of Electronics and Communication Engineering**

**Delhi Technological University (Formerly DCE)**
**Bawana Road, Delhi - 110042, India.**
**July, 2023**

# DECLARATION

I hereby certify that the research work, which is being presented in this Ph.D. Thesis titled "**Design of Compact Band Pass filter for UWB Application with multiple notches"** in fulfilment of requirements for the award of the degree of Doctor of Philosophy is an authenticated record of my research work carried out under the supervision of **Prof. N.S Raghava** and **Prof. Asok De**. The matter discussed in this Ph.D. Thesis has not been submitted elsewhere, in part or fully, to any other institute or university for the award of any degree. This thesis comprises completely original data, graphics, and information, with no content from other sources unless specifically acknowledged.

Date:

**Mohd Sazid**
**Enrollment no.:2K18/PHD/EC/507**
**Department of ECE,**
**Delhi Technological University,**
**New Delhi, India**

*DELHI TECHNOLOGICAL UNIVERSITY*

(Formerly Delhi College of Engineering)

Shahbad Daulatpur, Bawana Road,

Delhi- 110042, India

# CERTIFICATE

This is to certify that that the research work presented in the thesis titled **" Design of Compact Band Pass Filter For UWB Application with Multiple Notches"** submitted by **Mr Mohd Sazid** with enrolment number **(2K18/PHDEC/507)** is the result of his original research carried out in the Department of Electronics and Communication Engineering, Delhi Technological University, Delhi, for the award of **Doctor of Philosophy** under the supervision of **Prof. N.S. Raghava.** and **Prof. Asok De.**

It is further certified that this work is original and has not been submitted in part or fully to any other University or Institute for the award of any degree or diploma.

This is to certify that the above statements made by the candidate is true to the best of our knowledge

**Prof. N.S Raghava**
Supervisor
Department of ECE,
**Delhi Technological University,**
New Delhi, India

**Prof. Asok De**
Co-Supervisor
Department of ECE,
**Delhi Technological University,**
New Delhi, India

# ACKNOWLEDGEMENT

I would like to express my heartfelt gratitude and sincere appreciation to my esteemed supervisors, Prof. N.S Raghava and Prof. Asok De. They are not only exceptional professors with profound vision, but more importantly, they are kind-hearted individuals. I extend my deepest thanks to them for their exemplary guidance and unwavering encouragement. Their trust and support have been a constant source of inspiration, aiding me in making the right decisions. I feel fortunate to have the opportunity to work alongside them.

I extend my heartfelt gratitude to Dr. O. P. Verma, Head of the Department, ECE, DTU, and Dr. Neeta Pandey, Professor, ECE, DTU, for their unwavering support throughout this journey.

Furthermore, I would like to extend my heartfelt thanks to the entire faculty and staff of the Department of Electronics and Communication Engineering at Delhi Technological University, New Delhi. Their unyielding encouragement has played a significant role in my academic journey, and I am truly grateful for their invaluable contributions.

Lastly, I am greatly indebted to all my friends who have generously offered their moral support and provided valuable suggestions. Their selfless efforts have been instrumental in my growth, and I am sincerely appreciative of their unwavering assistance.

**Mohd Sazid**

**Date:**

**Place: New Delhi**

# TABLE OF CONTENTS

# Abstract

Radio frequency (RF) filters are essential components of the present wireless communication systems as it enables and enhances their functionality. RF filter's primary objective is to govern and control electromagnetic signals ensuring that they operate within a particular frequency spectrum. However, the upper stopband of conventional Ultra-Wideband (UWB) filters was limited, and they were sensitive to interference from other wireless services. To satisfy the need of integrated services and overcome the shortcomings of its forerunner, UWB filters have greatly improved. They are compact and have several notches which are strategically positioned to improve transmission efficiency. With the help of this development, UWB filters may be seamlessly integrated into several devices and applications, making more efficient use of limited space and spectrum allocations. UWB filters play an important role in minimizing interference and maintaining the smooth functioning of wireless services by targeting and suppressing undesirable frequencies. In today's technology-driven society, their advanced designs let numerous systems exist harmoniously, promoting an integrated and efficient wireless ecosystem. Revolutionary developments, such as high-speed data transfer, Internet of Things (IoT) applications, and the establishment of smart city infrastructure, have been made attainable by advancements in UWB filter technology. The capability of these filters to precisely filter specific radio frequencies provides reliable data transmission, allowing for smooth communication across a wide range of scenarios and environments.

The design of UWB filters poses a distinctive challenge of strategically incorporating notches at specific frequencies to effectively mitigate interferences. the design must achieve a wide bandwidth while maintaining acceptable performance characteristics across the entire frequency spectrum.

This thesis explains the design and analysis of band pass filters for UWB applications. In the present endeavour, six filters for UWB applications are fabricated and measured, namely: MMR-based filter, flexible and transparent filter using silver nanowire, stepped impedance resonator (SIR) based filter, broadside coupled filter based on microstrip to CPW transition filter, multiple notches filter based on CSRR, and Hybrid SIR and Modified CSRR based multiple notches filter. Extensive simulations are used to analyse and then experimentally validate the aforementioned structural designs. These all suggested filters are suitable for UWB applications.

The first chapter offers a concise and comprehensive introduction to UWB (Ultra-Wideband) technology, providing a foundational understanding of its concepts and applications. It explores the anticipated spectrums that UWB technology is expected to utilize, highlighting its potential to exploit a broad range of frequencies for diverse wireless communication purposes. The second chapter explores the complexity of UWB filter design and provides significant insights into the underlying concepts and modelling methodologies. The next section of the chapter explores numerous techniques used to enhance selectivity, passband flatness, stopband extension, and other frequency characteristics of UWB filters. In addition, the chapter investigates the implementation of single and multiple-notch functions within the filters, intending to eliminate any potential in-band interference. The in-depth examination offers a thorough grasp of the complicated design issues and modern techniques utilized to enhance the functionality of UWB filters, ensuring the effective suppression of undesirable signals while maintaining the integrity and quality of the desired UWB signals.

The third chapter describes the construction of planar structures that generate a passband utilising multimode resonators (MMRs) and interdigital capacitors (IDCs). The upper transmission zero (TZ) is regulated by the arm dimension of the IDCs, while insertion loss is reduced by tight coupling among the IDCs' arms. By integrating inverted L-type resonators in the design, the lower TZ is tuned. The result makes it possible to manage the TZ.

In the fourth chapter, silver nanowires are utilized for creating the circuit on a transparent and flexible PET substrate. The TZ is controlled by the length of the three pairs of arms that collectively make up the passband. The TZ of this structure is determined by the arm length of the IDCs, and it demonstrates an extended stop band of up to 50 GHz.

In the fifth chapter, a dual-notched band UWB-BPF was built using broadside linked techniques. This structure incorporates complementary split ring resonators (CSRRs) in the bottom plane to introduce two notches in the passband. These notches are positioned at 5.4 GHz and 8.2 GHz, and they can be independently controlled. By changing the dimension of the CSRRs, both notches can be positioned to desired frequencies. The incorporation of CSRRs in the design allows for precise control over the notches, enabling selective suppression of unwanted frequencies. This dual-notched band UWB filter offers improved interference rejection capabilities and enhances the overall performance of UWB systems. The design

methodology here involves optimizing the dimensions and placement of the CSRRs to achieve the desired notch frequencies.

In the sixth chapter, the planar structure has been designed for the application of triple-notched bands. In this the structure utilize a broadside coupled technique, employing a basic architecture of a BPF with microstrip-to- CPW transitions arranged on either side of the dielectric. This UWB-BPF exhibited favourable frequency characteristics, featuring two TZs located at the edges of the passband. To eliminate in-band interferences, DGS in the form of CSRRs and complementary folded split ring resonators (CFSRR) were incorporated, resulting in the placement of three TZs within the passband. The triple notches were centered at frequencies of 5.6, 6.42, and 8.03 GHz, attenuating over 19 dB. The measured 3-dB BW of the suggested filter spanned from 3.25 to 10.73 GHz and stopband attenuation was achieved up to 17 GHz.

The basic geometry of the BPF was built in the seventh chapter employing microstrip lines on the upper layer linked to an altered CPW on the bottom layer. Because of the presence of two TZs at the lower and upper edges of the passband, this design with a broadside alignment produced a highly desirable Ultra-Wideband (UWB) response. This concept was improved further by incorporating numerous circular resonator CRs and a CFSRR into the basic architecture. These additional components were added to the ground plane to efficiently mitigate interference from in-band RF sources. By effectively arranging the CRs and CFSRR, the filter was able to establish TZs at frequencies of 5.2, 6.5, and 8 GHz, effectively filtering undesirable signals from WLAN, C band, and X band, respectively.

In the eighth chapter, a compact quad-band notched filter was developed for UWB applications. This suggested filter was constructed using a single-layered Roger 6010 dielectric with a height of 0.635 mm and a dielectric constant of 10.8. In this design, Quad notches were introduced within the passband at frequencies of 3.6 GHz, 5.4 GHz, 7.5 GHz, and 8.7 GHz. These notches effectively eliminate interference caused by WiMAX, WLAN, C band, and the super-X band for satellite TV networks (ranging from 7.2 GHz to 8.4 GHz) within the UWB passband. The quad notches were implemented using SRR and CSRR. The suggested UWB-BPF was developed and simulated using IE3D EM simulation software.

Chapter 9 concludes this thesis by, summarizing the findings and contributions presented throughout the work. It also offers valuable insights and suggestions for potential future

enhancements and extensions of the research, particularly concerning diverse UWB filter design applications.

## List of Figures:

**List of Tables:**

## List of Acronyms

| | |
|---|---|
| ADS | Advanced Design System |
| BPF | Band-Pass filter |
| BSF | Band Stops filter |
| BW | bandwidth |
| CFSRR | complementary folded split ring resonators |
| CPW | coplanar wave guide |
| CR | circular resonators |
| CSRRs | complementary split ring resonators |
| Db | decibel |
| DGS | Defective Ground Structure |
| DMR | detached-mode resonator |
| DMS | defective microstrip structures |
| DSRR | defective split-ring resonator |
| EBG | electromagnetic bandgap |
| EM | Eectromagnetic |
| FBW | fractional bandwidth |
| FCC | Federal Communications Commission |
| fH | Higher cut off frequency |
| fL | lower cut off frequency |
| HPF | High-Pass filter |
| IDC | interdigital coupled |
| IDCL | Interdigital coupled line |
| IDCS | Interdigital coupled structure |
| IDL | interdigital lines |
| LPF | Low-Pass filter |
| MMR | Multi mode Resonator |
| MSCCPW | modfied short circuited coplanar waveguide |
| MSL | microstrip lines |
| PCB | Printed Circuit Board |
| RF | Radio Frequency |
| SCCPW | Short-Circuited Coplanar Waveguide |
| SF | Selectivity Factor |
| SIR | Step Impedance resonator |
| SIS | Step impedance stub |
| TEM | Transverse Electromagnetic |
| TRLSR | triangular ring loaded stub resonator |
| TZ | transmission zero |
| UWB | Ultra Wide Band |
| WiMAX | Worldwide Interoperability for Microwave Access |

| | |
|---|---|
| WLAN | Wireless Local Area Network |
| WPANs | wireless personal area networks. |
| YSSR | Y-shaped stub resonator |

# CHAPTER 1

# INTRODUCTION

## 1.1. Introduction:

Radio frequency (RF) filters are critical elements of present wireless communication systems, since they aid in the management and control of electromagnetic (EM) signals within certain frequency bands. These filters are critical for reducing interference while increasing the efficiency with the performance of RF circuits and devices. RF filters provide dependable and high-quality signal transmission and reception in a wide range of applications by selectively allowing certain frequencies to pass while attenuating others.

Here a filter works as a two-port device that controls the S-parameters of a system and it achieves this by permitting low insertion loss ($S_{21}$) at the desired frequency band while providing significant attenuation outside that band.

Figure 1.1 illustrates a schematic representation of a typical two-port filter configuration. In this configuration, there's an input voltage (Vs) that has a load impedance ($Z_L$) and source impedance ($Z_s$) that terminates the circuit and powers the filter. The transmission and reflection coefficient. are defined as the magnitude of the transmitted and reflected waves, respectively. These coefficients are denoted as R (ω) for reflection and T (ω) for transmission., where the angular frequency is denoted by ω.

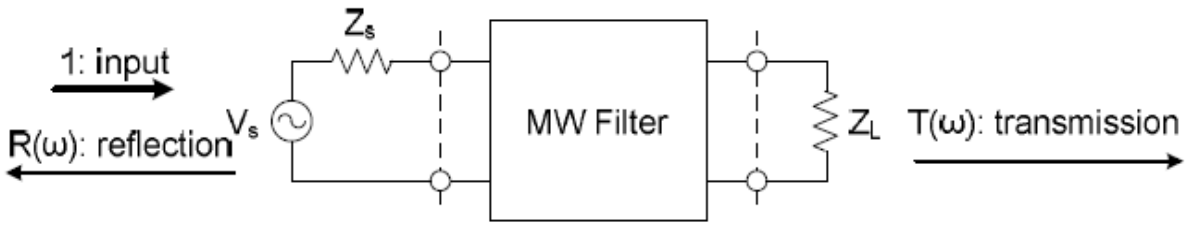


**Fig. 1.1.** A microwave two-port filter is defined by its reflection and transmission coefficients, which are represented by R (ω) and T (ω), respectively

Wireless communication has grown pervasive in today's globe, with technologies like cellular networks, Wi-Fi, Bluetooth, and satellite communications forming the backbone of our networked civilization. These systems rely on the effective use of the RF spectrum, which refers to the frequency range employed for wireless communication. However, as the number of wireless devices grows and frequency bands become scarce, the RF spectrum has become crowded and prone to interference.

RF filters protect the RF spectrum by ensuring that signals inside certain frequency bands are pure and undistorted. They achieve this by selectively attenuating unwanted frequencies, such as noise, harmonics, and other undesirable signals while enabling desired signals to flow through with little distortion. This selected frequency response is accomplished by carefully designing and implementing various filter technologies and topologies.

Four of the most popular types of filters are lowpass (LPF), highpass (HPF), bandpass (BPF), and bandstop (BSF) microwave filters. [1]. As seen in Figure 1.2, each of these filters has a distinct frequency response. LPFs used for the transmission of signals below the cutoff frequency $\omega_c$ are more effective than those above $\omega_c$ which are then discarded, as shown in Figures 1.2(a). HPFs, on the other hand, attenuate signals below $\omega_c$ while passing signals above it, as seen in Figures 1.2(b). BPFs and BSFs are designed to pass through and attenuate all frequencies in between, Figures 1.2(c) and 1.2(d) below illustrate $\omega_{c1}$ and $\omega_{c2}$ which are the lower and higher cutoff frequencies accordingly.

## 1.2. Prototype of a basic lowpass filter for the production of any filtering response:

The cutoff frequency, $\omega_c$, determines the normalized frequency, which is $\Omega = \omega/\omega_c$, and it can be used to characterize the LPF. The power insertion loss parameter is represented by the expression $L(\Omega) = 1/|T(\Omega)|^2$, which determines its frequency response. A general polynomial function $F_N(\Omega)$ may also be used where N is the order of the LPF to describe the function $L(\Omega)$. This is detailed in the reference [2].

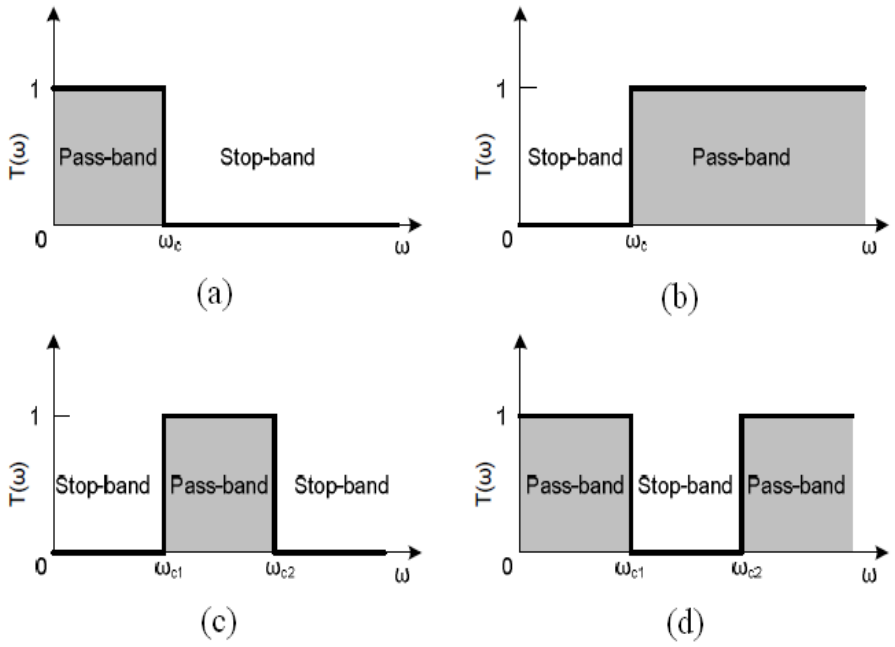


**Fig. 1.2.** The ideal frequency selective characteristics can be classified into four categories: (a) LPF, (b) HPF, (c) BPF, and (d) BSF.

$$L(\Omega) = 1+k^2F_N(\Omega) \tag{1.1}$$

The constant *k* in the polynomial function $F_N(\Omega)$ is connected to the passband ripple or tolerance. It is critical to consider the physical constructability of the network topology by picking the right $F_N(\Omega)$. In practice, two basic types can be specified as Butterworth filters and Chebyshev filters where Butterworth filters are a type of analog or digital filter characterized by their maximally flat passband response which have a steady gain across the passband and a smooth roll-off rate. Chebyshev filters, on the other hand, were developed to provide a sharp roll-off than Butterworth filters. However, the equal-ripple characteristic produces some distortion in the passband. The selection of these filter types is determined by the application's specific requirements. When a smooth frequency response is required, Butterworth filters are preferable, whereas Chebyshev filters are utilized when a steeper roll-off and tolerable passband ripple are required. The insertion loss parameters of these filter types are given by Equations (1.2) and (1.3), respectively, where $T_N(\Omega)$ indicates the Chebyshev function of Nth-order [2]. The insertion loss parameter for a Butterworth filter is given by.

$$L(\Omega) = 1+k^2\,\Omega^{2N} \tag{1.2}$$

And the insertion loss parameter for the Chebyshev filter is given by.

$$L(\Omega) = 1+k^2T^2N(\Omega) \tag{1.3}$$

Figures 1.3 shows the frequency responses for N=5 lowpass prototype filters. When these two curves are compared, it is clearly visible that the Chebyshev filter has a steeper transition beyond $\omega_c$ than its Butterworth equivalent. As a result, Chebyshev filters are preferred to approximate the optimum frequency response depicted in Figure.

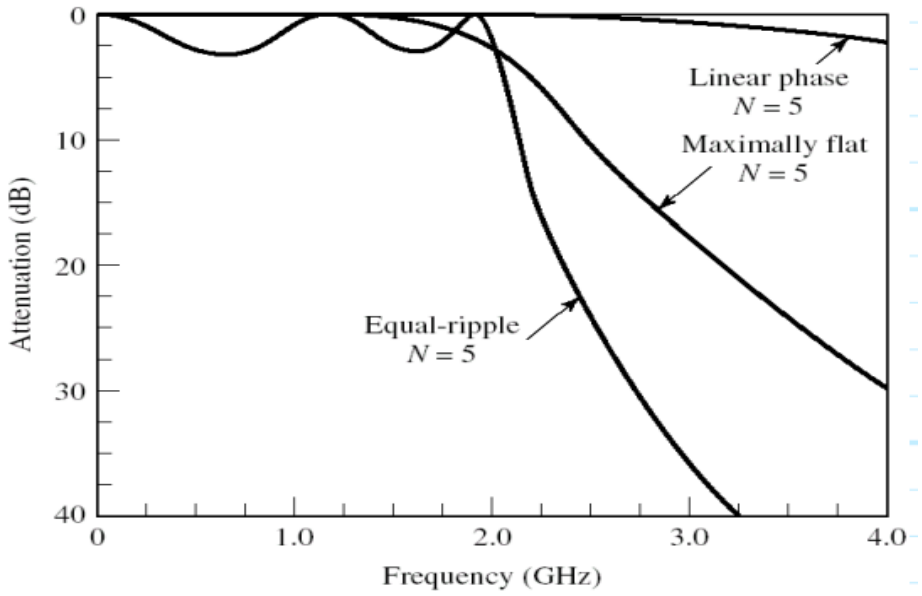


**Fig. 1.3.** Butterworth Chebyshev low pass responses.

Two ladder networks are shown in Figure 1.4 as low-pass filter (LPF) prototypes. These networks have different components, normalized inductance or capacitance of the kth level, where denoted by gk. Furthermore, at the input port $g_0$ symbol represents the normalized source conductance or resistance. Whereas the normalized load conductance or resistance at the output port is denoted by $g_{N+1}$. These ladder networks serve as a foundation for developing and analyzing LPF circuit. To initiate the design process, the first step involves deriving the input impedances and subsequently converting them into their corresponding insertion losses.

Consequently, the value of every element $g_k$ (where k = 1 to N) for $g_{N+1}$ load could be determined conceptually by equating with insertion loss of the two sets, as specified by Equations (1.2) and (1.3). These insertion losses are illustrated in Figure 1.4 which are obtained from the ladder networks. As an example, let's consider the prototype Butterworth low-pass filter with the specific value of Lc = 3dB at Ωc = 1, where k = 1. In this particular situation, Component's value (referred to as $g_k$) may be obtained using the following equations, which provide a direct and concise representation.

$$g_0 = g_{N+1} = 1 \tag{1.4}$$

$$g_k = 2 \sin\left(\frac{2k-1}{2N}\pi\right) \tag{1.5}$$

for k =1 to n

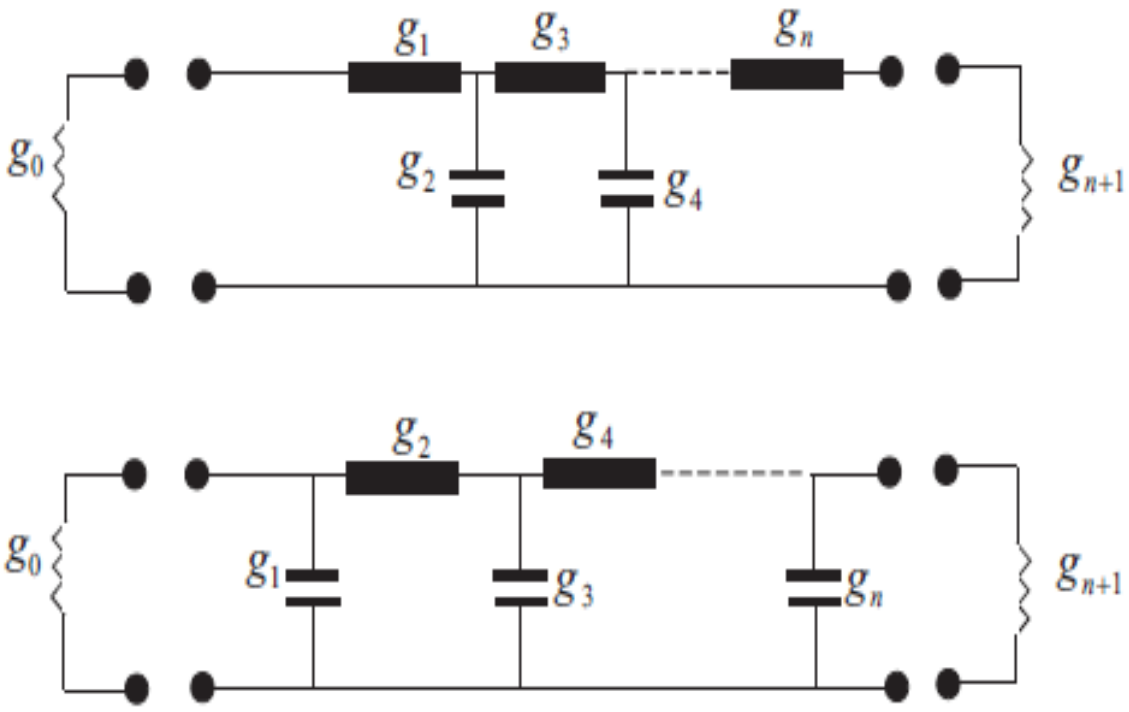


**Fig. 1.4** Lowpass prototype filters with lumped-element ladder networks that consist of both inductive and capacitive element types.

Equation (1.3) may be used to design to get the constant k for the kind of Chebyshev prototype filter at $\Omega c = 1$ with a desired insertion loss Lc.

Following that, for a given value of N, the values of each and every component individually of $g_k$ can be calculated according to the envisioned stop-band performance described at frequency $\omega_c$ by the insertion loss (Ls). Equations (1.6), (1.7), and (1.8) can be used to do this. In order to make sure that the filter matches the necessary specifications, N, an integer value, should be determined by the required stop-band performance.

By following this approach, the design process for the Chebyshev prototype filter, insertion loss may be managed and controlled precisely with the ripple characteristics in the low pass-band, providing the flexibility to meet specific application requirements. The calculated values of the elements gk enable the construction of the Chebyshev filter with the desired performance characteristics, facilitating effective signal processing and filtering in various applications. [2].

$$g_1 = \frac{2a_1}{\sinh\left(\frac{\beta}{2N}\right)} \tag{1.6}$$

$$g_k = \frac{4a_{k-1}}{b_{k-1}} \frac{a_k}{g_{k-1}} \tag{1.7}$$

$k = 2 \text{ to } N$

$$g_{N+1} = \begin{cases} 1, N \dots\dots\dots\dots\dots\dots\dots\dots\dots\dots\dots\dots\dots odd \\ 2k^2 + 1 - 2k\sqrt{1+k^2}, N \dots\dots\dots even \end{cases} \tag{1.8}$$

Where

$$\beta = \ln\left(\frac{\sqrt{1+k^2}+1}{\sqrt{1+k^2}-1}\right)$$

$$a_k = \sin\left(\frac{2k-1}{2N}\pi\right)$$

And

$$b_k = \sinh^2\left(\frac{\beta}{2N}\right) + \sin^2\left(\frac{k\pi}{N}\right)$$

## 1.3. BPF realization based on a LPF:

The LPF is characterized by the conductance ($g_0$ and $g_{N+1}$), normalized source/load resistance, normalized susceptance, or reactance (gk), with the domain of normalized frequency ($\Omega = \omega/\omega_c$). However, it is essential to do frequency transformation of the frequency response from ω to Ω for designing realistic lumped-element LPF, HPF, BPF, and BSF filters working with the real frequency domain (ω). An impedance scaling process is also necessary to make sure the low-pass prototype filter's response and in context of $S_{21}$, contrast it with the practical filter's response. The low-pass prototype filter's insertion loss response and its practical filter transformation are unchanged. This section offers an overview of the need to perform frequency and element transformations to achieve the desired objective for a BPF, Using the Fig. 1.5(a) network topology can be understood and its associated frequency characteristic is also visible in Figure. 1.5(b).

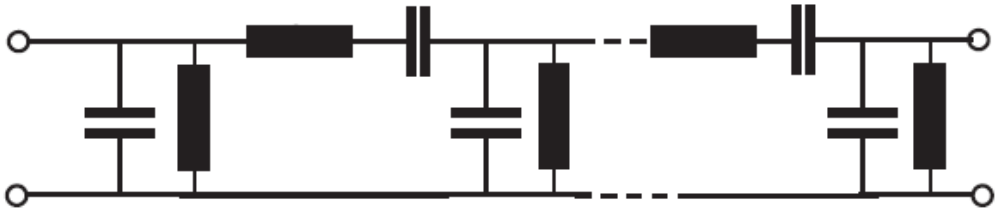

(a)

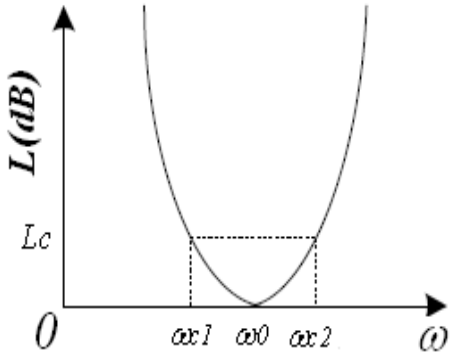


(b)

**Fig. 1.5**. (a) Ladder network of the microwave BPF. (b) Frequency-dependent microwave BPF's attenuation response.

To develop the BPF filter seen in Fig. 1.5(a), one must choose a frequency transformation that achieves a BPF response with the passband defined by Equation (1.9). According to the figure, when constructing BPF, it is advised to simultaneously transform the prototype's inductive and capacitive elements into series and parallel LC resonators. The capacitance and inductance values $C_{k\ and}$ $L_k$, for every LC resonator, may be determined using [2], to make sure that at the $\omega_{c1}$ and $\omega_{c2}$ the insertion losses (Lc) are seen in Fig. 1.5(b) are the same as those at $\Omega c = 1$ in the corresponding LPF prototype:

$$\Omega = \frac{\omega_0}{\omega_{c2}-\omega_{c1}}\left(\frac{\omega}{\omega_0}-\frac{\omega_0}{\omega}\right) \text{ where } \omega_0 = \sqrt{\omega_2\omega_1} \tag{1.9}$$

$$\text{Lk} = \frac{g_k R_L}{\omega_{c2}-\omega_{c1}}\ , \text{Ck} = \frac{\omega_{c2}-\omega_{c1}}{\omega_0^2 g_k R_L}, \quad \textit{for series LC} \tag{1.10}$$

$$\text{Lk} = \frac{R_{L(\omega_{c2}-\omega_{c1})}}{\omega_0^2 g_k}\ , \text{Ck} = \frac{g_k}{R_{L(\omega_{c2}-\omega_{c1})}}, \quad \textit{for parallel LC} \tag{1.11}$$

At lower frequencies, a variety of filters can be developed via effectively employing lumped element capacitors and inductors by using an efficient synthesis approach [1]. As the reactance or susceptance of the lumped components deviates nonlinearly in term to frequency when the operating frequency reaches the microwave region. Hence, while designing microwave filters, it is essential to consider the distributed nature of the components that are used in microwave circuits. Despite this, these elements are expressed in the low-frequency domain as quasi-lumped elements. As a consequence, the previously stated synthesis method may still be utilized successfully in the creation of a microwave filter. [2].

## 1.4. Conversion of a filter's lumped element form to its distributed form:

In the construction of realistic RF circuits, it is crucial to employ distributed transmission line (TL) components. To achieve this, an approximate equivalency between lumped and distributed elements is obtained through Richard's transformation [3].

### 1.4.1. Richards' Transformation

Richards demonstrated that distributed networks, composed of TLs with the same electrical lengths and lumped elements, can be analyzed as LCR networks of lumped elements through a transformation.

$$t = \tanh\frac{l_p}{v_p} \tag{1.12}$$

The transformation used by Richards is defined by Equation (1.12), where $p = \sigma + j\omega$.
*t* is defined as a Richards' variable, and its domain is the complex plane, also known as the t plane. Richards' transformation is usually known as Equation (1.12). We have $p = j\omega$ for lossless ($\sigma=0$) passive networks, and the Richards' variable can be written as

$$t = j\tan\theta \tag{1.13}$$

here

$$\theta = \frac{\omega}{vp} l \tag{1.14}$$

is known as the electrical length.

The phase velocity ($v_P$) of TEM TLs remains constant and irrespective of frequency, whereas the electrical length ($\theta$) and frequency are directly proportional. The relationship is written as $= \theta = \theta_0 (\omega/\omega_0)$, where electrical length is represented by $\theta_0$ at a specific frequency $\omega_0$. We choose $\omega_0$ as the reference radian frequency where all line lengths are equal to one-quarter wavelength, corresponding to an electrical length of $\theta_0 = \pi/2$. We can define the variable $\Omega$ as $\tan\theta$, so that:

$$\Omega = \tan\left(\frac{\pi\omega}{2\omega_0}\right) \tag{1.15}$$

Figure 1.6(a) illustrates the frequency mapping, which shows that $\Omega$ varies from 0 to $\infty$ as $\omega$ varies from 0 to $\omega_0$.

The periodic mapping from $\omega$ to $\Omega$ reflects the distributed network's periodic nature. We obtain the response of periodic frequency for the distributed filter network with a

periodicity of $2\omega_0$ by applying Richards' transformation for the Chebyshev prototype lowpass transfer functionas displayed in fig. 1.6 (b). This response can be identified as a distributed BSF with a centered frequency at $\omega_0$. As a result, depending on the design purpose, it is possible to change a p-plane lowpass or bandstop response into a t-plane lowpass or bandstop response. In similar way, it is possible to transform a highpass or bandpass frequency characteristics in the p-plane into a HPF or BPF response in the t-plane.

Richards' transformation demonstrates a substantial relationship among lumped capacitors and inductors, as there exist specific positions or regions in p-plane. Similarly, open-circuited and short-circuited TLs occupy particular locations or regions in the t-plane. Within the p-plane, the existence of an inductive element (inductor) of one port exhibiting an impedance Z = jXL is equivalent to line element (stub) which is short-circuited possessing an input impedance Z = tZc = jZc * tan(θ). In this case, Zc represents the line's characteristic impedance.

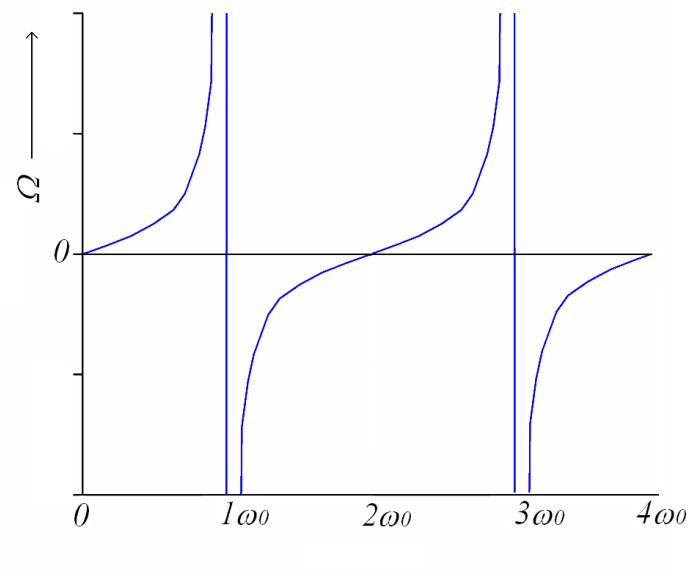


(a)

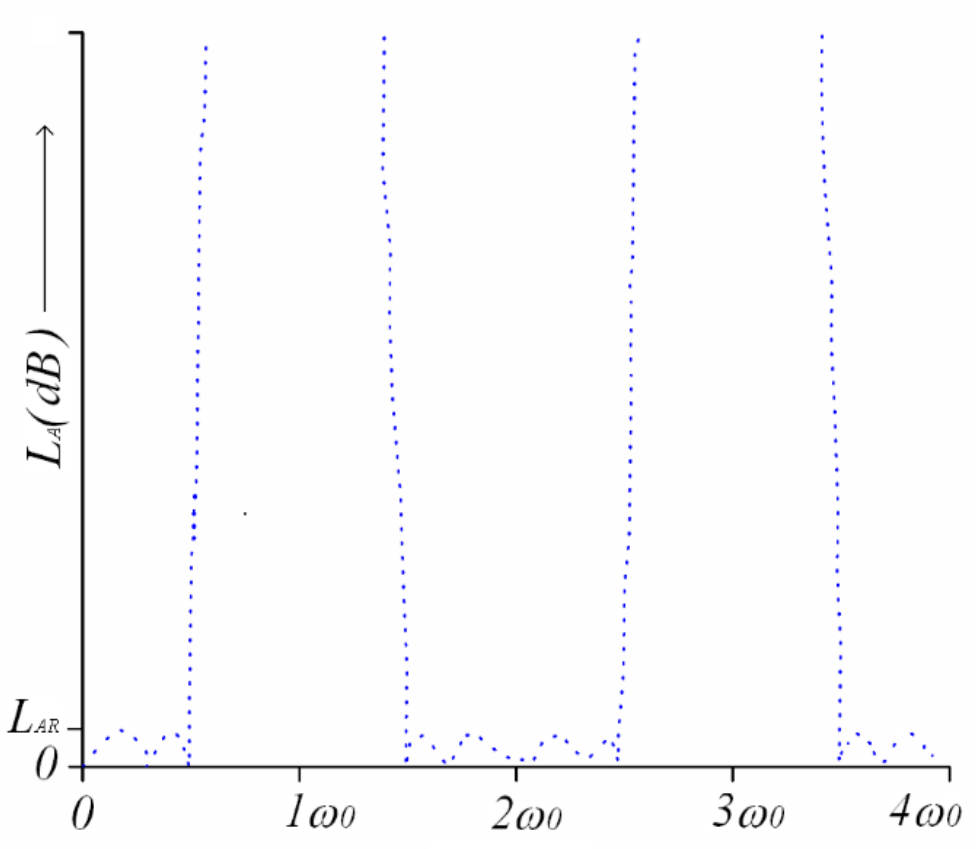


(b)

**Fig. 1.6.** Figure (a) illustrates the relationship between a distributed frequency variable and a real frequency variable in terms of frequency. The Chebyshev LPF utilizes the Richards' transformation for response which is illustrated in Figure (b).

In addition, Richards' transformation creates an equivalency between the lumped capacitors along with the inductors of the p-plane and for the t-plane's open- and short-circuited TLs.A lumped capacitor with impedance $Z = jB_C$ is equivalent to a line element (stub) which is open-circuited with input admittance $Y = 1/Z = tY_c = jY_c\tan\theta$ where $Y_c$ represents the line's characteristic admittance. The input impedance equal to $Z = tZc = jZc\tan\theta$ of the short-circuited line component which is equivalent to an inductor with impedance Z = XL. Figure 1.7 (a) and (b) depicts these relationships, and the short and open-circuited line components are often employed as the t-plane and inductor and capacitor, accordingly. The contrast across lumped and distributed components simplifies the analysis and construction of distributed filter networks based on the t-plane.

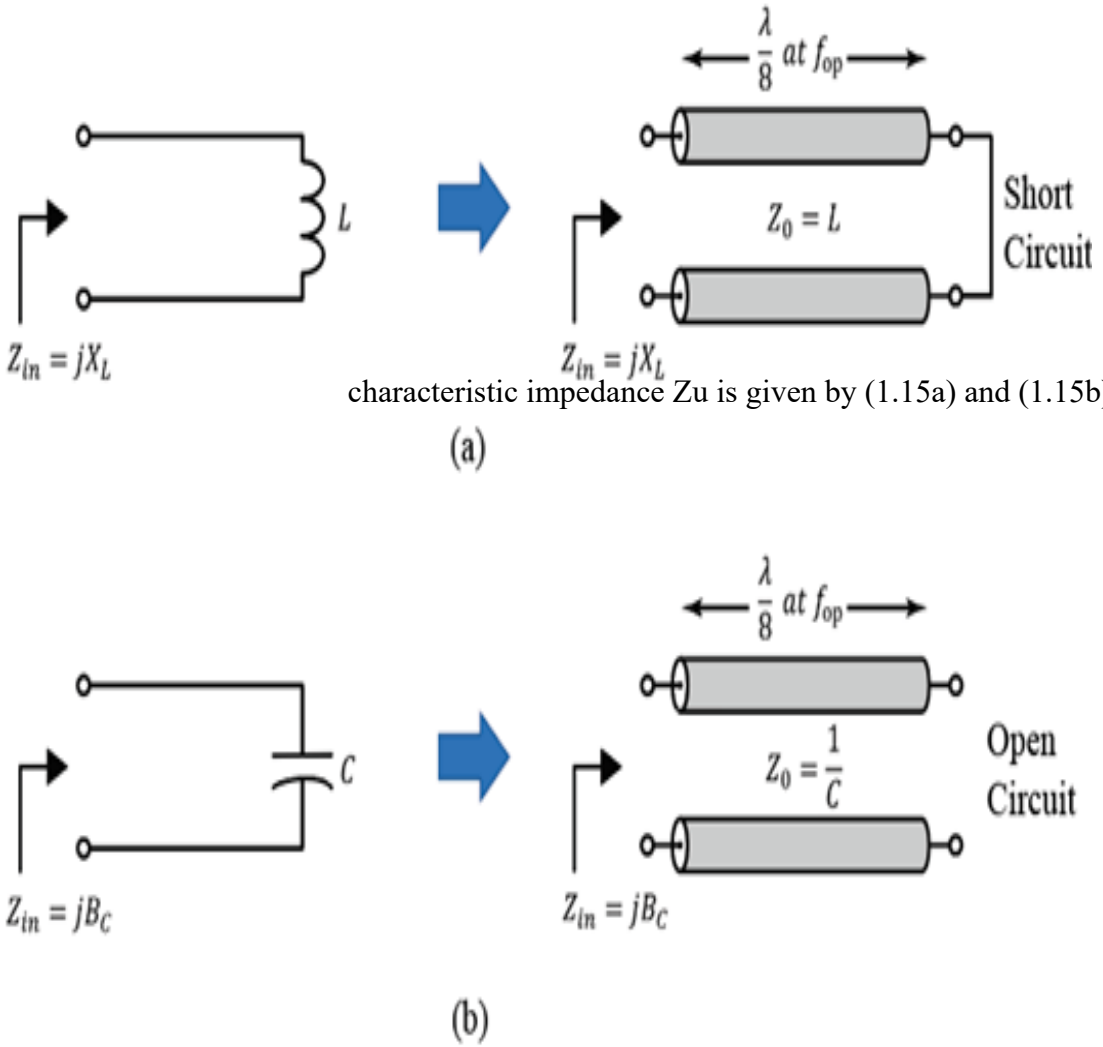


characteristic impedance Zu is given by (1.15a) and (1.15b):

**Fig. 1.7.** The correspondence between lumped and distributed elements for Richards' transformation.

Distributed elements are essential in microwave circuit design and include a two-port network made up of an identical dimension, also known as a unit element (UE). This element has no equivalent in lumped-element circuits. A TL with the ABCD matrix and characteristic impedance Zu is given by (1.15a) and (1.15b):

$$\begin{bmatrix} A & B \\ C & D \end{bmatrix} = \begin{bmatrix} cos\theta & jZusin\theta \\ jsin\theta/Zu & cos\theta \end{bmatrix} \quad (1.15a)$$

which becomes in terms of Richards' variable as

$$\begin{matrix} A \\ C \end{matrix} \begin{bmatrix} B \\ D \end{bmatrix} = \frac{1}{\sqrt{1-t^2}} \begin{bmatrix} 1 & Zut \\ t/Zu & 1 \end{bmatrix} \tag{1.15b}$$

The commensurate-length line, also known as the UE, is a significant distributed element without a comparable lumped element. The UE is a network of two-port which compromises a TL with characteristic impedance Zu, and its schematic representation is shown in Figure 1.8. An important feature of the UE (Unit Element) at t = ±1, is the presence of a half-order TZ. UEs are often used to differentiate distributed filter elements that are positioned at the same physical location. In filter design, UEs can be either redundant or non-redundant. Redundant UEs do not affect filter selectivity, while non-redundant UEs can enhance it.

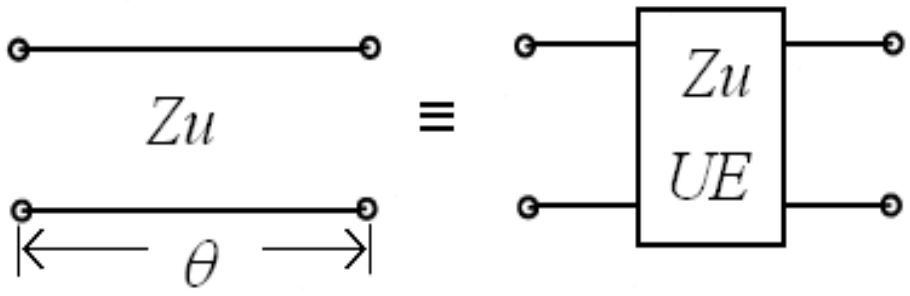


**Fig. 1.8.** Unit element (UE).

### 1.4.2. Kuroda Identities

The Kuroda identities [4], as seen in Figure 1.9, allow for transformations of Filter networks with the same electrical characteristics but different physical structures or component values. These transformations provide more design flexibility and freedom in developing physically realizable networks with precise dimensions. For every identity, the Kuroda identities assume commensurate line elements of equal electrical length. The initial pair of Kuroda identities encompasses the interchange of a UE having a shorted series stub or an open shunt stub, and vice versa. Conversely, the second pair of Kuroda identities

employs ideal transformers so that interchange stubs of the same type can be done. By comparing various networks for the ABCD matrices under discussion, these Kuroda identities are determined.

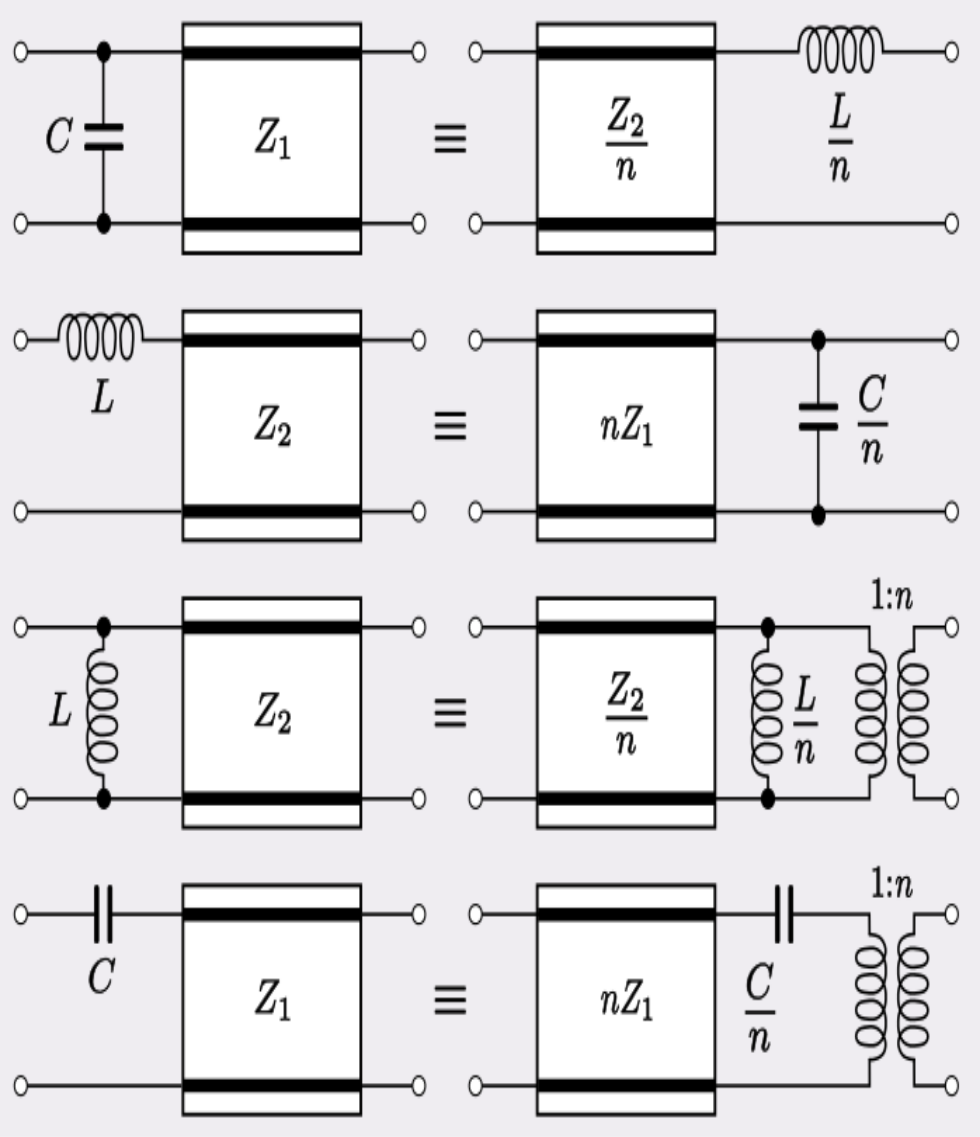


$$L = Z_1, \quad C = 1/Z_2, \quad n = 1 + Z_2/Z_1$$

**Fig. 1.9.** Kuroda Identities.

Various kinds of resonators are employed in the microwave spectrum, including coaxial, dielectric, waveguide, and micro stripline (MSL) resonators. Microstrip resonators (MRs) and MSL are commonly employed in microwave circuits because to their practical benefits,

such as their compact shape, ease of manufacture, simplicity of making, and interoperability with integrated circuits The basic architecture of a microstrip filter will be discussed in the next section.

## Microstrip Filter:

Microstrip filters are frequently employed in cutting-edge radio communication systems because of to its small size, ease of integration, and broad frequency range. These filters are made with microstrip TL technology, in which a conductor is put on a dielectric substrate to form a planar structure. The small size of microstrip filters is beneficial in miniaturized circuit designs with minimal space requirements. Additionally, their low cost makes them a popular choice for mass production. The planar structure also allows for easy integration with other microwave components and circuits, which simplifies system design and construction. Microstrip filters have a wide spectrum range, ranging from megahertz to gigahertz. Microstrip filters' design versatility allows for the realization of many filter types such as LPF, HPF, BPF, and BSF. They can be built with precise frequency responses and properties, such as narrow or wide bandwidth, excellent selectivity, and minimal insertion loss. Microstrip filter design characteristics like as conductor width, dielectric constant, and substrate thickness can be customized to match individual requirements. Conventional printed circuit board (PCB) manufacturing processes are used for manufacturing microstrip filters, which are well-established and readily available. These filters are used in microwave devices. As given in Figure 1.10, in microstrip structure of filter which consists of a width W conducting strip positioned on top and a height h dielectric with relative permittivity $\varepsilon_r$ isolating it from the bottom layer. Because the substrate material and the air above, the architecture becomes inhomogeneous, causing EM waves to disperse and propagate. As a consequence of this, the microstrip design, is incapable of directing pure transverse EM (TEM) waves.

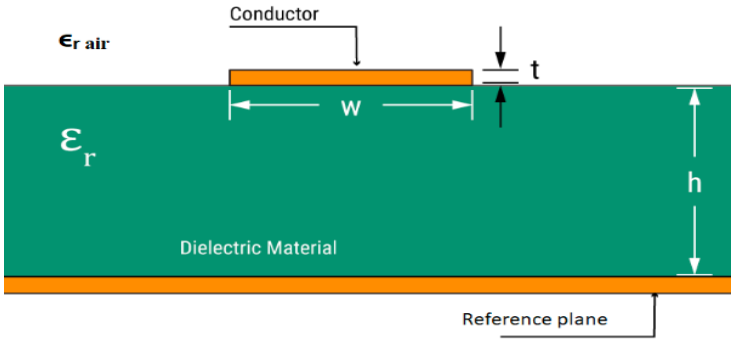


(a)

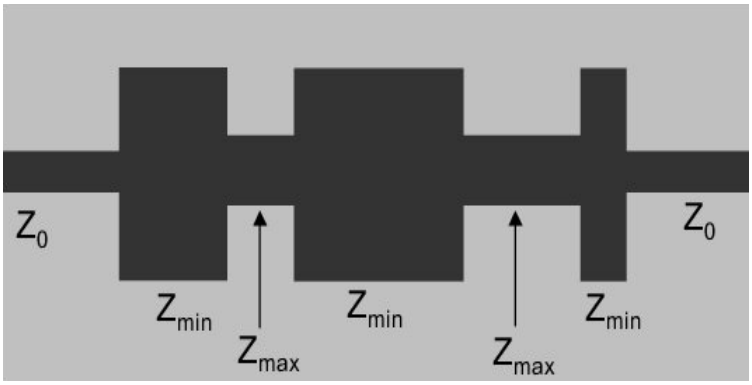


(b)

**Fig. 1.10.** Layout (a) cross section. (b) top view.

The presented approximation simplifies the MR structure by combining it into a single layer with an effective dielectric constant, $\varepsilon_{re}$, that accounts for the presence of both air and dielectric materials. By using this approximation, it is feasible to effectively characterize the behavior of microstrip TL by utilizing Zc for characteristic impedance and $\varepsilon_{re}$ for effective dielectric constant. The application of the quasistatic analytic techniques, as indicated in the literature [5-6], is widely used to determine the values for εre and Zc as depicted in Eqn. (1.16 ) and (1.17) respectively.

$$\varepsilon_{re} = \frac{\varepsilon_r+1}{2} + \frac{\varepsilon_r-1}{2}\left(1 + 12\frac{h}{W}\right)^{-0.5} \tag{1.16}$$

$$\text{Zc} = \frac{\eta}{2\pi\sqrt{\varepsilon_{re}}} \ln\left[\frac{F}{u} + \sqrt{1 + \left(\frac{2}{u}\right)^2}\right] \tag{1.17}$$

Where $u = W/h$, $\eta = 120\pi$ ohms, and

$$F = 6 + (2\pi-6)\exp\left[-\left(\frac{30.66}{u}\right)^{0.7528}\right]$$

## Microstrip Losses:

A microstrip TL 's total loss includes conductor loss, dielectric loss, and radiation loss. The propagation constant can be calculated when dealing with a lossy TL by $\gamma = \alpha + j\beta$ as a complex variable. Now $j\beta$ denotes the phase constant, which describes the phase shift experienced by the propagating wave along the TL, while $\alpha$ accounts for the attenuation constant (associated with conductor and dielectric losses). This complex propagation constant is essential in accurately modeling and understanding the behavior of signals in lossy microstrip structures. Attenuation which occurs through conductor loss is given by [7]:

$$\alpha_c = \frac{8.686\ Rs}{ZcW} \quad \text{dB/unit length} \tag{1.18}$$

The surface resistance of the bottom layer and conducting strip in ohms per square is denoted by Rs and is given by:

$$Rs = \sqrt{\frac{\omega\mu_0}{2\sigma}} \tag{1.19}$$

Here

$\sigma$ = Conductivity,

$\mu_0$ = Permeability of free space.

The attenuation caused in a microstrip by dielectric can be computed using existing research equations [7, 8].

$$\alpha_d = 8.686\pi\left(\frac{\varepsilon_{re}-1}{\varepsilon_r-1}\right)\frac{\varepsilon_r\ tan\delta}{\varepsilon_{re}\ \lambda_g} \quad \text{dB/unit length} \tag{1.20}$$

Where $tan\delta$ is the loss tangent of the dielectric.

## 1.5. UWB-BPF:

Ultra-wideband (UWB) technology has an extremely broad working bandwidth, allowing for fast speeds transmission of data, massive channel capacity. It has several uses, including short-range wireless communications, radar, imaging systems, and many others. In acknowledgment of its importance. The Federal Communications Commission (FCC) has allowed the utilization of unlicensed UWB spectrum (3.1-10.6 GHz) for worldwide deployment in limited coverage wireless transmissions in February 2002. [9]. Figure 1.11 provides a comparative illustration of UWB signals and narrowband signals.

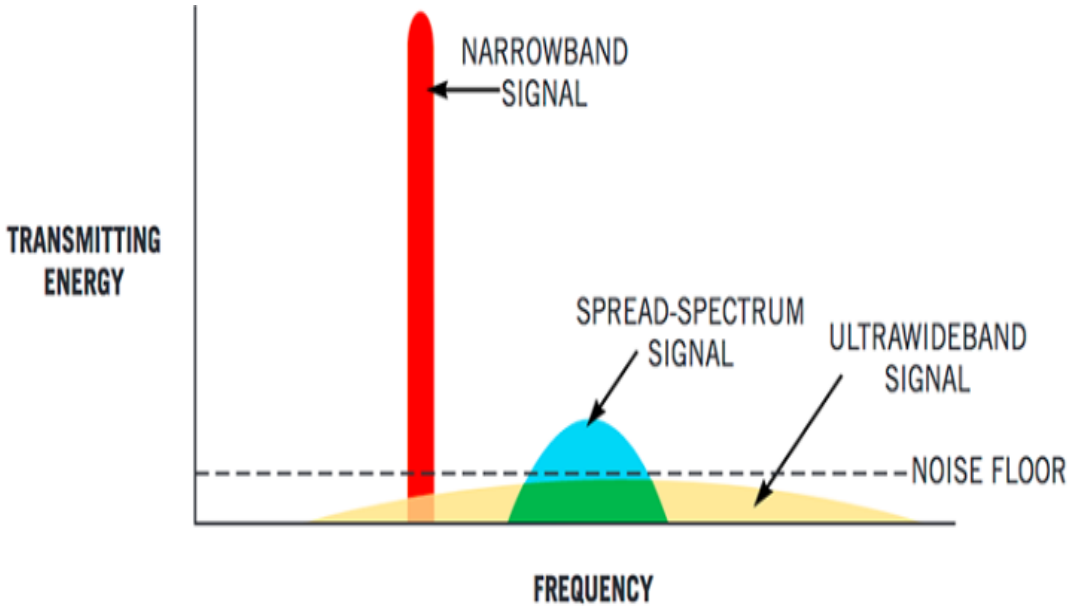


**Fig. 1.11.** A comparative illustration of narrowband and UWB signal**.**

According to the FCC, signal is considered to be UWB if it meets the criteria of either having a fractional bandwidth (FBW) of at least 20% or total at the center frequency is 500 MHz. This means that the signal occupies a wide frequency range, allowing for high-speed data transfer and increased channel capacity. A UWB pulse is seen in Figure 1.12.

$$FBW > 20\% \text{ and /or } BW > 500 \text{ MHz}$$

The FBW is defined using the -10 dB emission points and can be calculated using the formula (1.21):

$$FBW = 2(f_H - f_L) / (f_H + f_L) \quad (1.21)$$

The -10 dB emission points at the higher frequencies $f_H$ and lower frequencies $f_L$, are used to calculate the FBW as shown in Figure 1.12. However, for UWB systems, the FCC has set a stringent emission in the UWB mask with a power spectral density limit of -41.3 dBm/MHz [9].

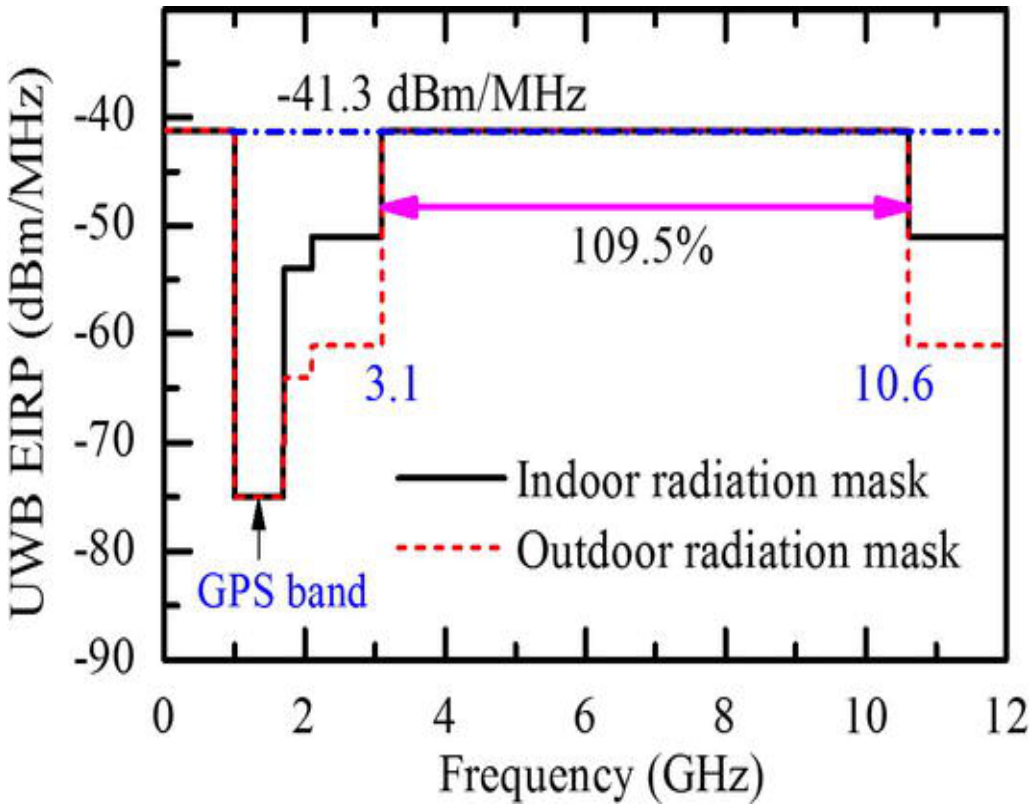


**Fig 1.12.** FCC approved UWB radiation mask for Indoor and outdoor systems.

**UWB Applications:**

UWB technology finds applications across various domains due to its unique characteristics and capabilities. UWB allows for high-speed data transmission in communication systems, making it suited for wireless personal area networks (WPANs),

and multimedia streaming. UWB is used in radar systems for high-resolution imaging, object detection, and localization in both indoor and outdoor contexts. In healthcare, UWB is utilized for precise tracking of medical devices, patient monitoring, and imaging applications. UWB is also important in automotive systems, enabling greater collision avoidance, radar-based sensing for autonomous vehicles, and vehicle-to-vehicle communication.

UWB is used in asset monitoring and localization systems, as well as accurate positioning in industrial contexts, inventory management, and logistics. Natural calamities such as earthquakes and avalanches are detected and tracked using UWB in environmental monitoring systems. UWB is used in security systems for monitoring, personnel tracking, and access control. UWB also has uses in entertainment and virtual reality, allowing for precise motion tracking and gesture recognition. The adaptability of UWB technology enables new solutions in a variety of industries by providing high data rates, precise positioning, and dependable communication in many different types of applications.

A UWB-BPF becomes a crucial component of the suggested system to govern the limited UWB mask and dominate the spectrum capabilities of the UWB technology. This need requires extensive research in the development and advancement of UWB-BPFs. The development of such UWB filters is difficult since it must take into account the following factors:

• At the center frequency, the FBW is 109 %.

• Low insertion loss.

• A small variation in group delay in passband.

## 1.6. Motivation:

Traditional UWB filters have limitations due to their small upper stopband and susceptibility to interference from other wireless services. These constraints offer substantial hurdles to the overall performance of UWB systems. Addressing these difficulties concurrently necessitates the use of specific filter structures, as there are only a limited number of planer filter structure available in the current landscape.

## 1.7. Objectives:

In this study major goal is to develop planar microstrip-based BPFs for UWB applications. These filters will be built to enable fine control over single or multiple notches in the frequency response while also extending the stopband region. At the same time, the goal is to ensure that the filters preserve a linear and flat group delay characteristic. By reducing interference and enhancing signal fidelity, these goals will improve the performance and adaptability of UWB systems. The suggested planar microstrip-based UWB BPFs provide a viable alternative for overcoming the constraints of existing UWB filters, allowing for improved signal filtering and spectrum utilization in a variety of applications.

## 1.8. Organization of the thesis:

This thesis' structure is summarized as-

The second chapter goes into the complexities of UWB filter design, providing significant insights into the underlying ideas and methodologies used in their modelling. The chapter then delves into the numerous approaches used to improve the frequency characteristics of UWB filters, including stopband extension, passband flatness enhancement, and selectivity enhancement. In addition, the chapter investigates the implementation of single and multiple notch functions within the filters, with the goal of eliminating any potential in-band interference. This in-depth examination provides the comprehensive understanding of the design complexities and advanced techniques used to optimize the performance of UWB filters, allowing for the effective suppression of unwanted signals while maintaining the integrity and quality of the desired UWB signals.

In the third chapter, planar structures are designed. The structure utilizes Multimode Resonators (MMRs) with interdigital capacitors (IDCs) to generate a passband. Tight coupling among the arms of the IDCs reduces insertion loss, while the upper transmission zero (TZ) is regulated by the IDCs' arm dimension. The lower TZ is tuned by integrating inverted L-type resonators into the structure. This allows for control over the TZ.

In the fourth chapter, a transparent and flexible substrate made of PET is used, and silver nanowires are employed to design the circuit. Three pairs of arms are used to develop the passband, and the length of these arms controls the TZ. This structure exhibits an extended stop band of up to 50 GHz, and the TZ is determined by the IDCs' arm length.

In the fifth chapter, a dual notched band UWB-BPF was built employing broadside linked techniques. The structure incorporates complementary split ring resonators (CSRRs) in the bottom plane to introduce two notches in the passband. These notches are positioned at 5.4 GHz and 8.2 GHz, and they are able to managed separately. By tailoring the dimension of the CSRRs, both notches can be positioned to intended frequencies. The incorporation of CSRRs in the design allows for precise control over the notches, enabling selective suppression of unwanted frequencies. This dual notched band UWB filter offers improved interference rejection capabilities and enhances the overall performance of UWB systems. The design methodology involves optimizing the dimensions and placement of the CSRRs to achieve the desired notch frequencies.

In the sixth chapter, planar structure has designed for the application of triple notched bands. The first structure utilized broadside coupled techniques, employing a basic architecture of a BPF with microstrip-to- CPW transitions arranged on the opposite side of the dielectric. This UWB-BPF exhibited favorable frequency characteristics, featuring two TZs located at the edges. In order to eliminate in-band interferences, DGS in the form of CSRRs and complementary folded split ring resonators (CFSRR) were incorporated, resulting in the placement of three TZs within the passband. The triple notches were centered at frequencies of 5.6, 6.42, and 8.03 GHz, attenuate over 19 dB. The observed 3-dB BW of the suggested structure spanned from 3.25 to 10.73 GHz, and stopband attenuation was achieved up to 17 GHz.

The basic geometry of the BPF was built in the seventh chapter employing microstrip lines (MSL) on the upper layer linked to an altered CPW on the bottom layer. Because there are two TZs at the lower and upper edges, this design with a broadside alignment produced a highly desirable Ultra-Wideband (UWB) response. The concept was improved further by incorporating numerous circular resonators CRs and a CFSRR into the basic architecture. These additional components were added to the ground plane in order to efficiently mitigate interference from in-band RF sources. The filter was able to establish TZs at frequencies of 5.2, 6.5, and 8 GHz by strategically arranging the CRs and CFSRR, effectively filtering undesired signals from WLAN, C band, and X band, respectively.

In the eight chapter, a compact shape quad-band notched filter was developed for UWB applications. The suggested filter was constructed using a single-layered Roger 6010

substrate. Quad notches were introduced within the passband at frequencies of 3.6 GHz, 5.4 GHz, 7.5 GHz, and 8.7 GHz. These notches effectively eliminated interferences caused by WiMAX, WLAN, C band, and the super-X band for satellite TV networks within the UWB passband. The quad notches were implemented using SRR and CSRR. The simulated and observed outcomes were obtained for the quad-notches UWB-BPF, both without the inclusion of complementary split ring resonators (CMSRR) and with CMSRR. Finally, Chapter 9 encapsulates the research provided in this thesis and gives proposals for subsequent enhancements and prospective adaptations of this work to various UWB filter design applications.

# CHAPTER 2

# REVIEW ON PLANAR ULTRA-WIDEBAND FILTERS

## 2.1. Introduction:

Extensive research has been conducted on UWB-BPF following the spectrum's allocation for unlicensed use in indoor and handheld devices. The design of UWB filters involves considerable challenges due to the requirement to address the following factors:

- Passband insertion loss.
- FBW
- Low Ripples in the passband.
- Upper stopband
- Multiple notches to mitigate the interference.

In this chapter a review on planar BPFs based on different design methodologies [10-27] are presented. The literature review also carries report on advanced planar UWB filters with extended stopband [28-37] and notched band [38-52].

## 2.2. Various UWB-BPF design methodologies:

There are numerous approaches to designing UWB-BPF filters. One typical strategy is to incorporate a LPF section into a HPF section [10, 11]. Another design strategy involves broadside coupling of top-plane MSL with ground-plane co-planar waveguides (CPW) via a shared dielectric material [12-19]. Furthermore, multiple mode resonators (MMR) are commonly used, either individually or on several TL topologies, such as hybrid MSL/CPW, [20-27]. Then the sections that follow provide a full description of each methodology.

### 2.2.1. UWB filters with cascaded HPF and LPF:

A simple method for creating a BPF is to sequentially combine a HPF and LPF section [10, 11]. The upper boundary is determined by the frequency of the LPF section's cutoff, while the lower boundary is determined by the frequency of the HPF section's cutoff. On the other hand, directly cascading the HPF and LPF sections, may result in an increase in circuit size. To overcome this issue, [10] proposes a UWB filter design technique in which the LPF portion is integrated into the HPF structure. The stepped impedance component serves as the LPF in Figure 2.1(a), while the shunt short-circuited stubs act as the HPF. Figure 2.1(b) depicts the frequency response of this arrangement.

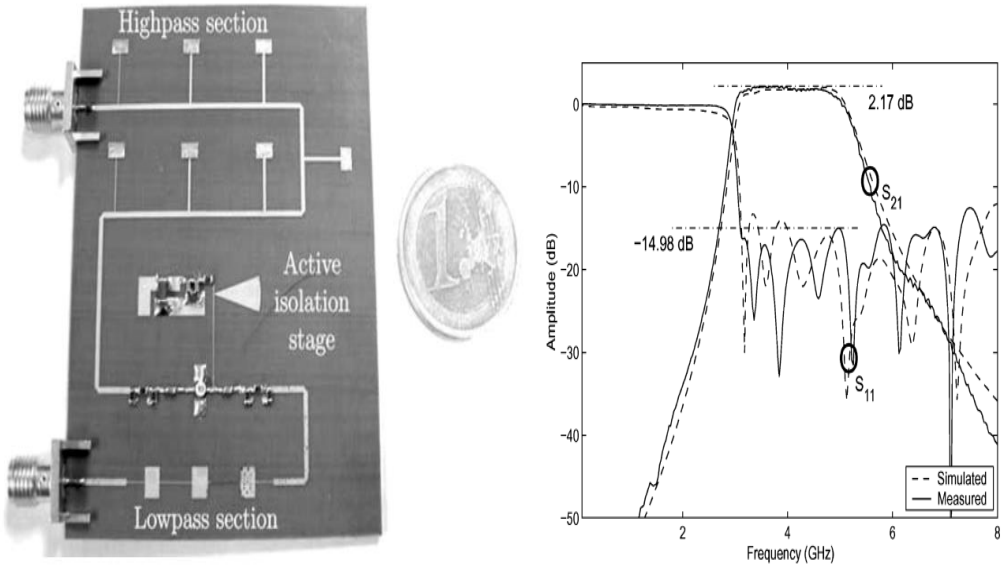


(a) (b)

**Fig. 2.1.** (a) BPF filter composed of lowpass filter embedded into highpass filter. (b) observed and simulated data [10].

Another UWB filter design solution reported in [12] connects a broadband BSF with a BPF using two short-circuit stubs. The BSF and BPF are designed independently by carefully selecting TLs impedances to meet the appropriate bandstop and bandpass characteristics, respectively. An alternate UWB filter design provided in [12] has an advantage over the one presented in [11], namely sharp selectivity.

### 2.2.2. Broadside coupled UWB filter:

Broadside coupling structures are another important technique used in UWB filter construction [12-19]. Through a shared dielectric material, MSLs are placed on the upper layer coupled with underneath bottom layer.

The broadside coupled structure was first implemented in [12], followed by the proposal of an equivalent circuit in [13]. The fundamental structure of filter consists of two MSL separated on the upper layer by a gap that are shown in Figure 2.2(a) which is broadside coupled on the bottom layer via the dielectric material to an open-end CPW. The existence of a dielectric substrate and the tight coupling achieved through broadside coupling lead to a wide bandpass operation. The coupled length of the UWB filter can be altered to control the bandwidth, whereas the distance that lies across the two sections determines the resonant frequency. The modifications in the spacing changes the TZ, increasing skirt performance at higher frequencies. It has no effect on bandwidth or passband performance. The stopband performance of the filter architectures illustrated in [12, 13] was unsatisfactory at both the lower and upper frequencies. Short-circuited stubs with series chip capacitors were integrated into the aforementioned arrangement to improve these features. This adjustment introduced attenuation poles at the upper and lower stopband frequencies. As a result, the skirt's performance was increased. This improvement, however, came at the expense of worsening passband performance, as seen in Fig.2.2(b).

In [15] introduces a novel UWB broadside coupled filter with similarities to the structure provided in [12]. The use of a MMR design for the CPW on the ground plane is a significant difference. In this design, three resonant modes: one at the lower end, one in the middle, and one at the top is supported by setting CPW at the end of the UWB passband.

Here [16-17] present apprised versions of the UWB broadside coupled filter proposed in [15]. The CPW is intentionally shorted in these enhanced designs to create a split mode resonator. Additional lower and upper TZs are obtained by inserting a cross-coupled capacitor. These zeros are intentionally placed near the passband's boundaries to improve selectivity. In addition, two MSL are employed to provide shunt inductances that resonate at higher frequencies, improving the out-of-band response [16]. The structure is enhanced further in [17] by incorporating a well-designed microstrip-to-CPW feeding mechanism.

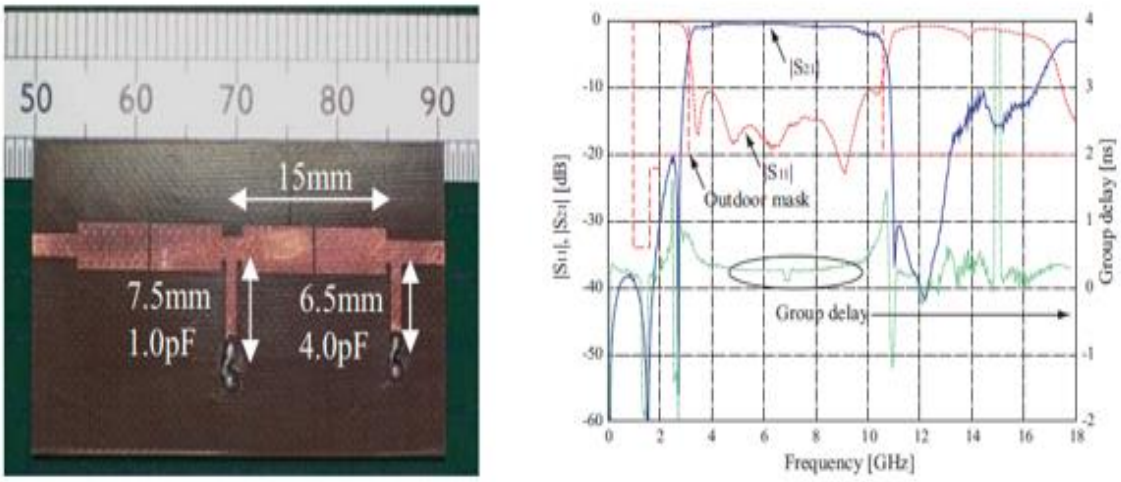


(a) (b)

**Fig.2.2.** (a) Photograph of UWB-BPF using broadside-coupled structure. (b) Simulated frequency response [14].

Here [18] Proposes a simplest broadside coupled structure consists on the ground plane with the λ/4 resonator, closely linked to the MSL on the layer at the top. These TZs are caused by the cross coupling present in between the two that is the feeding lines and the stubs, which improves the filter's selectivity. The spacing between the two open-circuited MSL is critical in setting the bandwidth (BW). The extent of this gap, in particular, is oppositely related to the filter's BW. Furthermore, altering the gap allows for manipulation of the TZ positions within the passband of the filter.

## 2.2.3. Multiple mode resonator (MMR) based UWB filter:

The MMR concept serves as the foundation for the basic category of UWB filter design [20-27]. UWB filters based on MMR theory have various advantages, including a simple construction and an easy design technique. The stepped variant of MMR, in instance, is usually known as a stepped impedance resonator (SIR). The appropriate UWB is achieved by simultaneous activation of numerous resonant modes inside the MMR. To further prolong and smooth passband response, the MMR is firmly connected with the input and output feeding lines. This concept was first introduced in [23], and it has been applied on

a various topologies of TL, including MSL CPW [24], and hybrid MSL/CPW configurations [25]. These many implementations have been added to the MMR-based UWB filters.

Figure 2.3(a) shows the classical MMR consists of wide center arm with low impedance, roughly λ/2 in length, and thin arms on both ends with high impedances, each around λ/4 in length. The goal is to optimize the MMR modelling in purpose of concurrently excite and place its resonant modes in a quasi-equal manner inside the UWB passband. The UWB bandwidth is influenced by the center arm portion, whereas the frequency characteristics filter is displayed in Figure 2.3(b). This is accomplished by inserting five TZs into the filter's response. The coupling degree is increased by stretching the narrow arms of the MMR.

The classical MMR was first reported in [23] and is composed of a wide central arm, of low-impedance, of approximately length λ/2 and narrow arms on either ends, of high impedances, of λ/4 each, as shown in Fig. 2.3(a). The idea is to optimize the modeling of MMR to simultaneously excite its modes which are resonant and insert into the passband. The wider arm section affects the UWB bandwidth while the length of narrow arms of the MMR enhances the coupling degree. As can be observed from its frequency response in Fig. 2.3(b), a five pole UWB filter with good in band performance has been constructed with five TZs.

Due to manufacturing limitations related to the coupled line's width, the edge coupled filter design faces problems in attaining tight coupling. [24] Introduces an innovative strategy to overcome this limitation and improve the coupled line’s coupling degree. This method employs a UWB filter based on a MMR with an aperture beneath the linked lines, in the bottom layer. When compared to the typical MMR design provided in [23], the inclusion of the aperture allows for substantially tighter coupling. This novel solution addresses the edge coupled filter's coupling issues and improves performance in UWB filter applications. [25] Proposes a UWB filter with a MMR with the bottom layer on CPW, linked to MSL on the upper layer, as seen in Figure 2.4(a). First three resonant modes are designed to allocate through MMR, which are centered at the UWB on the lower, middle, and upper ends.

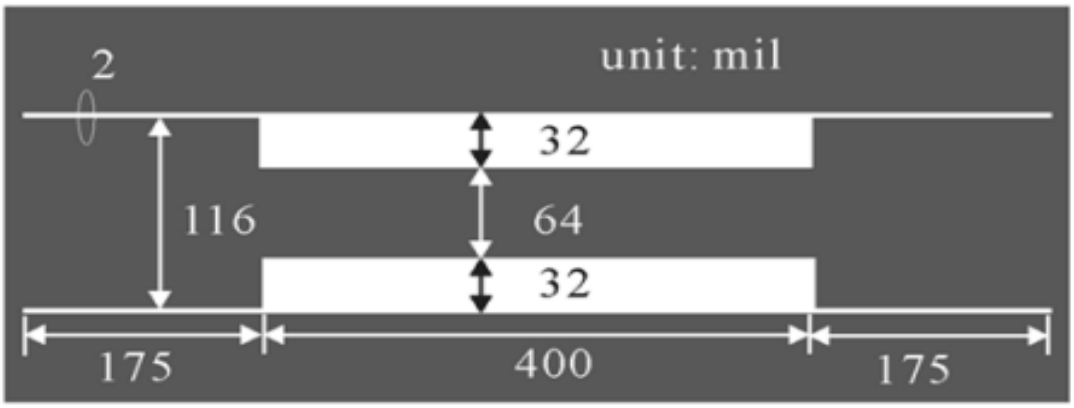


(a)

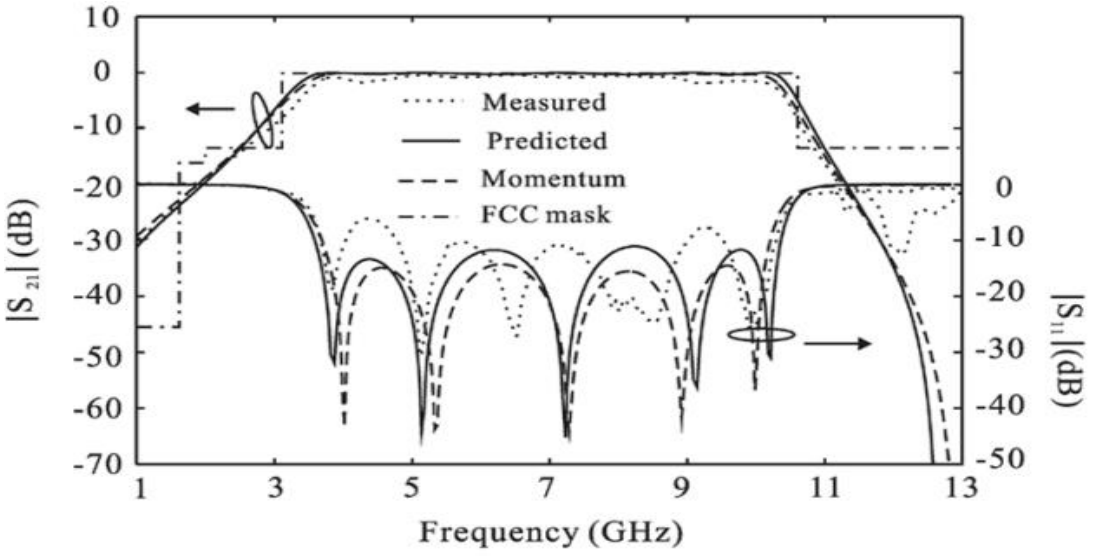


(b)

**Fig. 2.3.** (a) Schematic of design (b) observed and simulated data [25].

The dimension of the central CPW portion is chosen to excite the MMR's first and third resonant frequencies, which are linked with the upper ends and the lower ends of the UWB pass band, 10.4 GHz and 3.3 GHz accordingly, as displayed in figure 2.3.

A unique UWB filter based on MMR is explained in [27]. This structure is built by connecting IDC line (IDCL) portion with stepped impedance stubs (SIS) in a cascade. The parameters of the short-ended SIS are carefully modelled in the filter design to obtain a characteristic impedance of 50, whereas the default lengths are selected as λ/4.Proper modelling of this geometry allows for the required impedance matching. The structure is

discovered to produce a highly favorable UWB response, showing its efficacy in obtaining the requisite filtering properties as displayed in fig 2.4.

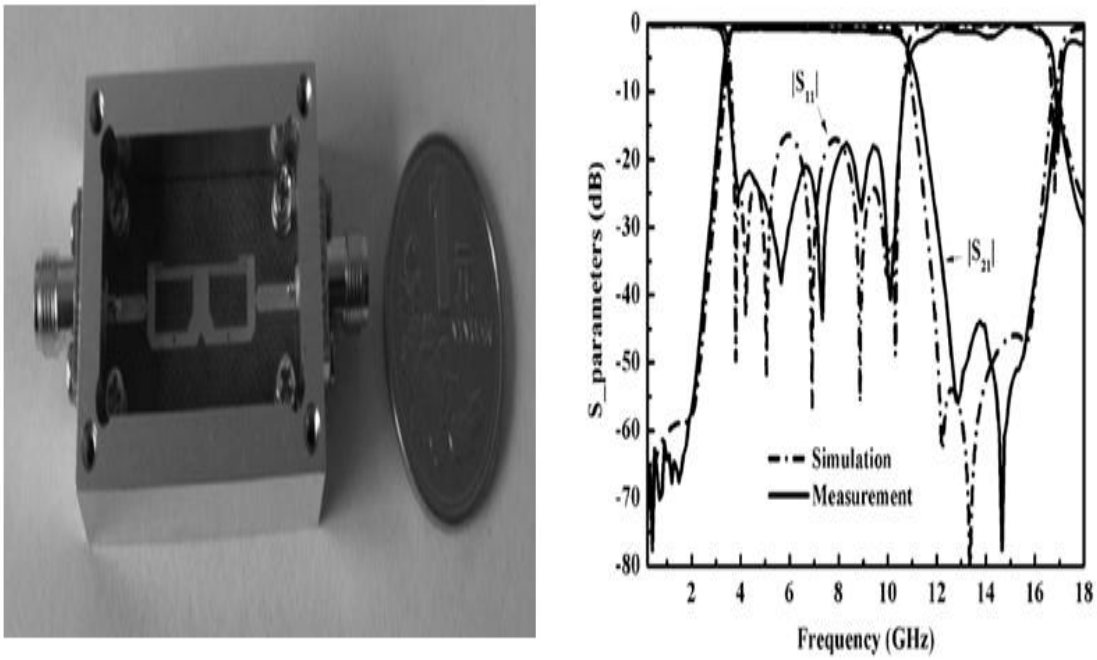


**(a)** **(b)**

**Fig. 2.4**. (a) Fabricated photo of MMR based UWB filter. (b Simulated and measured S parameter characteristics [27].

## 2.3. Advanced planar UWB filters:

Traditional UWB filters were limited by a small upper stopband and were susceptible to interference from other wireless services. Researchers developed microstrip-based planar advanced UWB filters to overcome these difficulties. These advanced filters used attenuation poles in the stopband [28-37] to decrease spurious harmonics and interference cancellation techniques in the passband [38-56]. These advancements sought to improve UWB filter performance by increasing stopband characteristics and minimizing interference from external sources, resulting in a more reliable and efficient UWB communication system.

### 2.3.1. UWB filters with the extended stopband:

Because of the presence of spurious harmonics, MMR-based filters frequently have a narrow upper stopband. Various strategies have been used to bypass this limitation and expand the stopband, such as integrating lowpass or bandstop structures on the MMR or embedding the MMR with an EM bandgap (EBG).

To solve these issues, Figure 2.5(a) depicts a unique MMR-based UWB filter that employs tapered interdigital lines (IDL) on both ends of the MMR. Initially the MMR is modeled so as to distribute, the UWB passband's first three resonant frequencies almost equally. As a result, the IDL's two outer arms are adequately tapered to compensate for the phase imbalance towards the UWB upper-end. As a result, a tight coupling degree is achieved, resulting in a nearly flat frequency response and significant return loss throughout the passband. Furthermore, as shown in Figure 2.5(b), the first spurious harmonic near 13.5 GHz is effectively suppressed by reallocating the TZ of the provided capacitive-ended stubs.

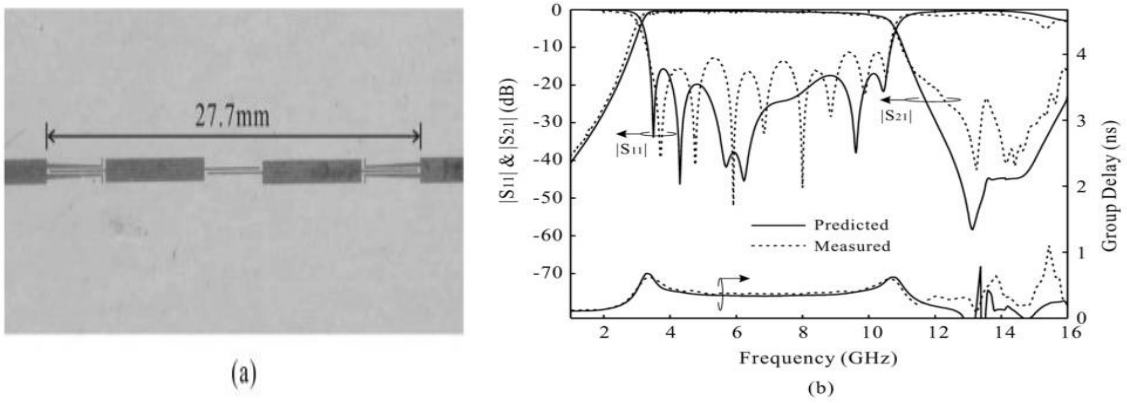


**Fig.2.5.** (a) Layouts of UWB BPF (b) Frequency responses for Simulated and measured values [28].

The article introduces a unique UWB filter frequency responses in shunt to a SIR [29]. By carefully regulating the lengths of these stubs, the first four resonant modes of the MMR are uniformly distributed across the UWB, where the fifth resonant frequency is exceeded beyond 15.0 GHz. As a result, the first four modes help to build the UWB, while the fifth resonant mode helps to reduce spurious signals in the stopband. This design method makes

optimal use of resonant modes to accomplish desirable passband properties as well as efficient spurious stopband suppression.

Enhanced versions of the UWB filter introduced in [29] have been presented in subsequent studies [30-33]. The original three symmetric stubs in [29] are replaced with alternative structures in these updated designs, greatly optimizing the filter's performance. To replace the symmetric stubs, [30] use shunt capacitive loaded EBG structures. The first three resonance frequencies of these EBG structures are carefully optimized so as to locate it into the UWB passband, while the fourth and fifth resonant frequencies are pushed to higher frequencies to function as spurious stopband harmonics. Furthermore, the interdigital coupled line (IDCL) utilized in this design has an attenuation zero, which allows the fourth resonant frequency to be adjusted closer to the IDCL's TZ. The EBG structure's bandgap behavior effectively suppresses the fifth resonant peak. SIR are used in [31] to substitute the original symmetric stubs. When compared to the previous design, these stepped impedance stubs contribute to a 33% reduction in total size while preserving the acceptable filter performance.

[32] Suggests a unique structure that combines features from [30] and [31]. It has a SIS at the center and symmetrical uniform-impedance two MSL on each side. This arrangement permits the presence of five resonant modes, all within the specified spectrum. The middle stepped-impedance stub generates two TZs at the lower and upper cut off frequencies.By varying the proportions of the center SIS, the behavior of the even mode varies whereas the odd modes stay constant, allowing for better control over their features.

[34] proposes an alternate technique that uses circular impedance-stepped stubs instead of the rectangular stubs used in [30-33]. A configuration is formed by coupling a high impedance MSL with multiple circular stubs interconnected in shunt. The resonant modes inside the UWB can be assigned, and the upper-stopband’s spurious harmonics can be suppressed, by modifying the radius of the circular stubs. By keeping the outer circle’s radius constant while decreasing the radius of the central circle, the even resonant modes will be shifted to lower frequencies but the modes that remains unaltered is the odd resonant modes. This enables for exact control of the resonance frequencies as well as the development of the filter response.

In [37], a brand-new multimode dual-ring UWB-BPF is demonstrated. The filter was built using open stubs in the dual-ring resonator's horizontal and vertical axes. This architecture ensures that the five modes are dispersed uniformly across the UWB passband. Furthermore, at the left and right transition bands, a pair of TZs are introduced, significantly increasing selectivity. Parallel-linked lines are used to establish appropriate external coupling capability in order to realize the UWB features. A cross junction is also used to attenuate spurious signals at high frequencies, hence increasing the filter's upper stopband.

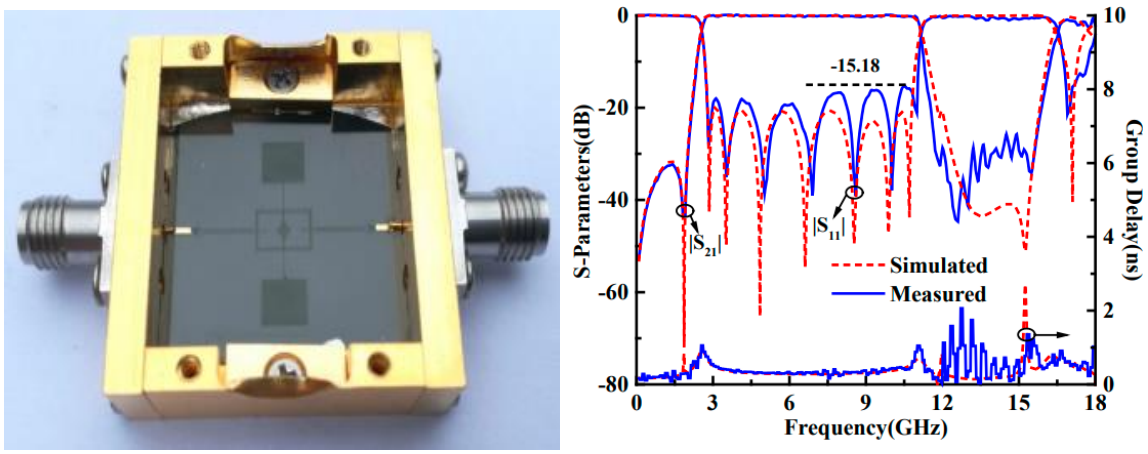


(a) (b)

**Fig. 2.6.** (a) Photo of the design. (b) observed and simulated data [35].

A novel UWB filter is presented in [36], which makes use of cross-junction transition in the back-to-back microstrip-slotline. The design procedure begins with the installation of a consistent slot line resonator on the ground that spans one full wavelength. A back-to-back microstrip-slotline transition is developed by the placement of two microstrip feed lines above the slotline resonator. The linear slotline resonator is converted into a W-shape to improve frequency selectivity, induce cross coupling, and reduce overall size. This change adds another coupling method that can generate single or multiple TZs outside of the specified UWB passband. These TZs, which have the same amplitude as the main transition-slotline-transition path but are out of phase with it, occur at certain frequencies outside the passband. Two lowpass filters (LPFs) are cascaded with the current structure

to boost out-of-band performance even further. This extra step improves the filter's capacity to attenuate undesirable frequencies outside the UWB passband.

### 2.3.2 UWB filters with single notched band:

Because of their low power density, UWB systems normally do not interfere with existing radio services. However, the inverse is not always true. WLAN, X band, C band, and other wireless services run at high power density and may cause interference for UWB systems. Several UWB filters have been developed to deal with this issue and reduce interference from these wireless services. UWB systems may efficiently minimize the impact of high-power density wireless services and assure reliable and interference-free communication by adding these notch filters. UWB filters were created in order to reduce interference from specific wireless services. To do this, these filters use a variety of ways. Some filters [38-49] use single notches inside the UWB passband, whereas others [50-56] use several notches. These notches are designed to selectively attenuate or reject frequencies associated with interfering wireless services. These UWB filters enable the UWB system to operate without interruptions caused by external interference by effectively suppressing undesirable signals.

[38] describes a notched band UWB filter design. Five stubs which are short-circuited are connected via non-redundant connecting lines in the design. Introduction of a passband notch, open stubs are incorporated into the first and last connecting lines. The notch's bandwidth is controlled by width adjustment of the width of the stubs/gaps, while the frequency position is identified by the dimension of the stubs. The UWB filter effectively attenuates specific frequencies within the passband as a result of these adjustments, resulting in a notch characteristic and precise control over the filter's frequency response.

[39] presents a design for a single notched band that employs a MMR. The notched band is formed by unequal placing stubs in the two outer arms of three parallel linked lines. A narrow passband notch is formed by varying the lengths of these stubs. The length difference between the two stubs can be used to alter the notch's bandwidth. This design allows for exact frequency response modification, which enables effective suppression of specific frequencies within the UWB passband.

[40] presents a modified non-uniform resonator-based design with a notched band. Attaching three pairs of SIS transversely creates the non-uniform resonator. Out-of-phase transmission cancellation produces the notched band. This is accomplished by greatly expanding one of the two arms of the IDCL that is connected to the resonator. A customized notched band can be achieved by using this design, allowing for selective suppression of specific frequencies within the UWB passband.

In [41], a hybrid microstrip and CPW construction is used to provide an ultra-narrow notched band for a small UWB filter. With the MSL on the upper layer of the structure acts as the feed lines for the detached-mode resonator (DMR) installed on the ground plane in a broadside configuration. A structure with the λ/4 meander slot-line is integrated inside the DMR so as to solve interference concerns from other wireless services. This meander slot-line incorporate in the filter design enables the formation of a notched band. The UWB filter effectively attenuates specific spectrum by deliberately employing this design, giving increased interference rejection capabilities.

In [42], metal lines embedded in a DGS are open circuited that are used to implement a notch in an UWB-BPF. The filter structure is made up of two layers: the top layer consists of two stubs and MSL while the bottom layer consists of two open circuited lines and a DGS. This arrangement enables the development of a notch within the UWB-BPF, resulting in increased selectivity and notch performance.

The physical parameters of the MSL define the location of the notch. the level of coupling in this gap determines the width of the notch. The suggested UWB-BPF architecture achieves notch functionality by adopting this approach, allowing for selective attenuation of specific frequencies within the passband. This method gives you more control over the notch location and bandwidth, which improves the performance and adaptability of the UWB-BPF.

[43] Presents a defective split-ring resonator (DSRR). The architecture consists of a TL on top layer and two units MSL. This arrangement improves selectivity, extended stop band performance, and contributes to the filter's compact size. A DSRR is implemented within the ground construction to introduce a notched band specifically targeting the WLAN frequency range. This DSRR produces a band rejection within the BW of the filter. The TL position is carefully tuned to create the appropriate coupling effect, resulting in optimal

filter performance. The suggested UWB filter creates a notched band by using this design method, efficiently attenuating signals inside the WLAN frequency range while keeping the desired UWB passband. This compact filter design, which has a split-ring resonator defective ground construction, provides higher selectivity, improved extended stopband performance.

The article [44] introduces a small size UWB-BPF with a notched frequency. The layout design employs a novel technique that employs a parasitic coupled line to create the UWB passband with a notch. The notched band's position and width can be changed by modifying the architectural parameters of the parasitic linked line. This novel approach allows for greater flexibility in getting the desired frequency response and successfully mitigating interference from unwanted signals. The suggested UWB BPF has the ability to improve interference immunity while also providing dependable performance in UWB radio systems.

In [45], a compact notched band with a slow-wave CPW based MMR is proposed. The UWB filter is built with feed lines on the top layer that are linked to the slow-wave MMR on the bottom layer in a broadside configuration. A passband notch is generated by a new bridge structure implemented on the top layer, allowing for controlled frequency suppression. The cascaded capacitive-loaded CPW lines in the slow-wave CPW MMR result in a larger capacitance per unit length between the interdigital fingers. Because of the enhanced capacitance, the electrical length is stretched, resulting reduction in compact size. Furthermore, two open-ended stubs connected to the top MSL generate TZs, which contribute to improved roll-off characteristics.

[46] Proposes a design with a notched band and a ring resonator for UWB-BPF as displayed in Figure 2.7(a). An IDCL feeds two stepped-impedance stubs in the layout. Harmonic suppression in the stopbands is performed by altering the length of the IDCL to approximately λ/4. Because of the IDCL's asymmetry, out-of-phase signals on the two pathways at a particular frequency create a notch at the appropriate frequency of interest as seen in Figure 2.7(b). These novel designs show the successful deployment of notched band UWB-BPFs with various resonator configurations. Slow-wave CPW MMR and ring resonator designs suggested here provide better performance, small size, and notch characteristics for tailored frequency suppression in the UWB passband.

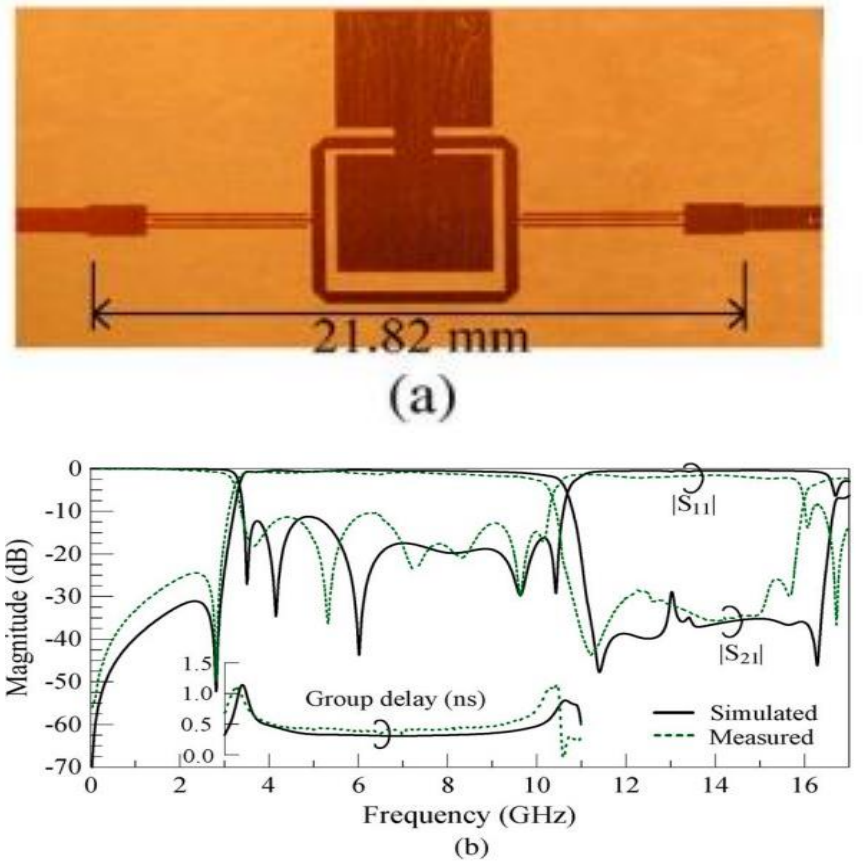


**Fig. 2.7.** (a) Photograph of notched band of UWB filter. (b) S-parameters for observed and simulated values [46].

## 2.3.3. UWB filters with dual notched bands:

[47] describes an UWB-BPF that has multiple notch bands. A SIR is used to attenuate higher order harmonics of the HPF. To create dual band notches at 5.75 and 8.05 GHz, the filter design features two stubs which are open implanted on the primary MSL. These notches are intentionally placed in the UWB passband to attenuate specific frequencies.

The paper [48] describes a unique triangular defective ground structures (DGS) UWB-BPF with dual notches. To enhance the BPF's performance, the design employs symmetrical dumbbell-shaped interdigital capacitors as shown in figure 2.8 (a). Furthermore, by intelligently aligning their TZs away from the required UWB frequency range, three pairs of tapered DGS are used to minimize spurious passbands. To produce the notched bands,

In the coupled-line parts, one of the arms has been extended and folded, generating in a notched band centered at 5.3 GHz. To produce another notched band centered at 7.8 GHz a meander line slot is also used as displayed in figure 2.8 (b).

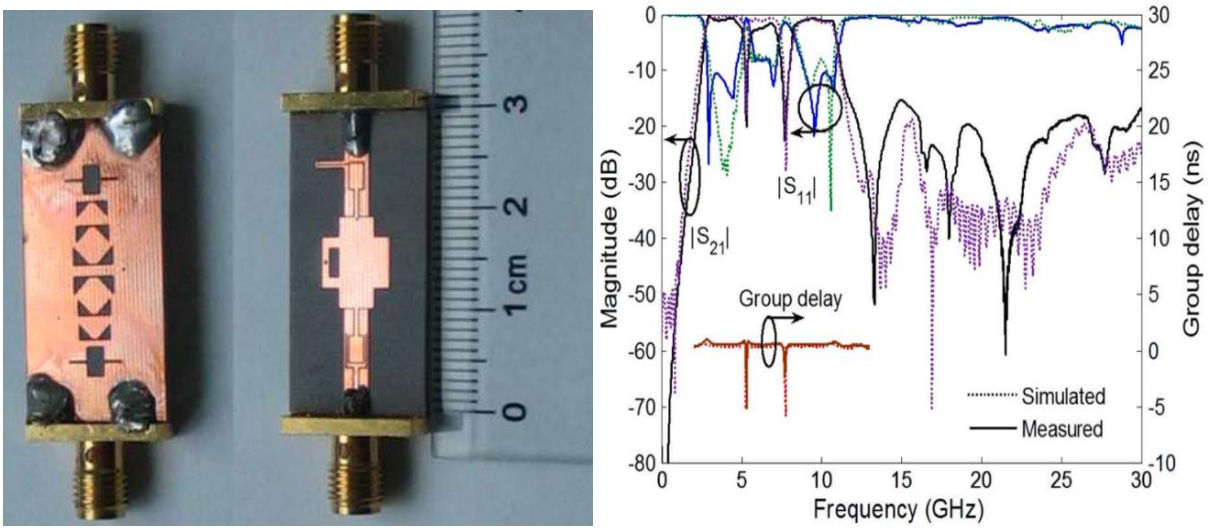


(a) (b)

**Fig. 2.8.** (a) Image of proposed dual bands UWB filter. (b) Characteristics of simulated and measured values [48].

The paper [49] describes a high rejection notched band miniature UWB-BPF. The filter consists of an open-loaded Y-shaped stub resonator (YSSR), a rectangular ring, interdigital feedlines and a DGS. The combination of these features leads to the UWB-BPF's miniaturization and performance. On a FR4 substrate, the suggested filter is developed, simulated and manufactured. The observed results match the simulated data very well. The filter has a 3-dB passband that covers the frequency ranges 2.73-4.36 GHz and 6.82-11.78 GHz, as well as having an in-band $S_{21}$ is less than 1.13 dB and $S_{11}$ is less than 10 dB (except at the notches).

## 2.3.4. UWB filters with triple notched bands:

[50] Describes a UWB-BPF compact filter with triple-notched bands. To accomplish the requisite filtering properties, the filter design utilizes SIR with a new triple-mode linking

lines with lengths of $\lambda g_0/4$ and $\lambda g_0/2$ separate the four folding shunt quarter-wavelength short-circuited stubs in the UWB BPF. This configuration serves as the basis for the UWB passband response. The suggested coupled triple-mode SIR improves the filter design by introducing triple-notched bands and allowing for more flexibility in adjusting the resonant frequencies. This enables exact control and customization of the filter's properties.

[51] Describes a UWB-BPF which is highly selective filters with three notches band. The filter design makes use of C-shaped and E-shaped resonators as well as a triangular ring loaded stub resonator (TRLSR) relied on the MMR. According to figure 2.9, the MMR structure is built with 50 feed lines connected at both ends to 50 parallel coupled lines and a uniform TL. This arrangement produces five even and odd modes, yielding a UWB passband response. The TRLSR introduces two TZs at the passband's lower and higher cutoff frequencies, resulting in a high skirt factor (SF), signifying sharp roll-off characteristics as given in figure 2.9 (b).

Also, the proposed filter incorporates a number of notch bands produced by $\lambda g/2$ resonators. These notch bands are placed deliberately to eliminate interferences. The notch frequency may be changed by adjusting the design's dimensions.

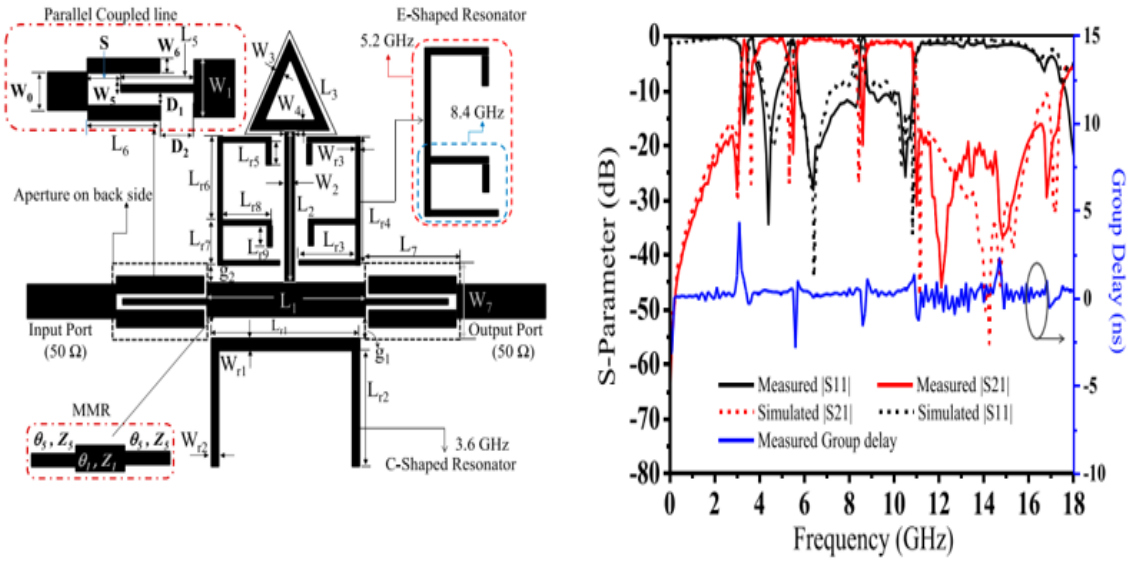


(a) (b)

**Fig. 2.9** (a). The triple-notch band UWB filter's layout. (b). Measured and simulated frequency response [51].

## 2.3.5. UWB filters with Quad notched bands:

The paper [52] describes UWB-BPF with quad-notches and an extended stopband. To attain the needed features, the design employs a quad-mode SIR (QMSIR) structure which is constructed using a square ring design with a λ/4 short-circuited stub, resulting in a square ring quad-mode resonator (SRQMR). The goal of the design is to produce a compact notched UWB BPF bands having the center frequencies of 5.2 GHz, 5.8 GHz, 7.0 GHz, and 8 GHz.

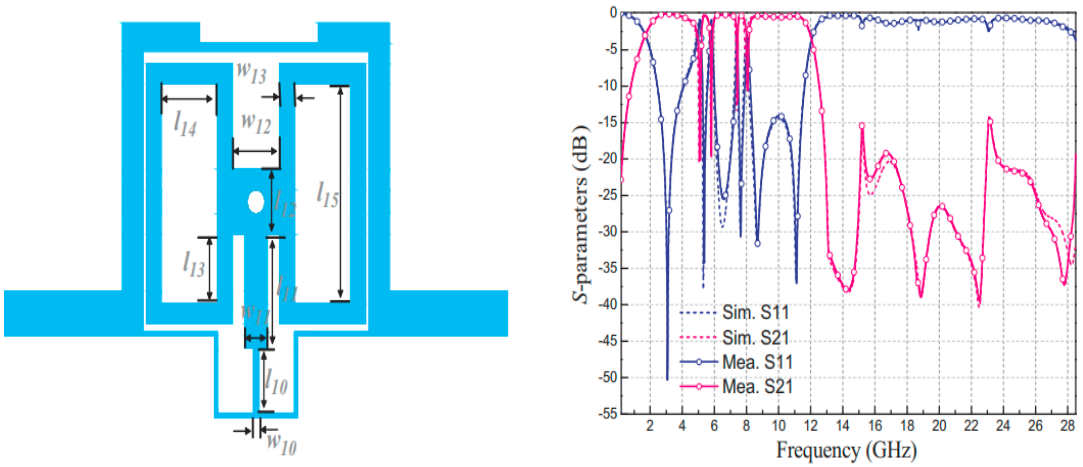


(a) (b)

**Fig. 2.10** (a). Quad notched band filter (b). Simulated frequency characteristics [52].

## 2.4. Summary:

This chapter presents a chronological overview of the approaches used to design and construct planar microstrip-based UWB-BPFs. The review focuses on three types of UWB-BPF design methodologies, with MMR-based designs being the most frequent. MMR-based UWB filters, on the other hand, frequently suffer from a narrow stopband and interference from other wireless services. To solve this, sophisticated designs of microstrip filters that expand the stopband by cancelling spurious harmonics have been proposed. The thesis also explores improved UWB filters that deal with passband interference by creating a passband notch at the desired frequency of interest. These enhancements are intended to improve the performance and usefulness of UWB-BPFs for variety of applications.

# CHAPTER 3

# MMR BASED UWB-BANDPASS FILTER WITH EIGHT POLES AND MULTIPLE TZs

## 3.1. Introduction :

The development and modelling of a proposed UWB-BPF using multimode resonators is the subject of this chapter. The MMR concept was introduced in the development of UWB BPF. This concept was used to achieve most desirable characteristics such as, smooth passband with high selectivity. In earlier reported work, interdigital coupled lines are used to reduce insertion loss in [53-55]. This concept preserves the filter's effectiveness while reducing its total circuit dimensions. The inclusion of radial stubs technique was further used in [56] for a significant reduction in filter size without sacrificing performance. Similarly, in [57-58] a rectangular stub resonator is used to generate tunable TZs with a wide stopband and appropriate UWB response. In the works [59-64], the appropriate frequency response was achieved by using the concept of a hybrid microstrip-coplanar waveguide. T-shaped slots are used in [65] to broaden the passband and improve the upper band rejection. Furthermore, to improve passband characteristics, [66] have used a precise closed-form relation of microstrip TLs and microstrip T-junction discontinuities. A multimode resonator, open-ended TL, parallel coupled-line sections, and DGS are used in [67] - [72] to create a BPF with improved stopband response for ultra-wideband applications. The first step in analyzing a MMR is to investigate its equivalent circuit to identify its inductance, capacitance, and resonant frequencies. In addition, the relationship between the MMR's dimensional characteristics and its resonant frequencies is examined, and the requirements for simultaneously activating the MMR's resonant modes are presented.

**Flow diagram of UWB-BPF Design:**

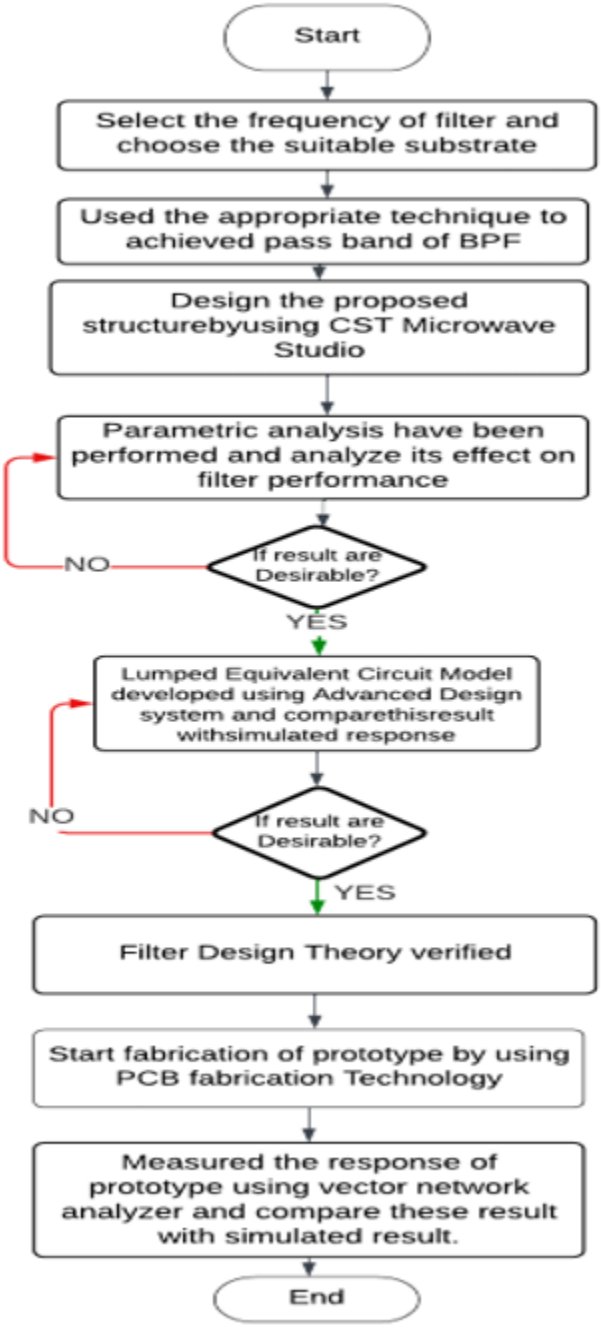


## 3.2. Analysis of the proposed design methodology:

The suggested BPF is realized using an MMR, with an ILSIR integrated at its center and IDS coupled at its ends. The ground plane has two rectangular DGS, arranged diagonally,

and exactly under the IDC structure (IDCS). Fig. 3.1 exhibits the architecture of the envisaged design.

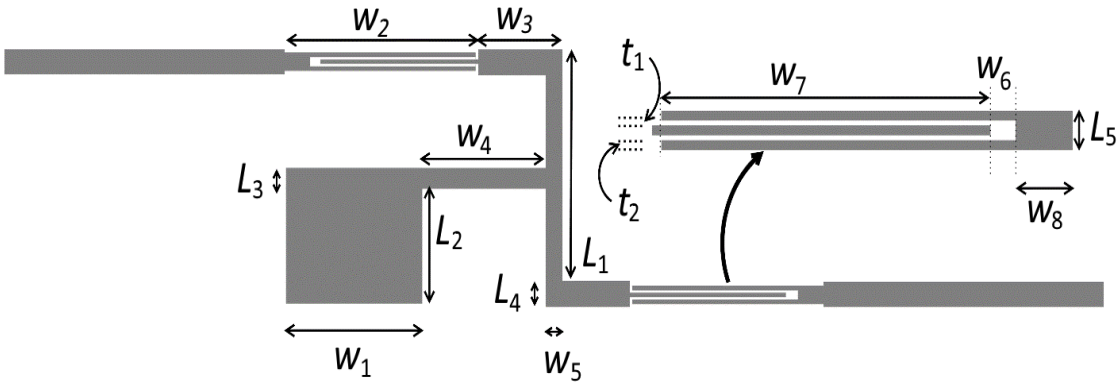


(a)

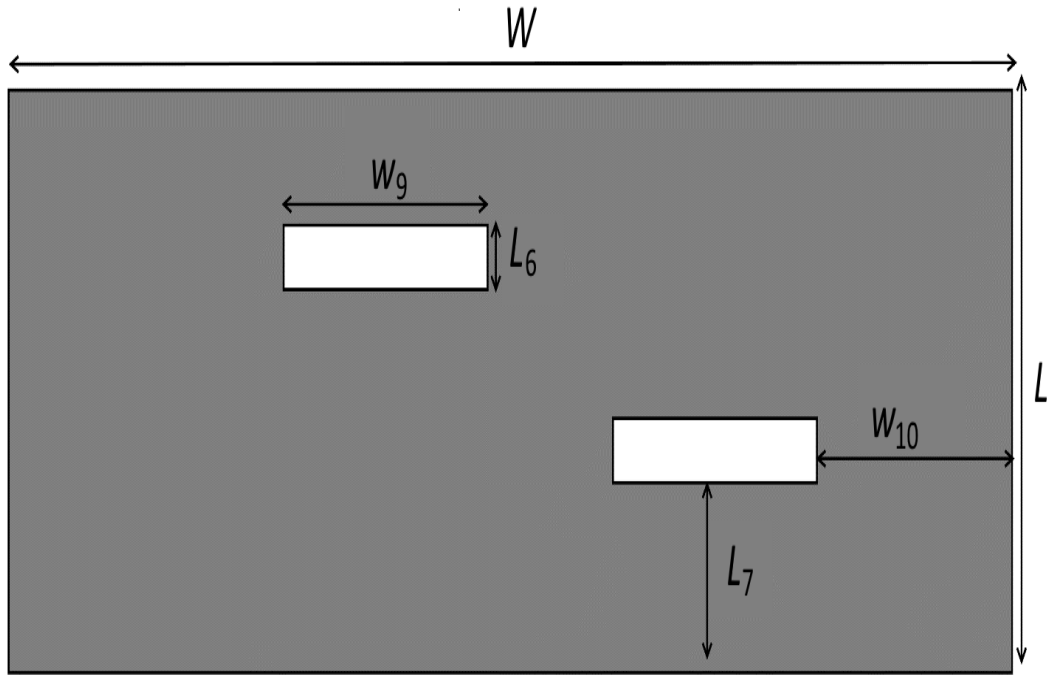


(b)

**Fig-3.1:** Suggested MMR based UWB filter (a) Upper and (b) Bottom layer

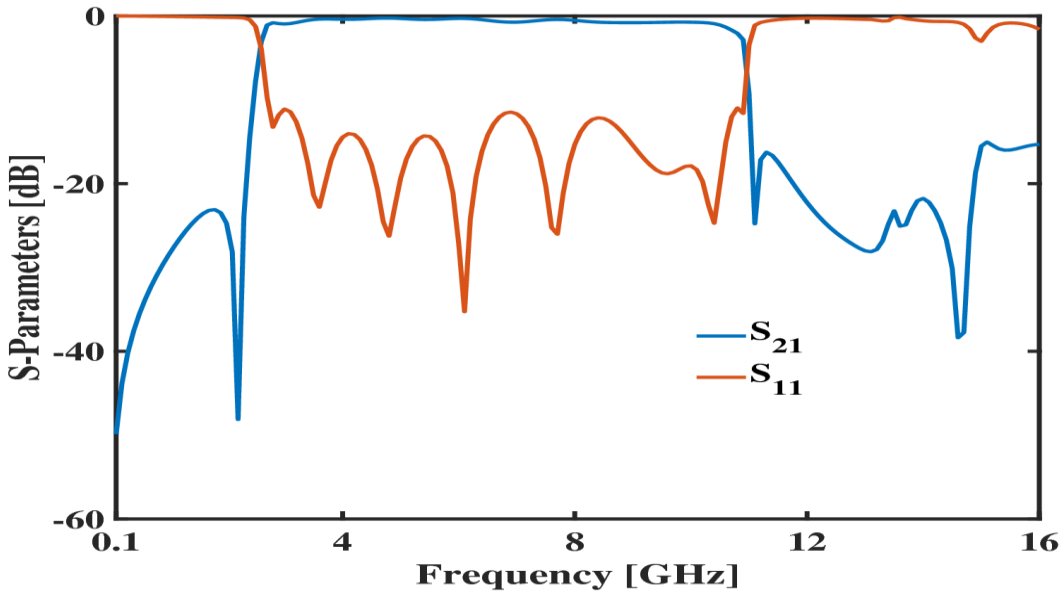


**Fig-3.2:** S-Parameters of suggested UWB filter

The simulated data in Fig (3.2) depict that IDCS has the potential to achieve outstanding quality of transmission over the whole passband, and provide steep transition. Upper TZ is tuned by the arm length of the IDCS as display in Fig (3.3),

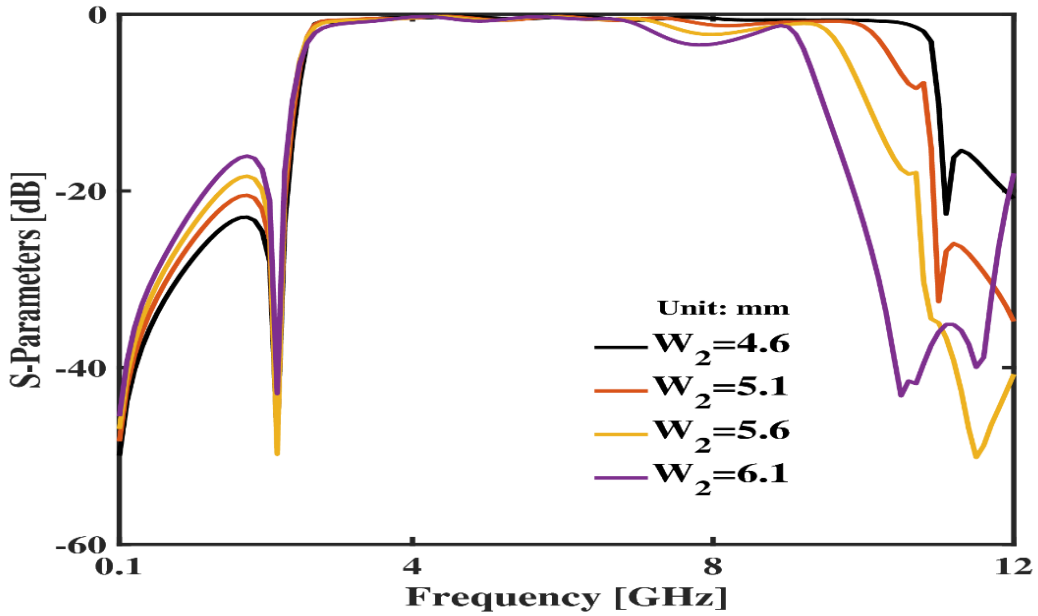


**Fig-3.3:** Parametric study ($W_2$) of upper TZ variations

The tuning range of upper TZ can be defined as the function of the arm Length ($W_7 \leq \lambda/4$) of the (IDS), and it is verified from Fig (3.3) and Fig (3.4), whereas the ILSIR tunes the lower TZ displayed in Fig (3.5) and Fig (3.6).

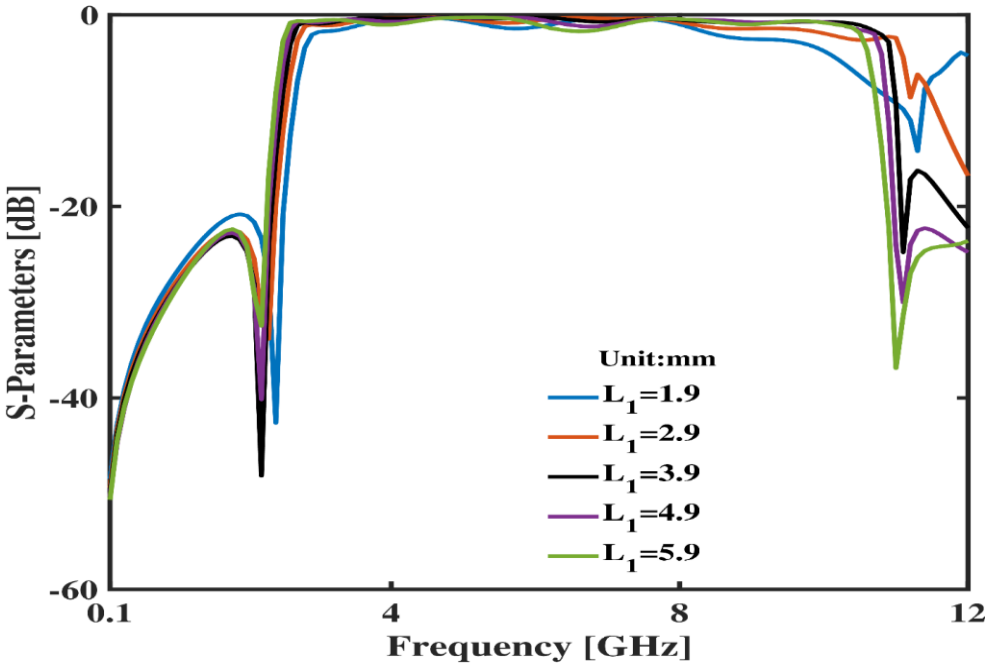


**Fig-3.4:** Parametric study ($L_1$) of upper TZ variations.

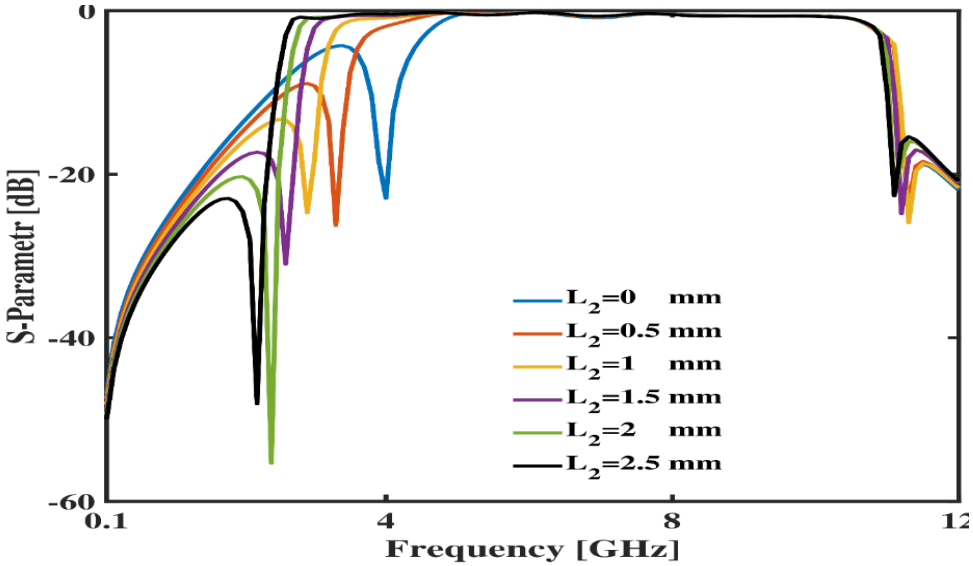


**Fig-3.5:** Parametric study ($L_2$) of $S_{21}$ and Lower TZ variations

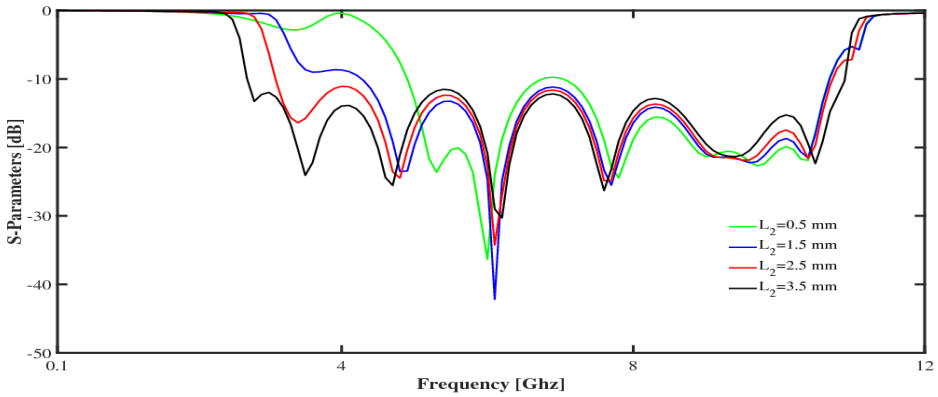


**Fig-3.6** Parametric study ($L_2$) of $S_{11}$ and Lower TZ variations.

whereas lower TZ frequency calculated by using following equation-

$$f_{TZ1} = \frac{c}{4(w_1+w_4+L_4)\sqrt{\varepsilon_r}}$$

The effect of DGS in bottom layer identified from Fig (3.7).

The physical parameters of the suggested design in figure (1) are given as (in mm) $L_1$ = 3.9, $w_1$=3.6, $L_2$ = 2.5, $w_2$ = 5.75, $L_3$ = 0.3, $w_3$ = 1.85, $L_4$ = 0.6, $w_5$ = 0.5, $L_6$ = 1, $w_6$ = 0.2, $L_7$ = 4.1, $w_7$ = 4.4, $w_8$ = 1, $w_9$ = 4.6, $w_{10}$ = 8.95, $t_1$ = 0.05, $t_2$=0.1, $L$=13.7, $W$ = 14.7.

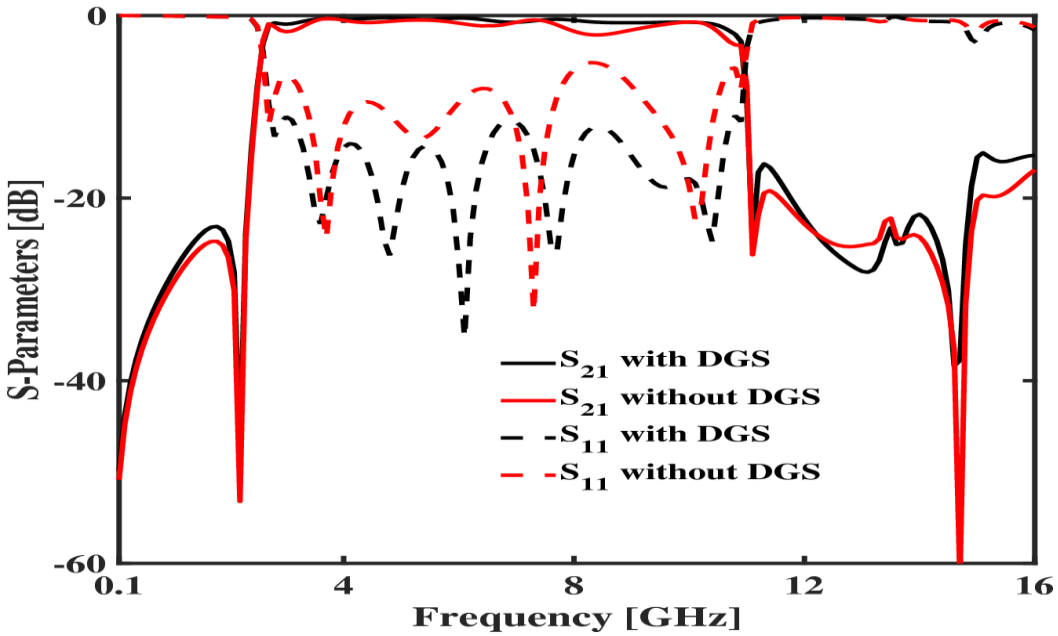


**Fig-3.7** Effect of DGS in bottom layer.

**Table: 3.1** Comparison of the designed filter with reported literatures

| Ref | S.F | IL/RL | Extended stop band | Structure | FBW (%) | TZs | Size (λg X λg) |
|---|---|---|---|---|---|---|---|
| [53] | na | na/10 | na | Step impedance | 116 | yes | 0.45X0.21 |
| [54] | 0.9 | 1.4/11.1 | 29.7 | Step impedance | 117 | yes | 0.32X0.23 |
| [55] | na | 0.94/12 | 18 | Step impedance | 123 | yes | - |
| [56] | na | 0.9/12.8 | 14 | Stub loaded | 109.5 | yes | 0.36X0.36 |
| [57] | 0.975 | 1.2/11.3 | 17.1 | Parellel coupeld line | NA | yes | 0.48X0.40 |
| [58] | na | 0.8 | 25 | Parellel coupled line | 101.9 | Lower TZ absent | 0.24X0.19 |
| [59] | na | 0.65/12 | 15 | Broadside coupled | NA | Lower TZ absent | 0.98X0.54 |
| [60] | 0.75 | 1.4/13 | 17 | Broadside coupled | 109 | yes | 1.04X0.66 |
| [61] | na | 0.9/20 | 14 | Broadside | 100.7 | yes | 0.67X0.54 |
| [62] | na | 0.85/16 | 15 | cpw-microstrip transition | 141 | yes, but poor roll off at high frequency passband edge | 0.99X0.90 |
| [63] | na | 0.5/20.5 | 12 | cpw-microstrip transition | 112 | Lower TZ absent | 1.15X0.24 |
| [64] | na | 2.5/10 | 10 | cpw-microstrip transition | 132 | Lower TZ absent | 0.76X0.32 |

| | | | | | | | |
|---|---|---|---|---|---|---|---|
| [65] | na | 0.5/17 | 20 | SIW | 62 | Lower TZ absent | 0.75X0.33 |
| [66] | na | NA/12 | na | least mean squares (LMS) | NA | Lower TZ absent | 2.60X0.28 |
| [32] | 0.921 | Na/na | 16 | MMR | 117 | yes | 0.32X0.20 |
| [67] | na | 1.5/na | na | MMR | 109 | Lower TZ absent and upper TZ around 14 GHz | 1.1X0.40 |
| [68] | 0.92 | 1.6/12 | 100 | MMR | 110.1 | yes | 0.60X0.54 |
| [69] | 0.89 | 0.9/na | 20 | MMR | 108 | yes | 0.28X0.14 |
| [70] | na | 0.4/20 | 20 | MMR | 109 | Lower TZ absent | 0.74X0.67 |
| [71] | na | 0.7/16 | 17 | MMR | 106.5 | yes | - |
| **This work** | **0.94 *** | **0.8/11.5** | **16** | **MMR** | **122** | **yes** | **1.01X0.34** |

*Selectivity factor $\zeta = \frac{BW_{3dB}}{BW_{25\,dB}}$

S.F=Selectivity factor

## 3.3. Odd and Even Mode Analysis `of suggested UWB-BPF:

The MMR-based suggested structure is displayed in figure 3.8. Since the suggested design is symmetrical about the Z'-Z plane, this structure could be analyzed using even-mode and odd mode analysis. Fig. 3.8(b) and 3.8(c) display the even- and odd-mode circuits.

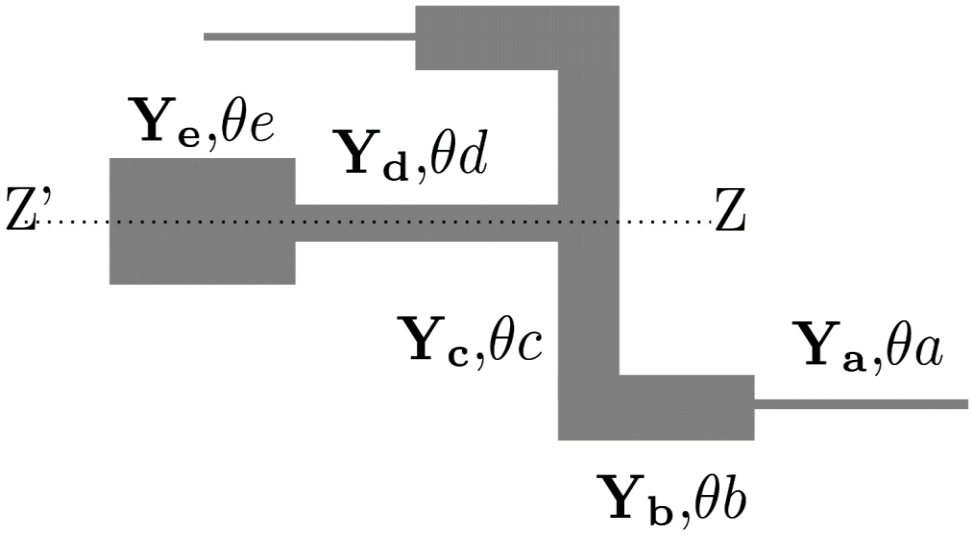


(a)

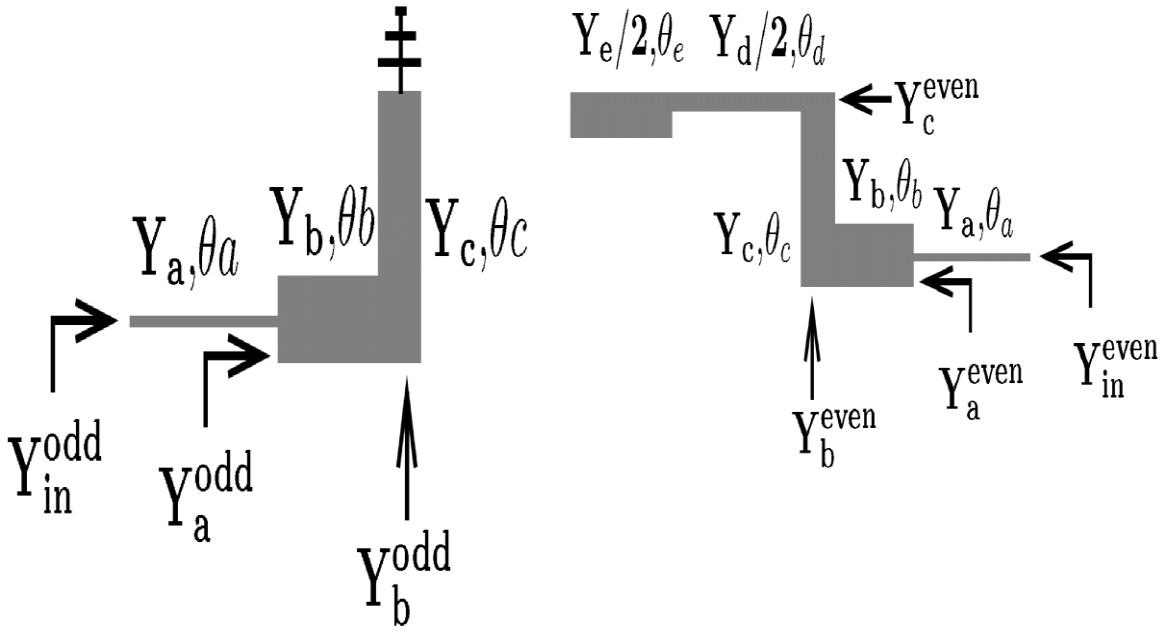


(b) (c)

**Fig-3.8** (a)Even Mode and odd mode circuits (b) Odd mode circuit (c) Even mode circuit.

### 3.3.1. Odd Mode Analysis:

The open-circuited transmission-line resonator has characteristic admittances Ya, Yb, and Yc. when odd mode excitation is applied, the voltage is null along the plane Z'-Z. The odd mode layout is demonstrated by the circuit design as shown in Figure 3.8.b, and all calculations and analysis are performed in the admittance domain. The determination of each specific input admittance follows the equation mentioned in section (3.b) and (3.c). The resonate modes could be extracted from the resonance condition $y_{in}^{odd} = 0$ in Equation (3.a).

Input Admittance of the circuit displayed in figure 3.8.b are represented as

$$y_{in}^{0dd} = y_a \left[\frac{y_a^{odd} + jy_a tan\theta_a}{y_a + jy_a^{odd} tan\theta_a}\right] \quad (3.a)$$

Where

$$y_a^{odd} = y_b \left[\frac{y_b^{odd} + jy_b tan\theta_b}{y_b + jy_b^{odd} tanb}\right] \quad (3.b)$$

$$y_b^{odd} = -jy_c cot\theta_c \quad (3.c)$$

for odd mode structure analysis, putting the value of Eqn. (3.b) and (3.c) in Eqn. (3.a) and further simplifying this equation at resonance $y_{in}^{0dd} = 0$ ,we get

$$y_b(y_a tan\theta_a + y_b tan\theta_b) = y_c cot\theta_c(y_b - y_a tan\theta_a tan\theta_b) \quad (3.d)$$

Hence, odd mode resonance frequencies can be deduced by Equation (3.d)

### 3.3.2 Even Mode analysis:

The even mode layout is demonstrated by the circuit design shown in Figure 3.8.c, and all calculations and analysis are performed in the admittance domain. The determination of each specific input follows the equation mentioned as 3.f to 3.j.

For even mode, the input admittance of the circuit is displayed in Fig 8(c), represented as (3.e)

$$y_{in}^{even} = y_a \left[\frac{y_a^{even} + jy_a tan\theta_a}{y_a + jy_a^{even} tan\theta_a}\right] \quad (3.e)$$

Where

$$y_a^{even} = y_b \left[\frac{y_b^{even} + jy_b tan\theta_b}{y_b + jy_b^{even} tan\theta_b}\right] \quad (3.f)$$

$$y_b^{even} = y_c \left[\frac{y_c^{even} + jy_c tan\theta_c}{y_c + jy_c^{even} tan\theta_c}\right] \quad (3.g)$$

$$y_c^{even} = \frac{jy_d}{2} \left[\frac{y_d^{even} + jy_d tan\theta_d}{y_d + jy_d^{even} tan\theta_d}\right] \quad (3.h)$$

$$y_d^{even} = \left[\frac{jy_e tan\theta_e}{2}\right] \quad (3.i)$$

From equation (3.h) and (3.i) we get

$$y_c^{even} = \frac{jy_d}{2} \left[\frac{y_e tan\theta_e + y_d tan\theta_d}{y_d - y_e tan\theta_d tan\theta_e}\right] \quad (3.j)$$

At resonance, even mode frequency can be analyzed using

$$y_{in}^{even} = 0 \quad (3.k)$$

Further equation (3.e) can be simplified by using (3.k),

$$y_a^{even} = -jy_a tan\theta_a \quad (3.l)$$

From equation (3.l) and (3.f), we get

$$y_b^{even} = -jy_b \left[\frac{y_a tan\theta_a + jy_b tan\theta_b}{y_b - y_a tan\theta_a tan\theta_b}\right] \quad (3.m)$$

And from equation (3.m) and (3.g), we get

$$-jy_b \left[\frac{y_a tan\theta_a + jy_b tan\theta_b}{y_b - y_a tan\theta_a tan\theta_b}\right] = y_c \left[\frac{y_c^{even} + jy_c tan\theta_c}{y_c + jy_c^{even} tan\theta_c}\right] \quad (3.n)$$

After simplifying equation (3. n), we get

$$-jy_b(y_a tan\theta_a + jy_b tan\theta_b)(y_c + jy_c^{even} tan\theta_c) = y_c(y_c^{even} + jy_c tan\theta_c)(y_b - y_a tan\theta_a tan\theta_b) \quad (3.o)$$

By putting the value of $y_c^{even}$ From (3. j), we can deduce even mode frequency using equation (3.o).

### 3.4. Analysis of Interdigital structure:

Upper TZ in pass band introduce by this parallel coupled stub and position of this TZ is adjusted by its length. The circuital model and equivalent circuital model of IDC are shown in Fig (3.9) interdigital capacitance calculated by using [72]. From Fig (3.1),

$$C = \varepsilon_{re} \frac{\varepsilon_{re}}{18\pi} \frac{N(n)}{N(n')} (k-1)W_7 \ pF$$

where $W_7$ is in mm, $t_1$=Slot width of MSL, $t_2$= Width of microstipline, and $W_7 \leq \lambda/4$,
k= Number of fingers in arm pair of IDCS.
The elliptic integral ratio of n and n' is

$$\frac{N(n)}{N'(n)} = \frac{1}{\pi}\ln\left(2\frac{1+\sqrt{n}}{1-\sqrt{n}}\right) \qquad 0.707 \leq n \leq 1$$

$$= \frac{\pi}{\ln\left(2\frac{1+\sqrt{n'}}{1-\sqrt{n'}}\right)} \qquad 0 \leq n \leq 0.707$$

where n and n' can be calculated as
$\alpha = t_1/2$, $\beta = (t_1+t_2)/2$, $n=\tan^2\left(\frac{\alpha\pi}{4\beta}\right)$, $n'=\sqrt{1-n^2}$
This MMR-based BPF is developed on Roger 6010 substrate (thickness h= 1.6 mm and dielectric constant =10.2).

## 3.5. Lumped Equivalent circuit model:

An approximated Lumped Equivalent circuit was introduced in Fig (3.10) to analyze the proposed structure using commercial software ADS, the lumped elements are retrieved. The obtained results of this lumped equivalent model are approximately the same as those retrieved from IE3D EM Simulator.

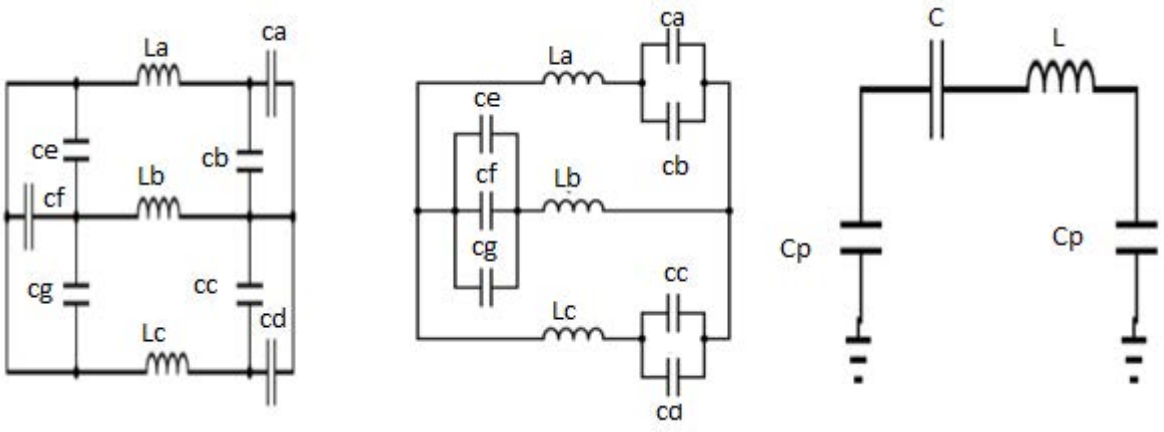
La
ca
ce
cb
Lb
cf
cg
cc
cd
Lc
La
ca
ce
cf
Lb
cb
cg
cc
Lc
cd
C
L
Cp
Cp

(a) (b)

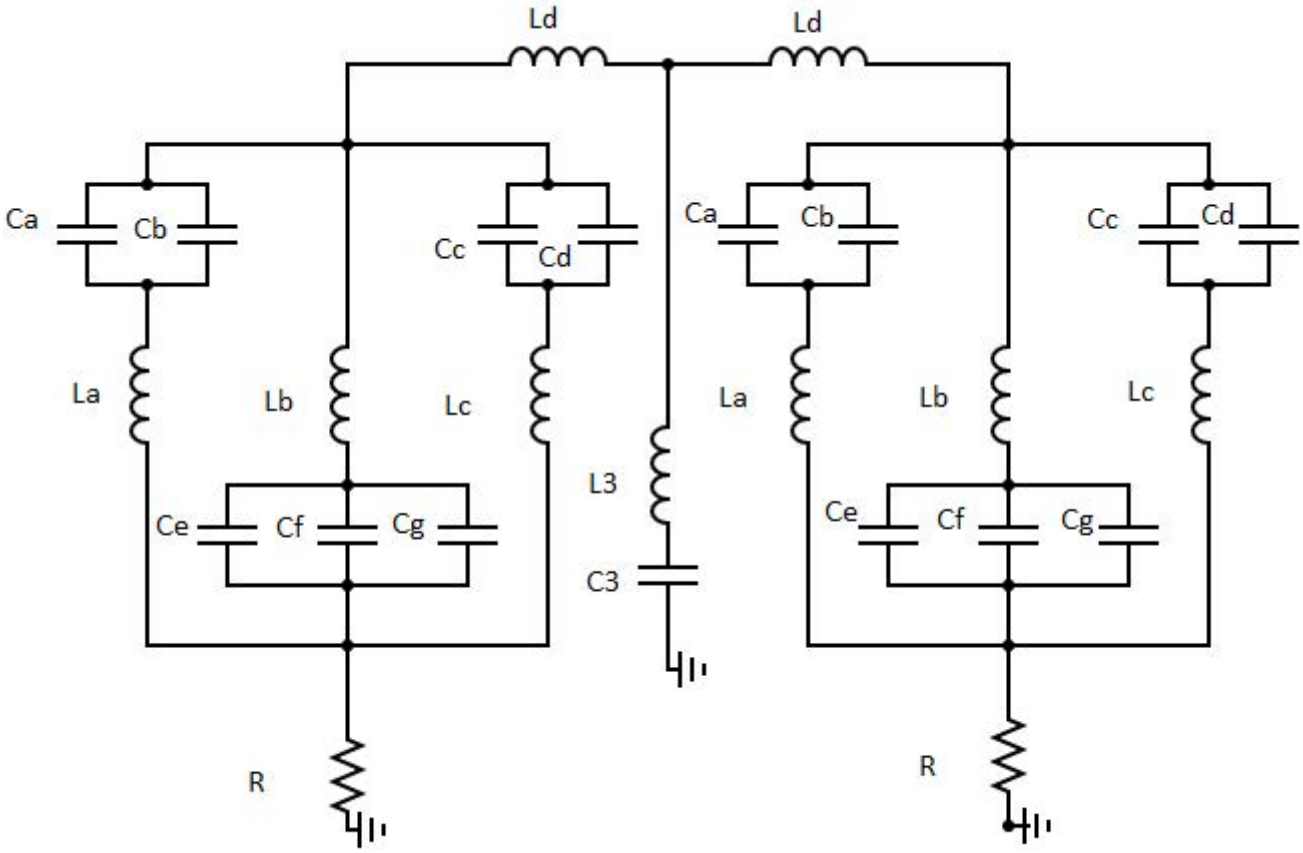
Ld
Ld
Ca
Cb
Cc
Cd
Ca
Cb
Cc
Cd
La
Lb
Lc
La
Lb
Lc
L3
C3
Ce
Cf
Cg
Ce
Cf
Cg
R
R

(a)

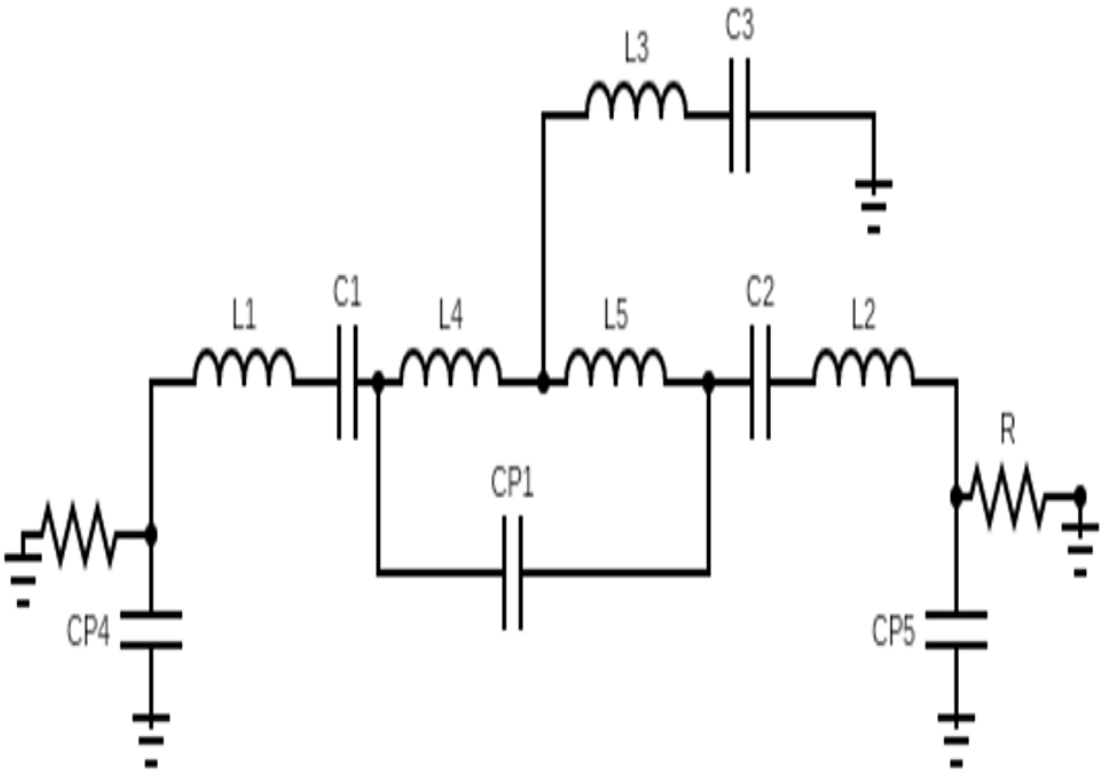


(b)

**Fig-3.10:** (a) Circuital model of suggested filter. (b) Equivalent circuit [L1 = L2 = 0.1 nH, L3 = 2.7 nH, L4 =0.1 nH, L5 = 0.1 nH, C1 = C2 = 1.5 pF, C3 = 2 pF, Cp1 =0.95, pF, Cp4 = Cp5 = 0.2 pF.

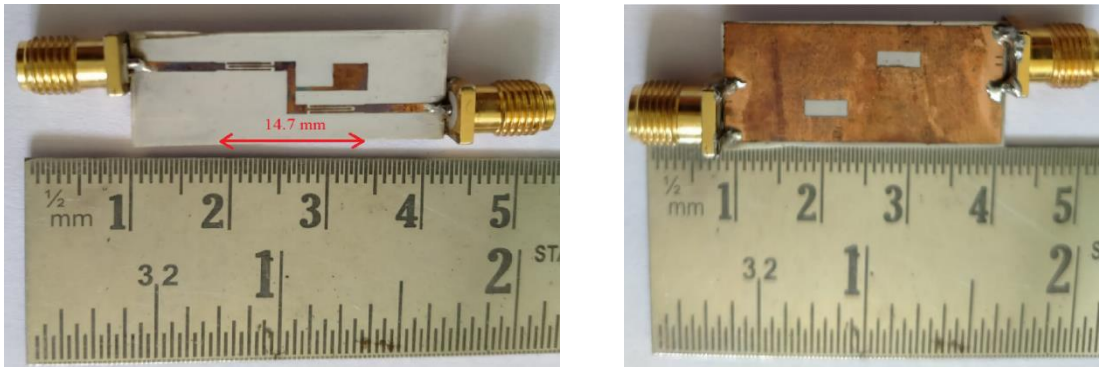


(a) (b)

**Fig-3.11:** Suggested filter photo (a) Top view (b) Bottom view.

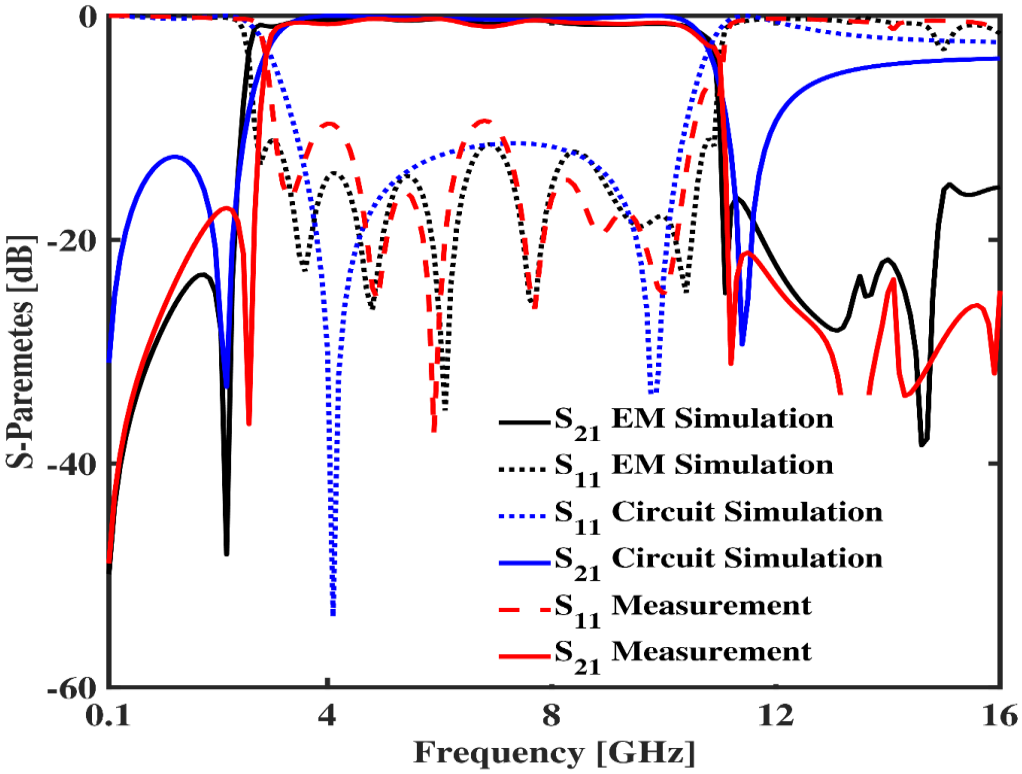


**Fig-3.12:** S-Parameters Comparisons of EM Simulation, Circuit Simulation and Measured Result.

## 3.6. Summary:

This chapter described a unique MMR based UWB-BPF. The UWB filter basically made up of MMR on upper layer and CSRR on ground plane. Initially the MMR was analyzed based on its equivalent circuit model and its topology was designed in order to position its resonant modes quasi-equally within the bandwidth. The optimized modeling of the MMR topology leads to simultaneous excitation of its resonant modes which in turn generates the requisite passband. Various dimensional parameters of the MMR were varied to study its effect on the UWB passband. Finally, the proposed UWB filter was designed based on its optimized dimensional parameters.

# CHAPTER 4

# DESIGN OF UWB-BPF UTILIZING SILVER NANOWIRES

## 4.1. Introduction:

The flexible UWB-BPF has become a substantial element of RF and microwave circuits, especially since the UWB spectrum spans 3.1 to 10.6 GHz [9,63], was available for commercial communication applications. These filters are often used in transparent smartwatches, vital sign tracking, imaging devices for healthcare, and remote patient tracking equipment. Traditional UWB-BPF are used to improve communication system performance and have critical qualities such as a wide upper stopband, lightweight design, low $S_{21}$, high $S_{11}$, and superior sensitivity. To adapt to a wide range of applications, modern wireless systems require UWB filters that are extremely flexible, transparent, and compatible with a variety of fabrication processes. Several strategies for achieving miniaturization and ultra-wideband features in BPF have been published. A transversal resonator and asymmetrical IDC lines are used to produce a wide passband by applying a transversal signal-interference approach, which results in the formation of a pair of TZ on either side of the passband edges. To enhance the filter's performance even further, two asymmetrical IDC lines are used to drive the transversal resonator, yielding five additional TZ in the lower and upper stopbands. [73], A differential-mode (DM) wideband BPF with adjustable bandwidth is based on a slotline MMR. The BPF made up of two pairs of microstrip feed lines and a cross-shaped slotline MMR engraved on the bottom plane. The linking between DM feed lines and MMR can be regulated by strategically positioning the slotline MMR to achieve the required DM passband. [74], A novel MMR design based on IDC MSL sections and stepped impedance stubs is presented. The suggested MMR structure has seven distinct resonances, which are investigated using a TL model. The

MMR resonances have various modes of operation, providing for a wide range of frequency response characteristics [27]. Four resonant modes from a pair of parallel-coupled lines loaded with EBG structures, are included in the design. The suggested design's combination of resonant modes allows the filter to demonstrate exceptional selectivity while delivering a super wide stopband. The filter achieves wideband performance by combining these resonant modes, allowing for effective signal filtering within the appropriate frequency range while simultaneously offering excellent stopband characteristics [68]. A MMR arrangement is used in the design, which combines an altered SIR with a stepped-impedance open-end stub in a shunt configuration. The open-end stub introduces two TZs, which contribute to increased band edge steepness. To improve coupling strength, external couplings are accomplished utilizing interdigital coupled-lines. [75], and coupling between two MMRs [69] are examples of these techniques. The literature also discusses several ways to design adaptable and small bandpass filters. Examples include the utilization of flexible PerMX polymer substrates [76] and a novel single-layer CPW BPF with exceptional selectivity. To accomplish its distinctive properties, the filter employs interdigital spoof surface plasmon polaritons (SSPP) with bow-tie cells. The independent adjustment of the lower and upper TZ is a remarkable feature of this system. The SSPP of bow-tie cells controls the upper TZ, whereas the IDC structure of the SSPP controls the lower TZ [77, 78] employs inkjet printing technique to create a two-sided flexible device. Furthermore, [79,80] shows how to make filters using spoof surface plasmon polariton lines. [81] creates a hybrid circuit employing an aerosol jet printed pad as well as a surface-mount device utilizing silver nanoparticle-based aerosol jet ink. Longitudinal and four-by-four slot array antennas are proposed in [82] for a flexible SIW-based slot antenna capable of operating at 79 GHz. Compactness in a multilayer open-loop MR is obtained by developing two four-pole, quasi-elliptic microwave BPF using low-loss organic substrate [83]. In [84], a flexible filter for wireless area network applications is built employing a liquid crystal polymer substrate.

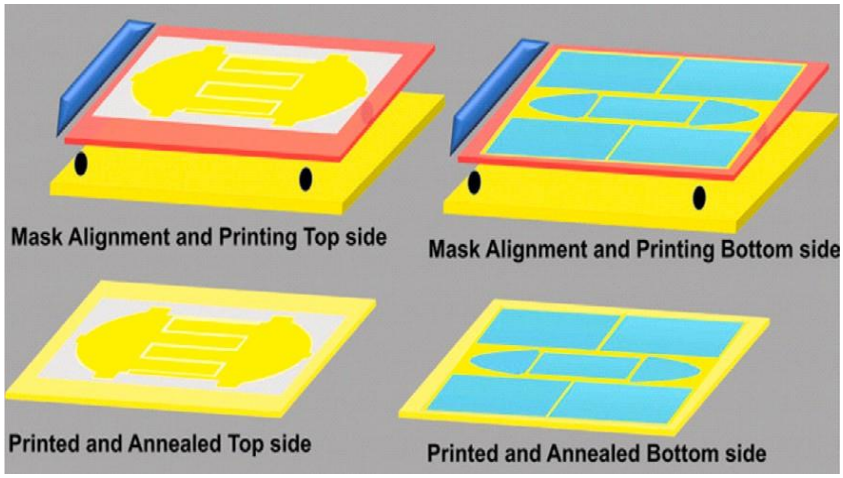


**Fig.4.1:** Steps for screen printed UWB filters on PET substrate.

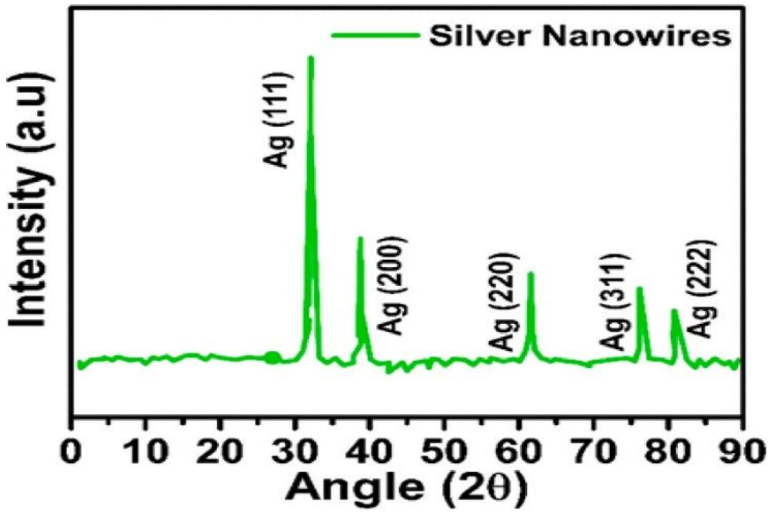


**Fig.4.2.** Silver nanowire X-ray diffraction pattern produced on PET substrates.

## 4.2. UWB filter fabrication utilizing silver nanowire ink:

Screen printing UWB filters on PET substrates with silver nanowire ink was used in the fabrication procedure. The procedure included multiple steps, as illustrated in Fig.4.1. To begin, a pattern mask matching the dimensions of the UWB filter was created. The mask was then precisely positioned on the PET substrate by using camera. The desired UWB filter design was then screen printed onto the patterned mask using silver nanowire ink. Few modifications were made to the preparation of silver nanowire ink mentioned in

previously published papers [85]. The printed design was then annealed for 10 minutes on a hot plate at 80°C. The substrate was subsequently flipped, and a bottom mask was precisely positioned utilizing cameras. The bottom pattern of the UWB filter has been printed with silver nanowire ink and then annealed.

## 4.3. Characterization of silver nanowire ink:

The application of silver nanowires in radio frequency circuit design on PET substrates was investigated, as well as their important attributes such as sheet resistance, conductivity, and transmittance. To ensure the existence of silver nanowires, X-ray diffraction (XRD) investigation was carried out. The XRD pattern in Fig.4.2 shows unique peaks at different diffraction angles, especially (111), (200), (220), (311), and (222). These peaks were contrasted. to the JCPDS file:04-0783, demonstrating that silver nanowires were successfully deposited on the PET substrate. The existence of silver nanowires present on the PET substrate is demonstrated by the well-matched XRD peaks.

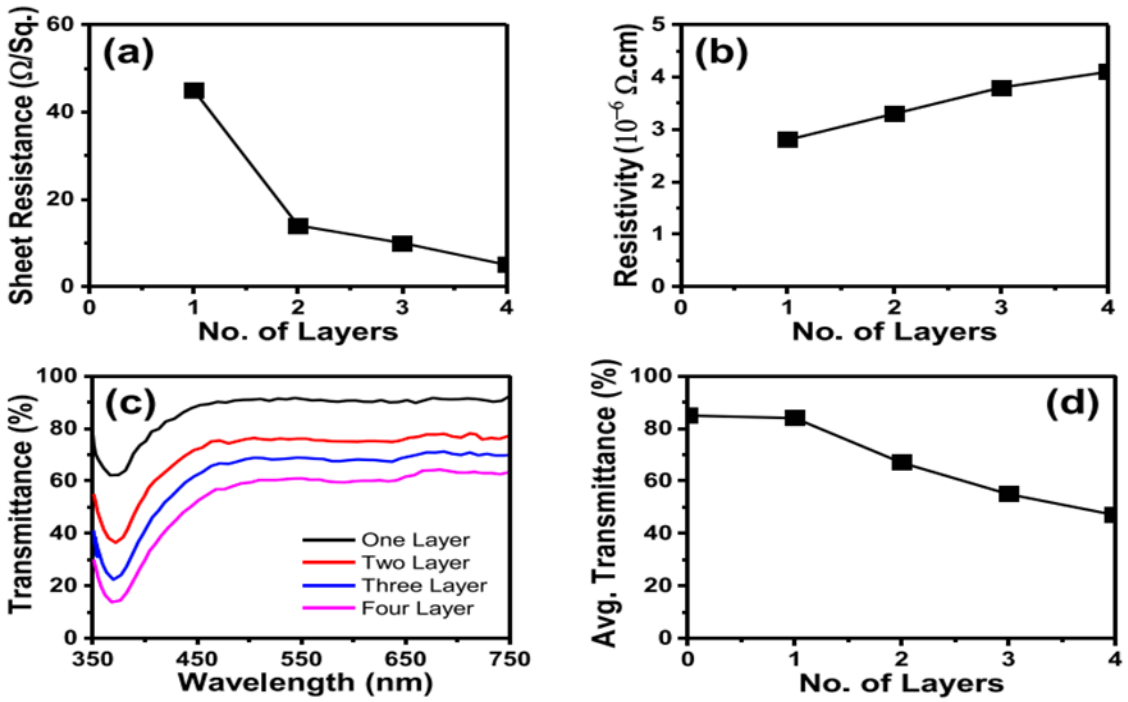


**Fig.4.**3. (a) Sheet resistance as the layer count increases, (b) Resistivity as the layer count increases, (c) Transmittance across wavelength range of 350 to 750 nm. (d) Average transmittance as the layer count increases

when displayed in Fig. 4.3(a), the sheet resistance steadily reduces from 45 Ω/Sq to 5 Ω/Sq. when the layer count increases from 1 to 4. As shown in Fig. 4.3(b), the resistivity of silver nanowire films fluctuates between (2.8-4.1) $10^{-6}$ Ω cm as the layer count increases from 1 to 4. Furthermore, for wavelengths spanning from 350 to 750 nm, Fig. 4.3(c) shows that the transmittance falls as the layer count increase from 1 to 4. Finally, Fig. 4.3(d) exhibits the average transmittance, which shows a linear fall as the layer count increases, possibly due to increased silver nanowire thickness.

## 4.4. Filter Configuration & working mechanism:

Figures 4.4(a) and 4.4(b) display the structure of the suggested UWB-BPF. It's constructed from three pairs of interdigital coupled (IDC) open-circuited rectangular stubs, put together on a flexible polyethylene terephthalate (PET) substrate with a height of 0.114 mm, relative permittivity $\varepsilon_r$ =3, and a loss tangent tanδ = 0.002. The width of the silver nanowire layer is 514 nm. The parameters of the suggested structure are as follows:

**Table 4.1:** Dimensions (in mm) marked in 4(a) and 4 (b)

| Parameters | Size | Parameters | Size | Parameters | Size |
|---|---|---|---|---|---|
| $L_1$ | 5.8 | $W_4$ | 0.2 | $W_8$ | 0.5 |
| $W_1$ | 1.15 | $L_5$ | 0.6 | W | 20.0 |
| $L_2$ | 0.5 | $W_5$ | 0.1 | S1 | 0.1 |
| $W_2$ | 0.3 | $L_6$ | 7.65 | S2 | 0.2 |
| $L_3$ | 1.5 | $W_6$ | 6.7 | t1 | 0.3 |
| $W_3$ | 0.5 | L | 16.2 | | |
| $L_4$ | 2.75 | W7 | 4.0 | | |

The interdigital capacitance is generated by three pairs of IDC arms. The wave cancellation method was used in the design. The IDC structure and the defective ground structure, respectively, tune the lower and upper TZ. The simulated data is seen in Figure 4.5.

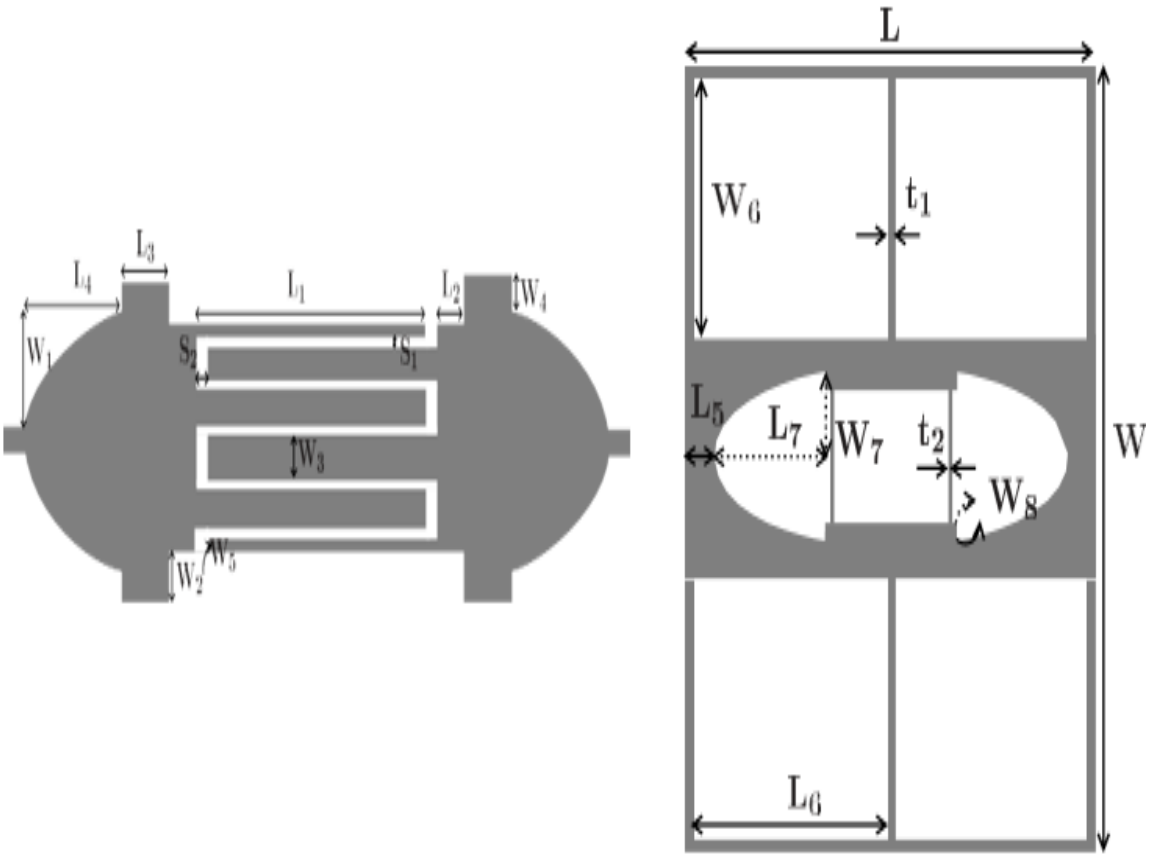


(a) (b)

**Fig.4.4.** The suggested filter's geometry is shown in (a) Top plane (b) Bottom plane.

According to the simulated data in Fig. 4.5, the suggested UWB filter design achieves a 3 dB passband of 9.7 GHz, covering the spectrum of 1.05 to 10.75 GHz. Throughout the whole 3 dB passband, the insertion loss remains lower than 1.6 dB. The simulation shows that combining three pairs arm of IDC structures with a DGS, not only assures good transmission efficiency in the UWB, but it also allows for extended stopband performance.

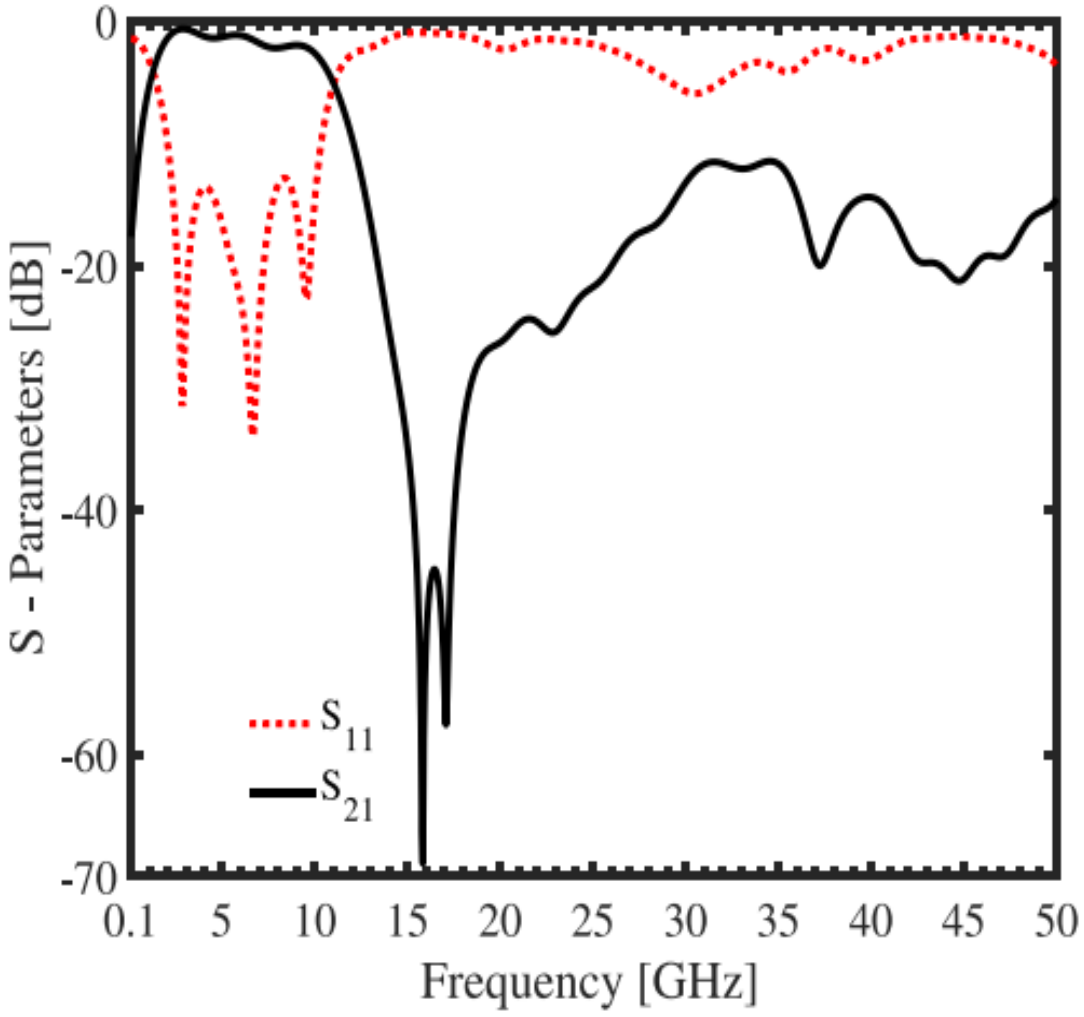


**Fig.4.5.** S-parameter simulations of the suggested design

## 4.5. Interdigital coupling (IDC) structure analysis:

Increasing the IDC arm pairs enhances filtering effectiveness, resulting in lower insertion loss $S_{21}$ within the BW, as shown in Figs. 4.6(a) and 6(b). However, by varying the count of arm pairs in the IDC Lines. The simulation results show that using of interdigital structures allows good transmission efficiency across the full passband while preserving the appropriate filtering performance. The lower TZ is tuned independently by the IDC arm length, which ranges from L1 = 5.8 to 3.5 mm as shown in Figs. 6(c) and 6(d), on the other hand, the upper TZ is tuned by DGS, length ranging from W6 = 6.7 to 5.2 mm, as displayed in Figs. 4.6(e) and 6(f).

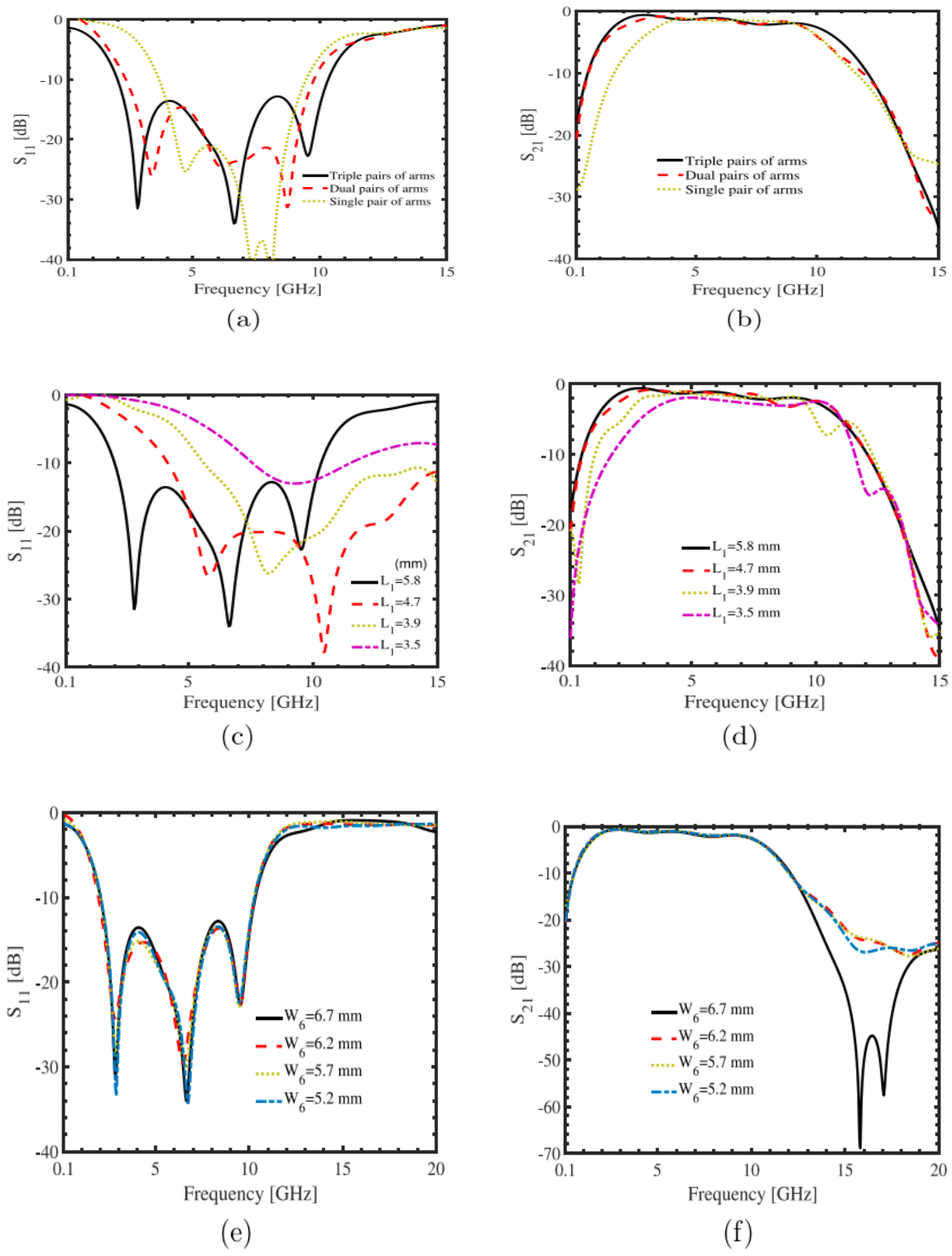


**Fig.4.6.** **(**a) S11, (b) S21 by varying IDC arms count, **(**c) S11, (d) S21 by varying IDC arm length $L_1$ (e) S11, (f) S21 by varying of DGS length $W_6$ (e) $S_{11}$, (f) $S_{21}$.

It's worth noting that changes to one TZ have little effect on the other, allowing for independent control and optimization of the two TZ.

The suggested UWB BPF was simulated using CST Microwave Studio software. The interdigital structural parameters of the filter were set to L1 = 6.4 mm, S1 = 0.1 mm, and W5 = 0.1 mm, with the arm width equal to the gap width (W5 = S1). The interdigital coupled (IDC) circuit are presented in Figs. 4.7(a) and (b), illustrating the setup depicted in Fig. 4.4(a). Capacitances Cij represent the capacitive coupling between the fingers, where i and j denote the finger counts. In this case, neglecting inductive coupling is justified. The equivalent circuit's circuit parameters were calculated using the Advanced Design System (ADS).

The interdigital coupling structure of the circuit produces a capacitance that can adjust the flexible bandpass filter's lower TZ. Using the method outlined in [72], the capacitance C of the IDC structure can be determined.

The observed center frequency of the manufactured device is 5.90 GHz, as shown in Fig. 4.8, with a 3-dB BW covering the spectrum from 1.20 to 10.65 GHz, corresponding to 160% FBW.

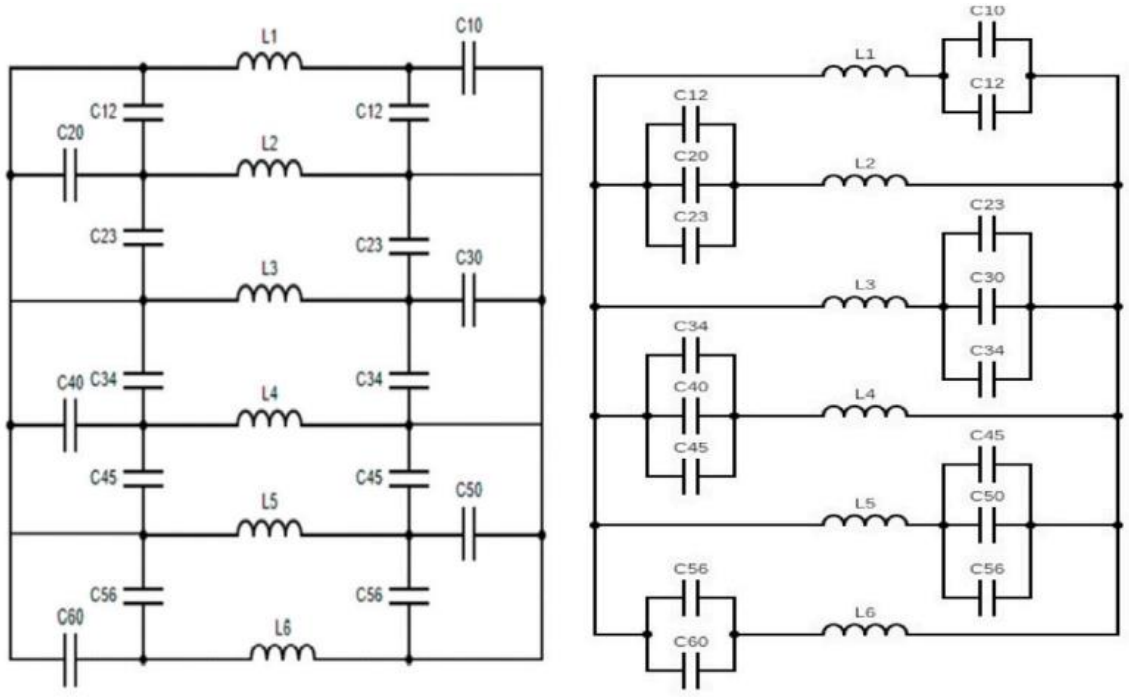


(a)

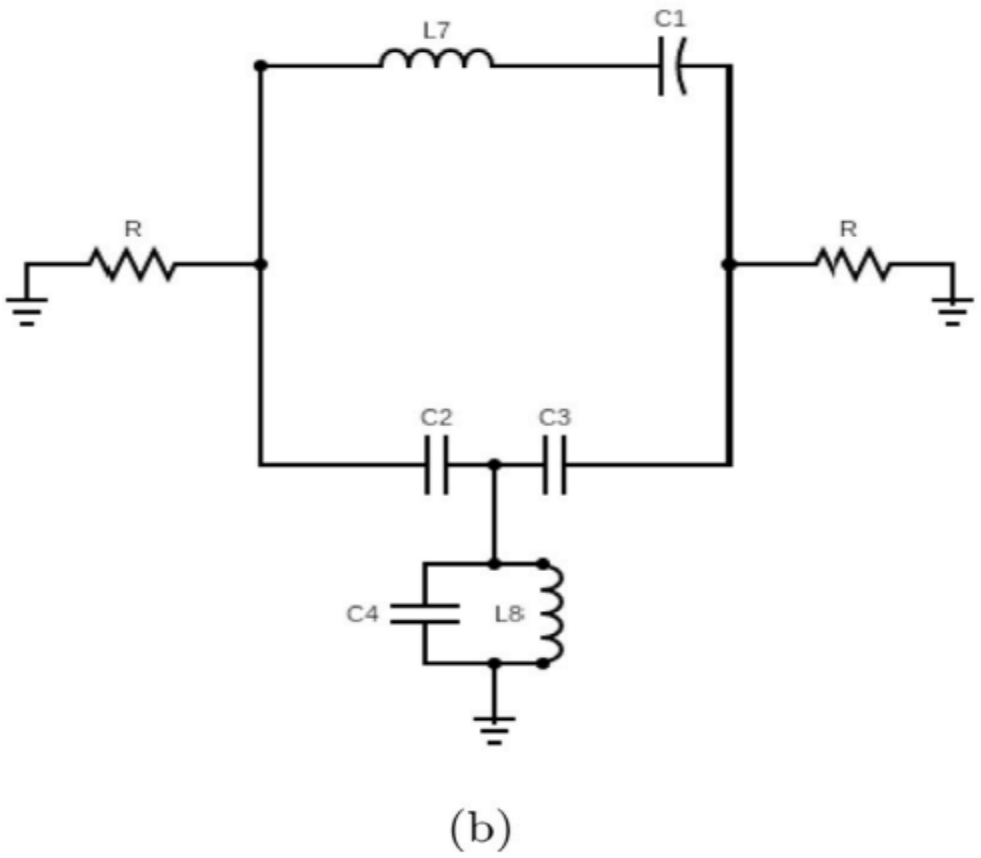


**Fig.4.7.** (a) Circuital model (b) Lumped equivalent circuit model of an IDC structure [$L_7$ = 1.81 nH, $L_8$ = 0.15 nH, $C_1$ = 1.1 pF, $C_2$ = 0.22 pF, $C_3$= 0.22 pF, $C_4$ = 1.05 pF].

## 4.6. Measurements and testing:

The manufactured device has high selectivity, indicating that it has outstanding filtering capability. Furthermore, an extended upper stopband up to 50 GHz may be detected, emphasizing the device's broad frequency range of operation.

The manufactured device's measured center frequency is 5.90 GHz, with a 3-dB BW spanning from 1.20 to 10.65 GHz, representing a FBW of 160%. The insertion loss ($S_{21}$) is lower than 1.60 dB. Moreover, the manufactured device has excellent selectivity and a 50 GHz upper stopband is observed.

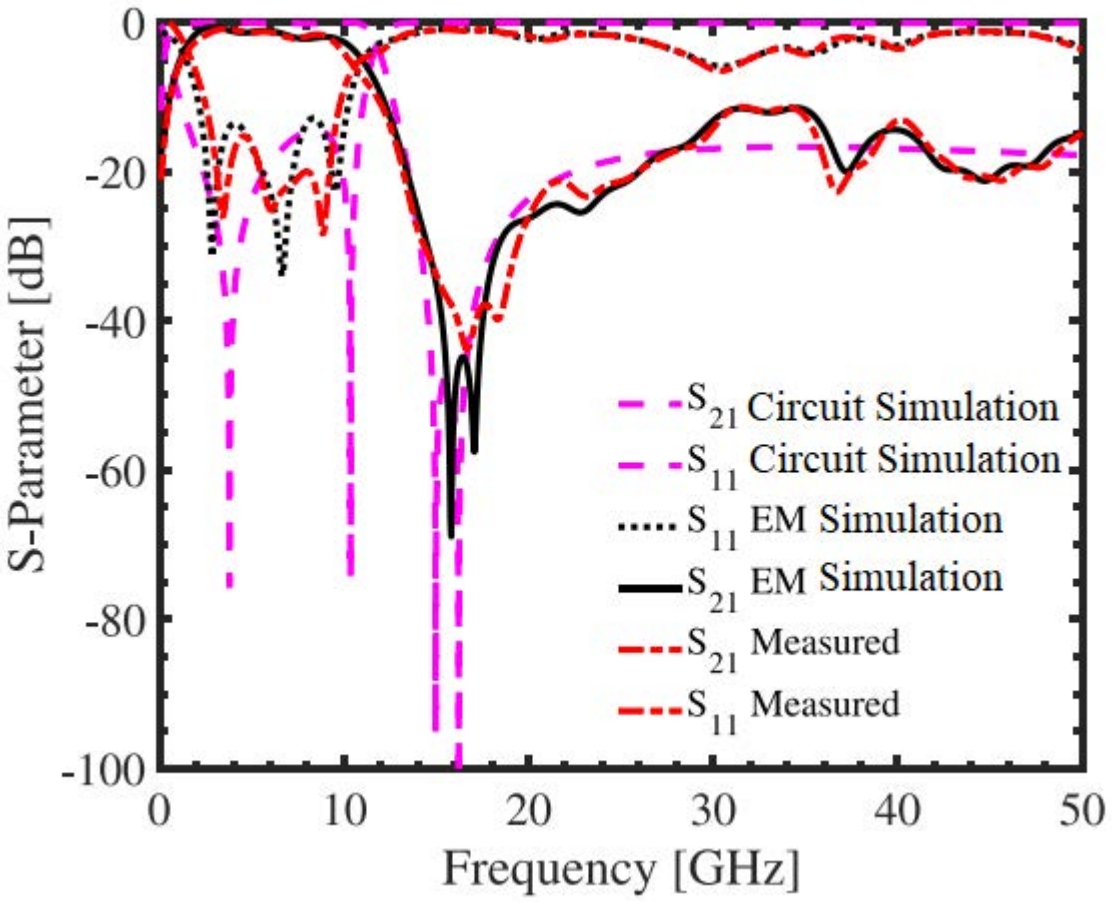


**Fig.4.8.** The Equivalent Circuit, EM simulation and observed S-Parameter responses.

Figure 4.9 shows photos of the UWB-BPF in various states, including bent and folded forms. Figures 4.10(a) and 4.10(b) display the bandpass filter's measured results in the flat, bending, and folded states.


**Fig.4.9.** The proposed designs are (a) flat, (b) bent, and (c) folded.

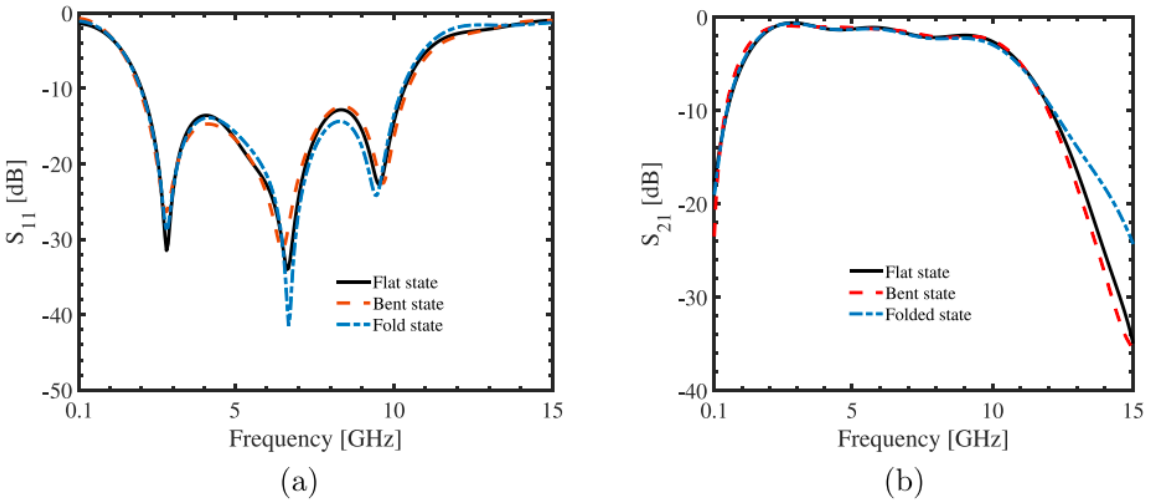


**Fig.4.10. (a)**$S_{11}$ and (b)$S_{21}$ of the suggested UWB-BPF in flat, bending, and folded states.

The reflection coefficient $S_{11}$ is less than -11 dB in all states. Table 4.2 provides a detailed comparison of the measured data for the UWB-BPF in these three states. In particular, the observed results in the bent and folded states nearly match those in the flat state, indicating that the suggested design is effective for transparent and flexible device applications.

**Table.4.2:** Data comparisons in flat bent and folded state

| **Device state** | **$f_L$ (GHz)** | **$f_H$ (GHz)** | **S21(dB)** |
|---|---|---|---|
| Flat state | 1.05 | 10.75 | 1.6 |
| Bent state | 1.0 | 10.8 | 1.6 |
| Folded state | 1.3 | 10.6 | 1.6 |

And Table 4.3 compares the performance of the constructed UWB-BPF to previously reported filters.

**Table.4.3:** Performance comparisons of reported UWB-BPF

| **Ref** | **Filter design** | **Size (λgXλg)** | **BW** | **IL (dB)** | **Upper stop band (GHz)** | **Transparency** | **Flexibility** |
|---|---|---|---|---|---|---|---|
| [77] | CPW and interdigital structure with bow-tie cells | 0.92 × 2.92 | 2.14–4.95 | 0.8–1.4 | 6–8 | No | Yes |
| [79] | Substrate integrated plasmonic waveguide | 0.91 × 3.4 | 7.5–13 | 2 | NA | No | No |
| [80] | Quasi-spoof surface plasmon polaritons | 0.71 × 1.58 | 8.8–17 | 1.3 | 30 | No | No |
| Proposed work | Interdigital structure with modified DGS | 0.79 × 0.64 | 1.05–10.75 | 1.6 | 50 | yes | Yes |

# CHAPTER 5

# DUAL NOTCHED UWB-BPF

## 5.1. Introduction:

UWB radio technology is extensively utilized for indoor short-range communications. However, due to the availability of many radio signals such as WLAN, X band, etc., these signals interact with the UWB system, causing interferences. Researchers developed multiband BSF to avoid such scenarios. However, increasing the circuit size by adding the BSF to the current UWB-BPF weakens the structure's compactness, which is undesirable. Several strategies for developing UWB-BPFs have been proposed. One extensively used strategy for UWB filter design is the integration of MMRs, which was initially introduced in [86-87].

In particular, folded triple-mode resonators have been employed to create dual-notched band UWB-BPFs [88]. Additionally, UWB-BPFs based on broadside-coupled [89], ring resonators [90], step impedance stub-loaded resonators [91], slotline structures [92] and open-circuited stub [47] have also been investigated.

The proposed design is unique compared to previous studies. Unlike other designs incorporating multiband bandstop filters, which resulted in larger circuit sizes, this design integrates the band stop filter within the bandpass filter. Previous designs also had issues such as a lack of proper TZs, complex geometries, and large sizes. The proposed design eliminates these issues and provides a compact and efficient solution. Using the method of moment-based IE3D, full-wave EM software, the filter was developed and optimized for a Roger 6010 substrate. The suggested design was verified to be effective based on the simulated data as displayed in figure 5.2. and observed experimental results. Parametric study of proposed structure is shown in fig.5.3 to fig.5.6

## 5.2. Filter Configuration & Working Mechanism:

Figure 5.1(a) displayed the fundamental structure of the Short-Circuited Coplanar Waveguide (SCCPW). This allowed its resonant modes to be assigned to the Ultra-Wideband (UWB) spectrum. We built MSL on the upper plane, connecting them to the bottom plane using the broadside technique, as illustrated in Figure 5.1(b).

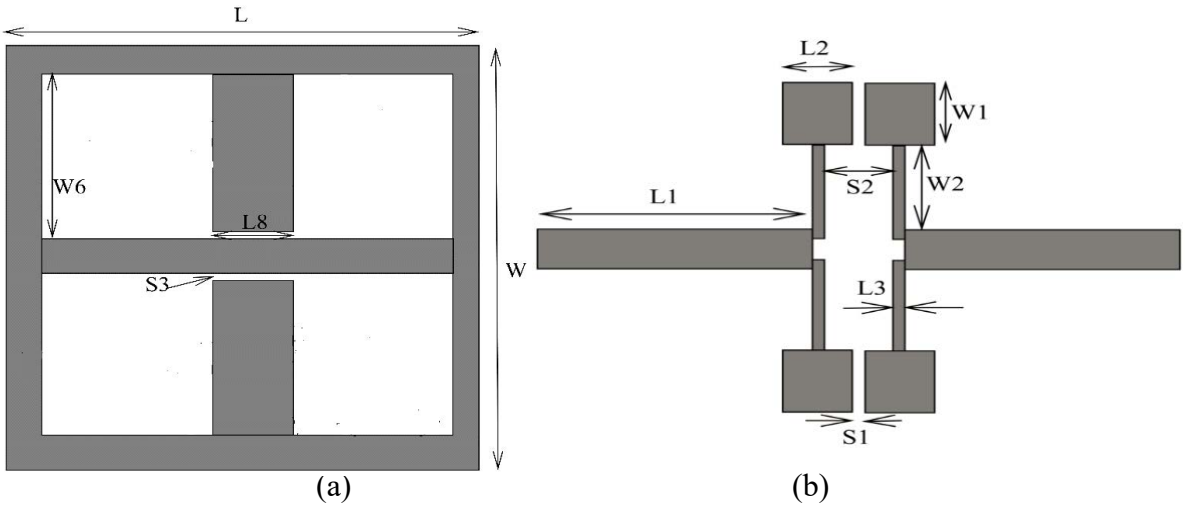


**Fig.5.1:** Fundamental Geometry of suggested UWB-BPF (a) Modified short circuited coplanar waveguide (MSCCPW) (b) Microstrip line on top plane

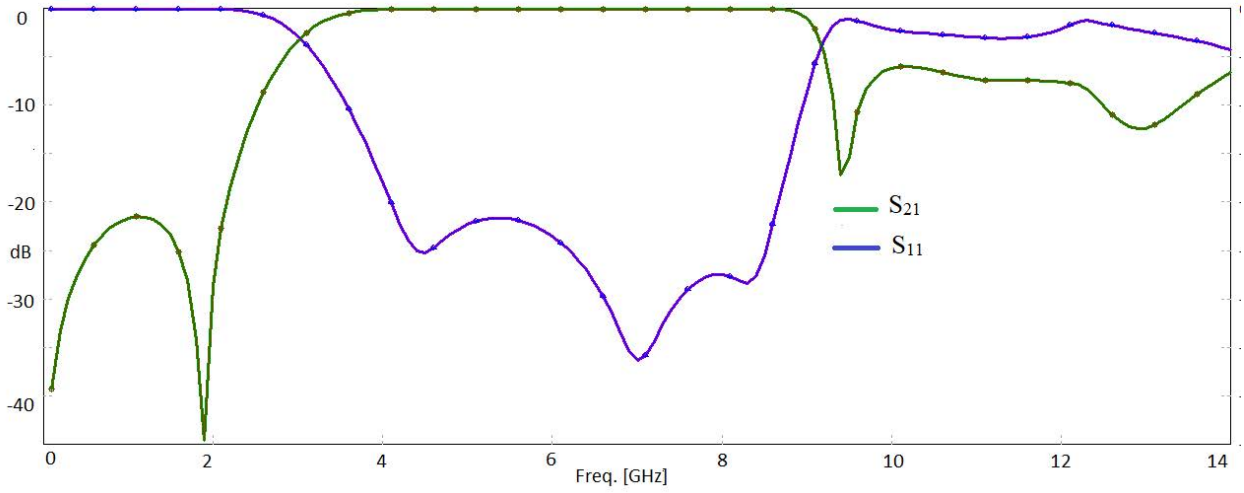


**Fig.5.2:** Simulated S-Parameter response.

The simulated response of the suggested UWB-BPF is seen in Figure 5.2 The existence of two TZs at the lower and upper passband edges, in particular, adds greatly to the outstanding frequency characteristics exhibited in the fundamental BPF response.

The first notch is created by incorporating a step impedance stub into the bottom layer, as displayed in Figure 5.3. A specific frequency notch is created by deliberately inserting this stub, giving specific signal filtering and suppression capabilities in the system.

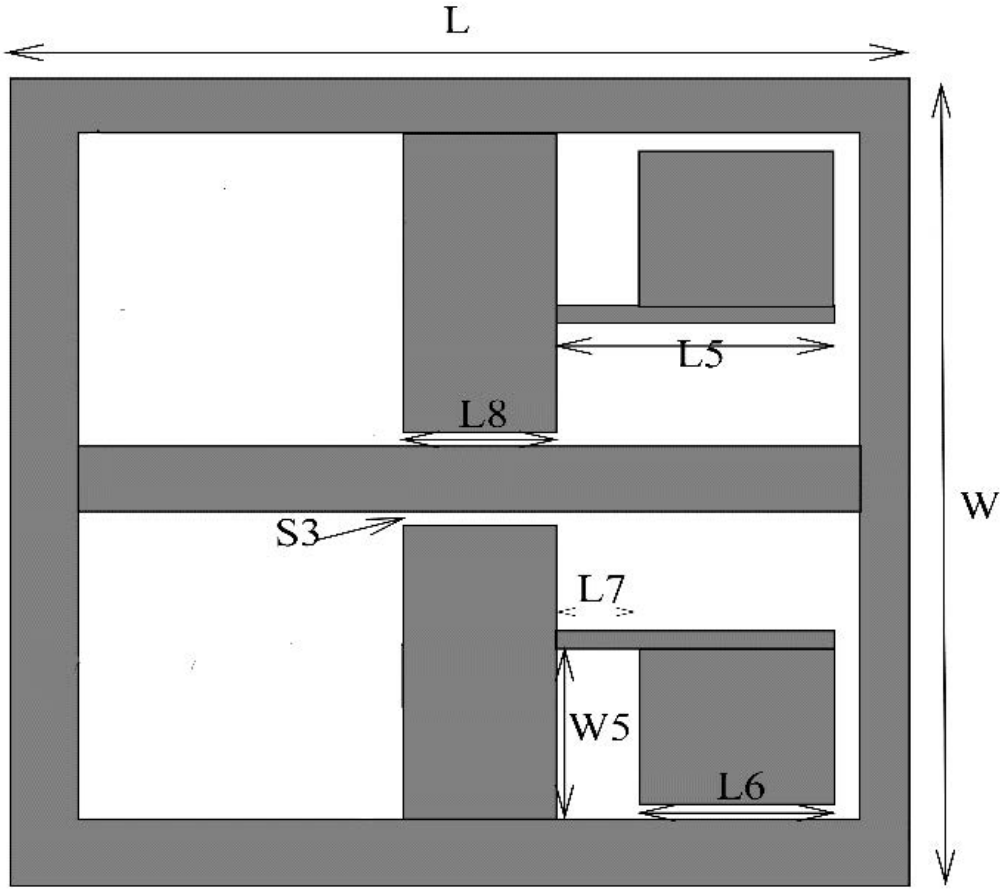


**Fig.5.3:** Bottom plane integrated with step impedance stub

The simulated response of suggested structure is displayed in figure 5.4. To finely adjust the notched frequency, one can manipulate the length of the step impedance stub. This alteration allows for precise control over the frequency at which the notch occurs. As shown in Figure 5.5, a second notch is formed by inserting a stub into the ground plane. This additional stub introduces another frequency notch, improving the system's overall performance and capabilities.

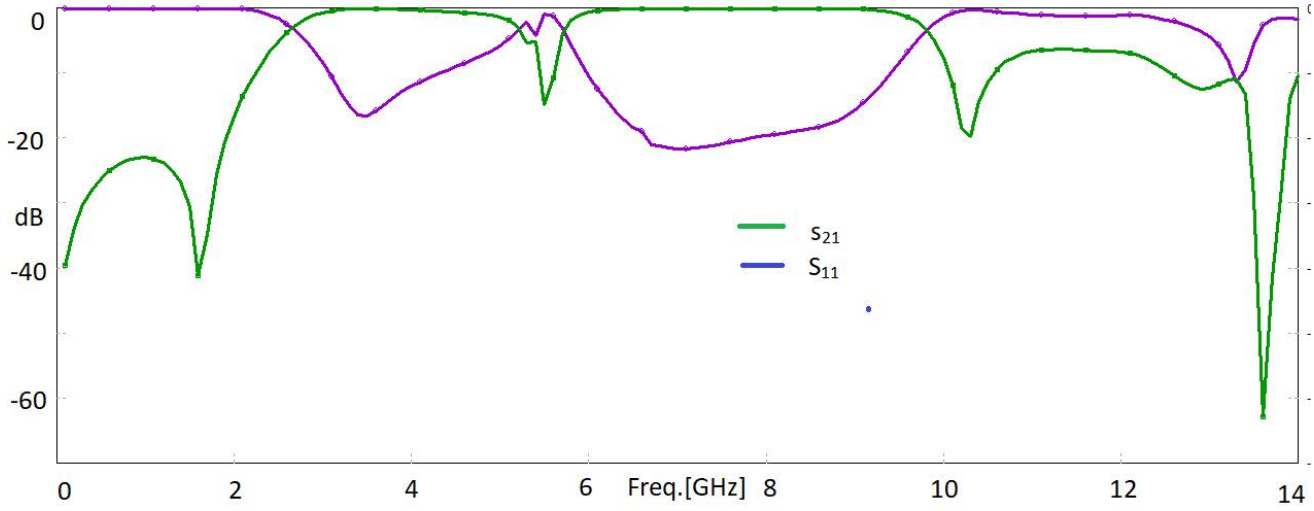


**Fig.5.4:** Simulated S-Parameters response of first notch.

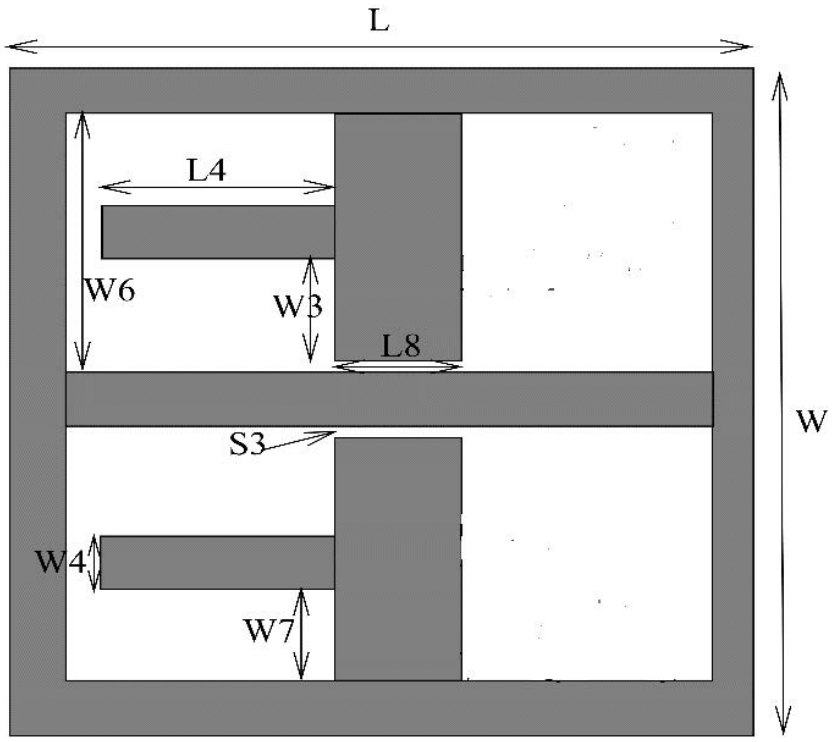


**Fig.5.5:** Suggested geometry integrated with stub in ground plane

The simulated data of suggested structure is displayed in figure 5.6. The dimension of the step impedance stub(SIS) can be modified to obtain exact frequency tuning, allowing us to fine-tune the notched frequency. The simultaneous integration of stub and step impedance stub on the bottom plane results in a dual notched design, as depicted in Figure 5.7 (b)

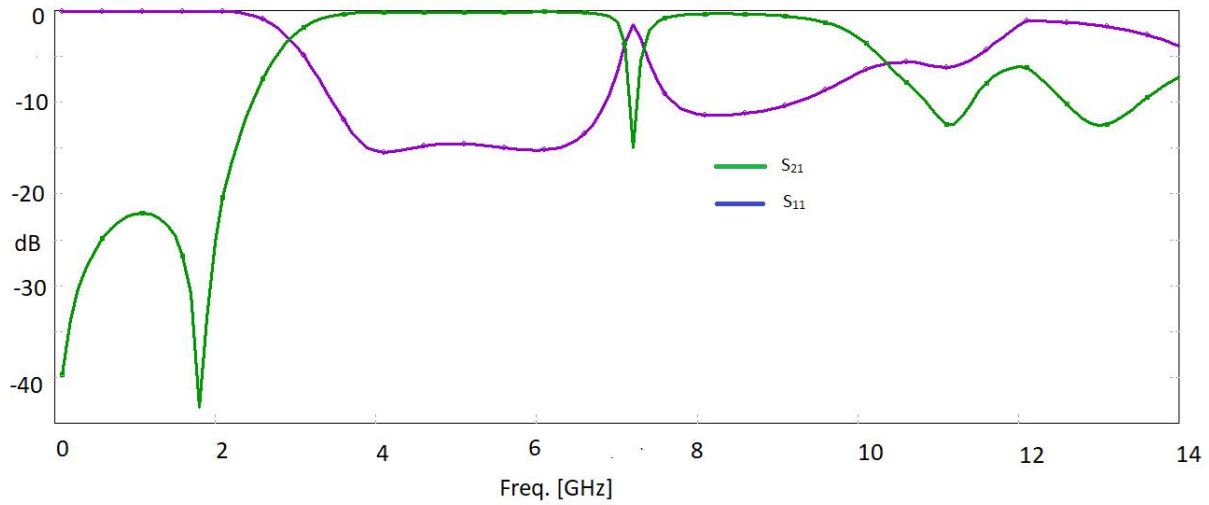


**Fig.5.6:** Simulated S-parameters response of second notch.

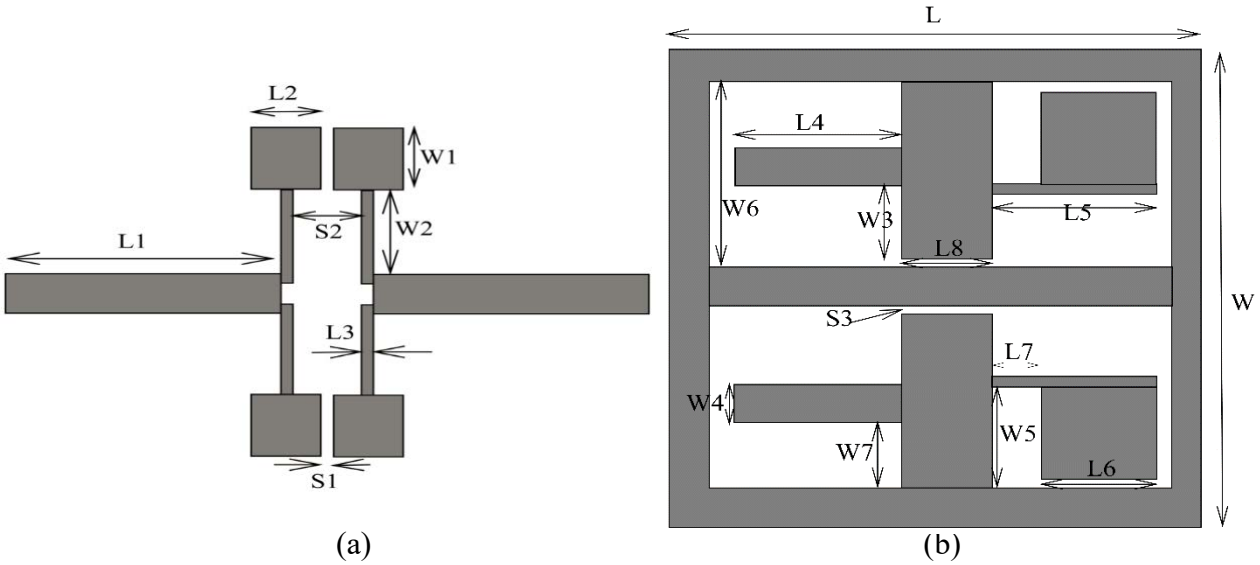


**Fig.5.7:** Final geometry of suggested filter (a) Top plane (b) Bottom plane.

Optimized dimensions (mm), L1=3.9, W1=1.25, L2=0.9, W2=3.05, L3=0.15, W3=1.55, L4=2.45, W4=0.8, L5=3.3 , W5=1.85, L6=2.8, W6=3.95, L7=0.6 , W7=1.25, L8=1.5, L=9, W=9.6 , S1=0.15, S2=0.9, S3=0.35..

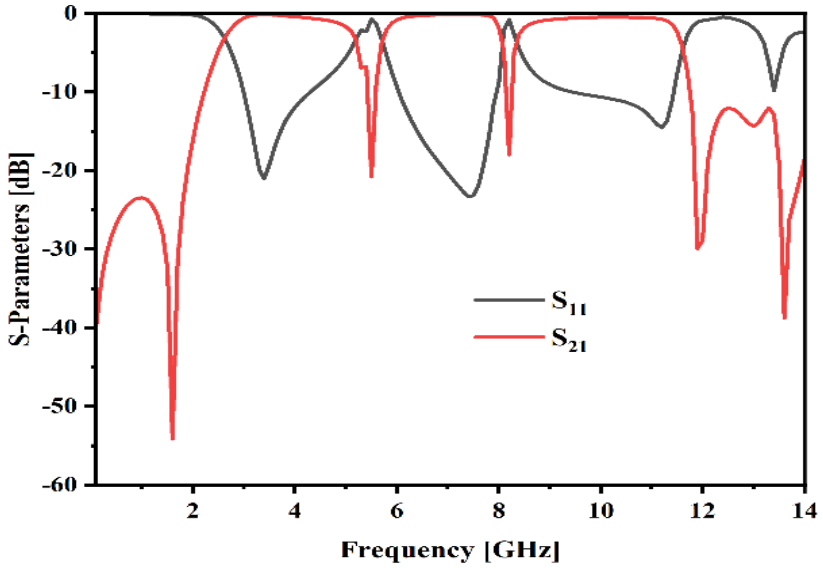


**Fig.5.8:** Simulated s21 and s11 of the suggested filter

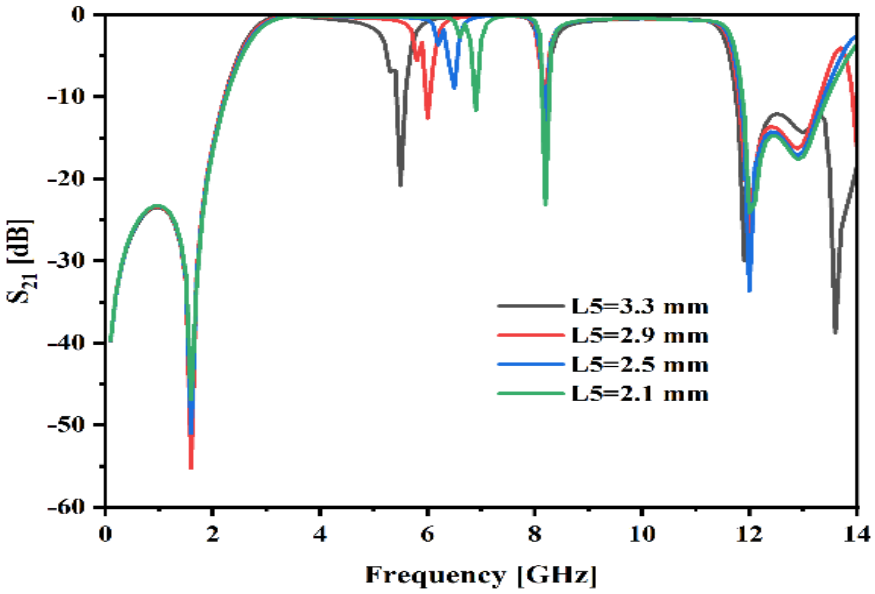


**Fig.5.9**: Parametric study of first-notch $S_{21}$

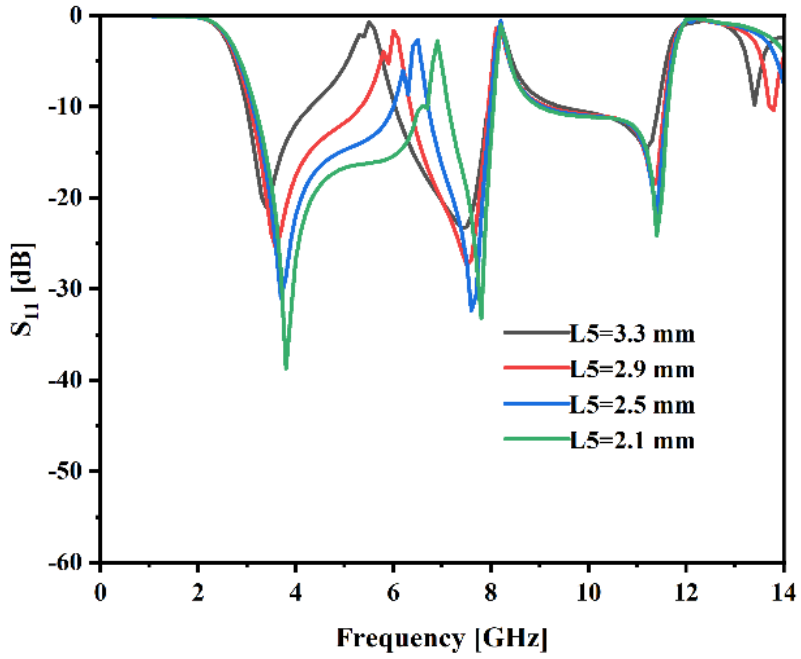


**Fig.5.10:** Parametric study of first-notch $S_{11}$

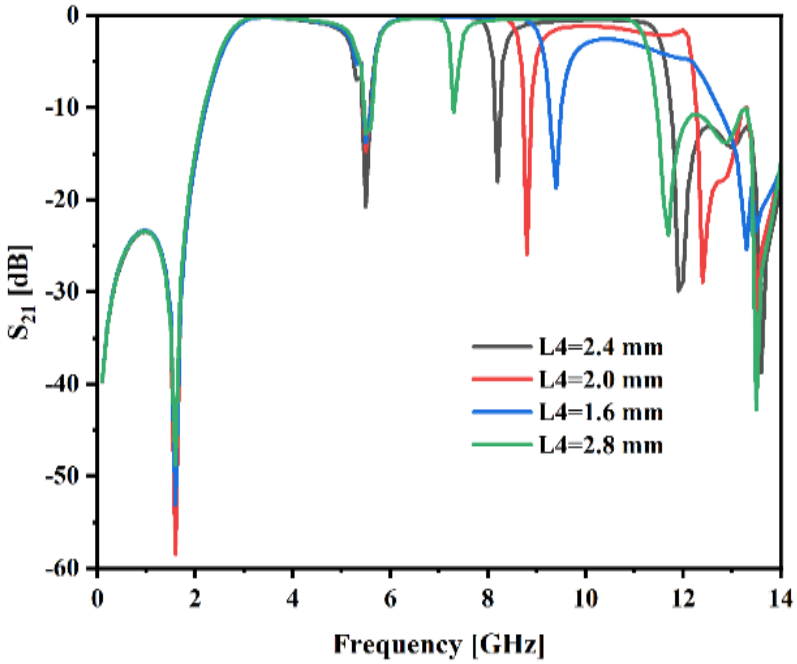


**Fig.5.11:** Parametric study of Second notch $S_{21}$

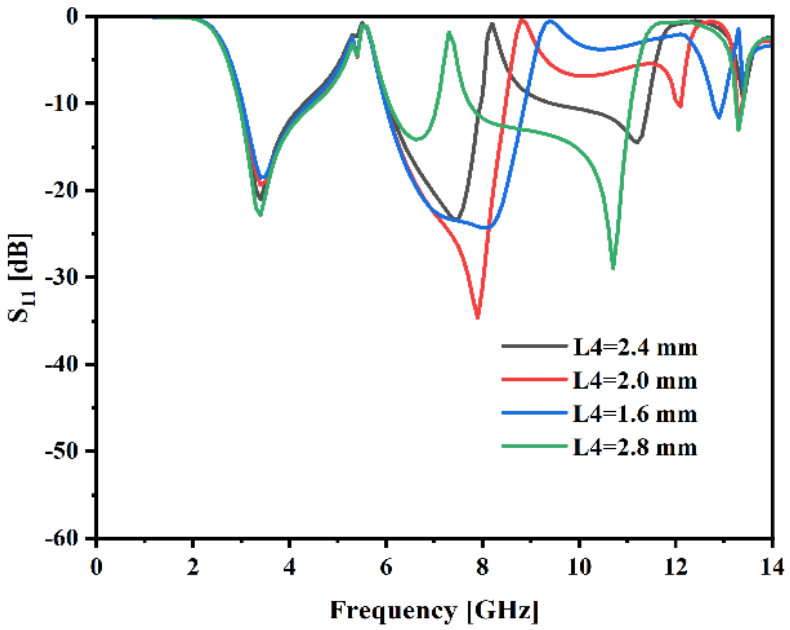


**Fig.5.12:** Parametric study of second-notch $S_{11}$

## 5.3 Measurement of the suggested design:

To verify the frequency characteristics obtained from simulations, in this study prototype of the suggested designed layout is fabricated and subjected it to testing using VNA. Observed frequency characteristics were then contrast to the simulated results. Any discrepancies between the observed simulated data were attributed to factors such as unexpected fabrication tolerances, the finite size of the substrate, reflections from connectors, and other similar factors.

## 5.4. Summary:

This study introduces a compact UWB BPF that features two notches at 5.5 GHz and in 8.2 GHz. The suggested design is based on broadside coupled technology, enabling the creation of a passband with two TZs at the edges, leading in low insertion. Incorporating step impedance stub and simple stub into the ground enables the achievement of dual

notches and an enhanced stopband. The frequency response of the built prototype was observed using VNA, and it validated the simulation results. The proposed UWB-BPF exhibits highly desirable frequency characteristics and compact size, making it a promising component for integrating a wide range of UWB communication systems.

# CHAPTER 6

# TRIPLE-NOTCHED PASSBAND UWB-BPF

## 6.1. Introduction:

The UWB BW, which spans 3.1 to 10.6 GHz, is susceptible to interference from a different type of EM wave sources. These sources can interfere with UWB signals, potentially causing communication and performance concerns. This interference makes it difficult for UWB systems to work optimally. To overcome this issue, researchers created UWB Bandpass Filters (BPFs) with several notched passband features integrated. To introduce triple passband notches, these filters employ several techniques such as DGS [93], wave cancellation [60,94,95], step-loaded resonators [96–97], and other resonators [98–109].

## 6.2. Filter Configuration & working mechanism:

Figure 6.1 shows a triple passband notched UWB-BPF built with broadside linked technique, as described in references [110]. On either side of the substrate, microstrips and SCCPW are used in the design. A pair of circular resonators (CRs) CFSRR is used to generate passband notches. The entire structure is optimized using the IE3D software on an RT/Duroid dielectric 6010.

To begin, simulate SCCPW to discover its resonant modes into the UWB frequency range, the coupling is further optimized using top-plane MSL. Figure 6.2a depict the basic design of the SCCPW and its TL counterpart. The narrow and wide parts of the SCCPW exhibit impedances Z1 and Z2, along with electrical lengths θ1 and θ2, respectively. The input impedance (Zin) of the left end is determined as [25].

The impedance ratio is represented by R = Z1/Z2. When Zin = 0, we have equations that, when solved, Provide the resonant frequencies fa, fb, and fc. For an easier solution, we use R = 1.0 and 1 2, which gives us the middle section lengths of the SCCPW as a1 = 5.24 mm (gCPW1/4), Z1 = Z0(CPW1) = 39, s = 0.4 mm, b1 = 5.56 mm, and θ1 = 39.33°. Similarly,

a2 = 2.46 mm, s = 0.4 mm, and b2 = 6.84 mm, Z2 = Z0(CPW2) = 37.87 correspond to and θ2 = 36.35° for the end segments.

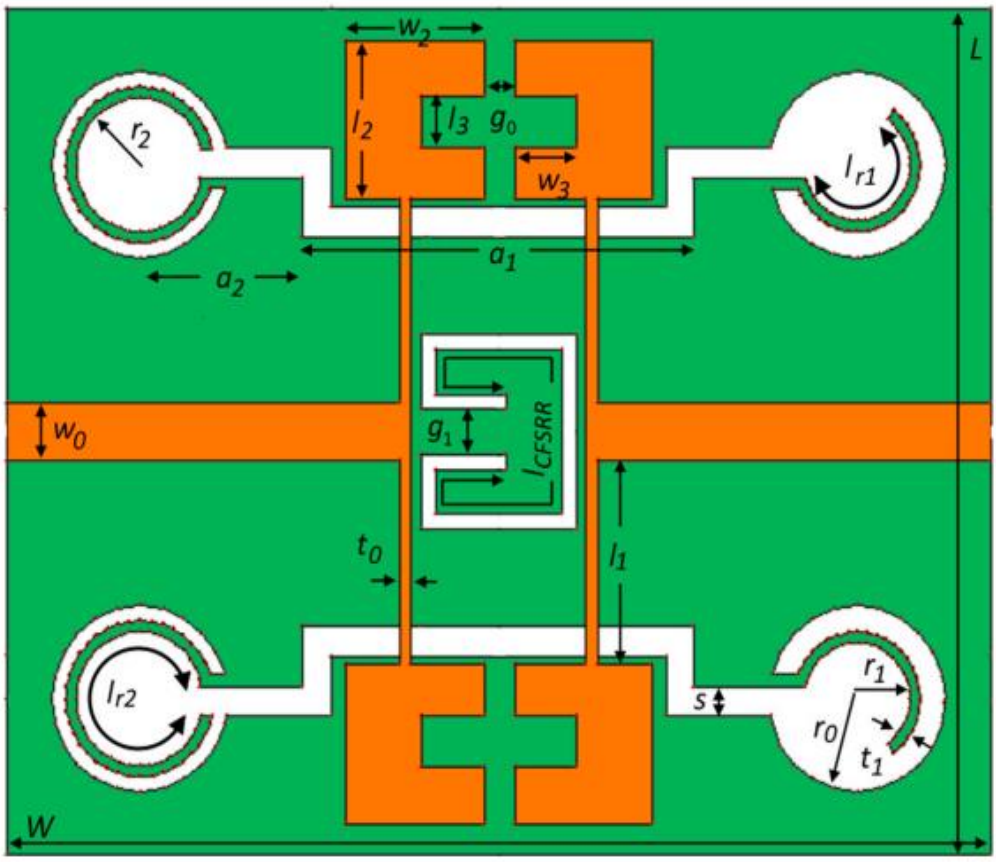


**Fig.6.1:** Suggested triple-notched UWB filter.

Within the UWB band, resonant frequencies of 3.6, 7.15, and 10.74 GHz were identified as the three lowest frequencies to be nearly equidistant from one another. For an easier solution, we choose R = 1.0 and 1 2, which gives us the length and width of the middle portion of the SCCPW as a1 = 5.24 mm (λgCPW1/4), b1 = 5.56 mm, s = 0.4 mm, for which Z1 = Z0(CPW1) = 39 and 1 = 39.33°. likewise, for the ends of the portions, a2 = 2.46 mm, b2 = 6.84 mm, and s = 0.4 mm, resulting to Z2 = Z0(CPW2) = 37.87 and 2 = 36.35°.

Figure 6.2b displays that when the variable impedance ratio (R) is equal to one, the resonant frequencies are completely equally spaced from each other, however, for R 1/R > 1, they

diverge/converge. The SCCPW can be optimized for coupling with MSL. The relationship between each of their characteristic impedances as [21].

$$Z0(\text{microstrip}) = 2Z0(\text{CPW1}) \tag{6.1}$$

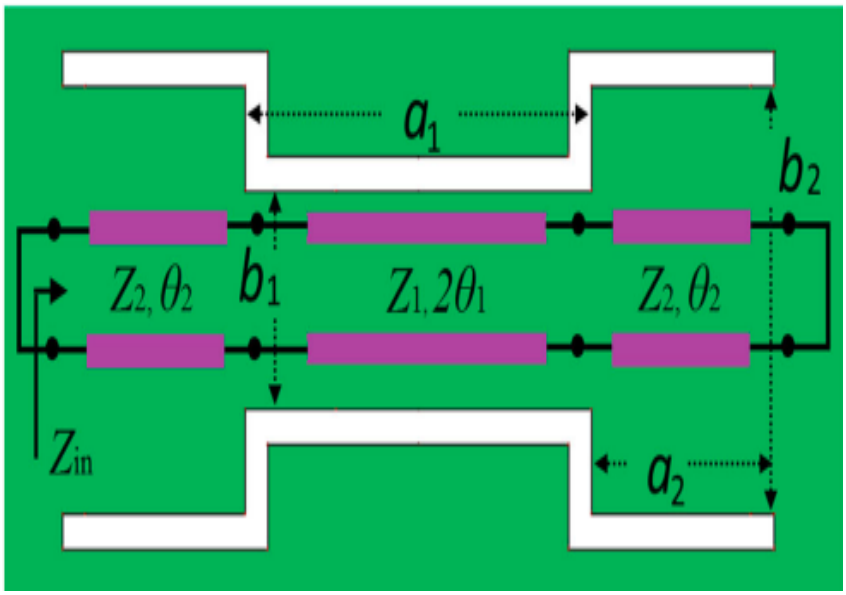


(a)

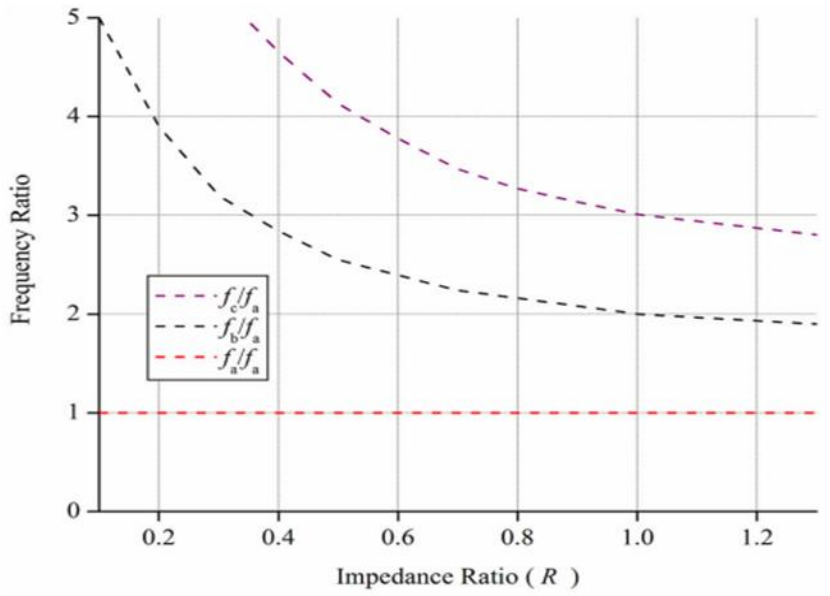


(b)

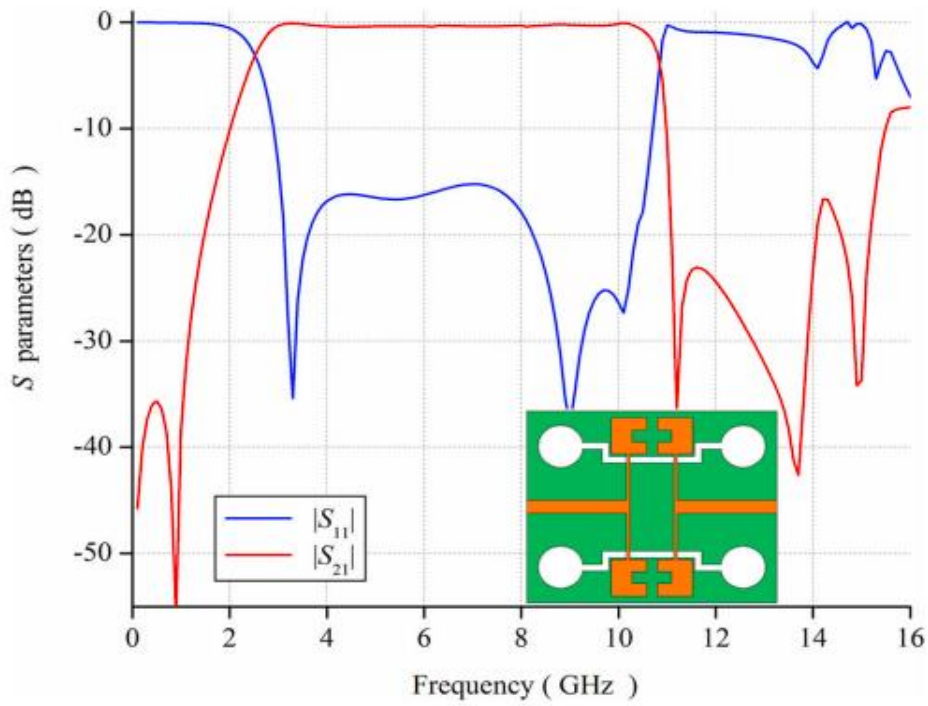


(c)

**Fig.6.2:** (A)SCCPW design incorporating TL network overlay. (B) Normalized frequency variation versus R. (C) The basic UWB-BPF's response has been optimized. BPF stands for band pass filter; SCCPW stands for short-circuited planar waveguide; and UWB stands for ultra wideband.

Subsequently, the slot adjacent to CPW2 is formed into a circle to tune the 3dB cutoff frequency of the suggested filter. As demonstrated in Figure 6.2C, the passband covers 2.53 to 10.76 GHz, with a return/insertion loss of a value below 16 dB and 0.41 dB respectively. The UWB bandwidth indicates TZs at 0.9, 11, 13.8, and 14.5 GHz, in that order.

The existence of a TZ at 0.9 GHz is critical in attaining remarkable attenuation more than 35 dB in the lower stopband. The upper TZs at 11, 13.8, and 14.5 GHz, on the other hand, increase the stopband coverage up to an astonishing 15.5 GHz while maintaining an attenuation level more than 12.5 dB. This multi-TZ arrangement not only guarantees exact frequency control, but also allows the filter to block undesired signal throughout a wide frequency range. Furthermore, there are two TZ at 0.9 and 11 GHz, results in a considerable

roll-off, which aids in maintaining a steep transition, resulting in little signal distortion and interference.

The dimensions with values that have been optimized are as follows: w0 = 0.76 mm, l2 = 2.15 mm, w2 = 1.95 mm, l3 = 0.7 mm, w3 = 0.875 mm, g0 = 0.46 mm, g1 = 0.6 mm, a1 = 5.56 mm, a2 = 3.57 mm, r0 = 1.25 mm, r1 = 0.88 mm, r2 = 1. To prevent interference from in band RF sources, we augment the basic BPF (in the ground plane) with multiple CRs and CFSRR. TZs are produced by the CRs and CFSRR at 5.2, 6.5, and 8 GHz, accordingly to restrict WLAN, C band, and X band. Figure 6.3A depicts the notche's configurable spectrum for various resonator/DGS. The physical dimension of the resonators/DGS and the layout of the notches have a relationship using the formula Eq 6.2 to 6.6:

$$\text{f @5.2 GHz} \approx \frac{C}{(2\pi l_{r2}\sqrt{\varepsilon_{reff2}})} \tag{6.2}$$

$$\text{f @6.5 GHz} \approx \frac{C}{(2l_{CFSRR}\sqrt{\varepsilon_{reff}})} \tag{6.3}$$

$$\text{f @7.9 GHz} \approx \frac{C}{(2\pi l_{r1}\sqrt{\varepsilon_{reff1}})} \tag{6.4}$$

$$l_{r1} = (\pi r_1 + (\pi/3)\, r_1 - s/2) \tag{6.5}$$

$$l_{r2} = (2\pi r_2 - s) \tag{6.6}$$

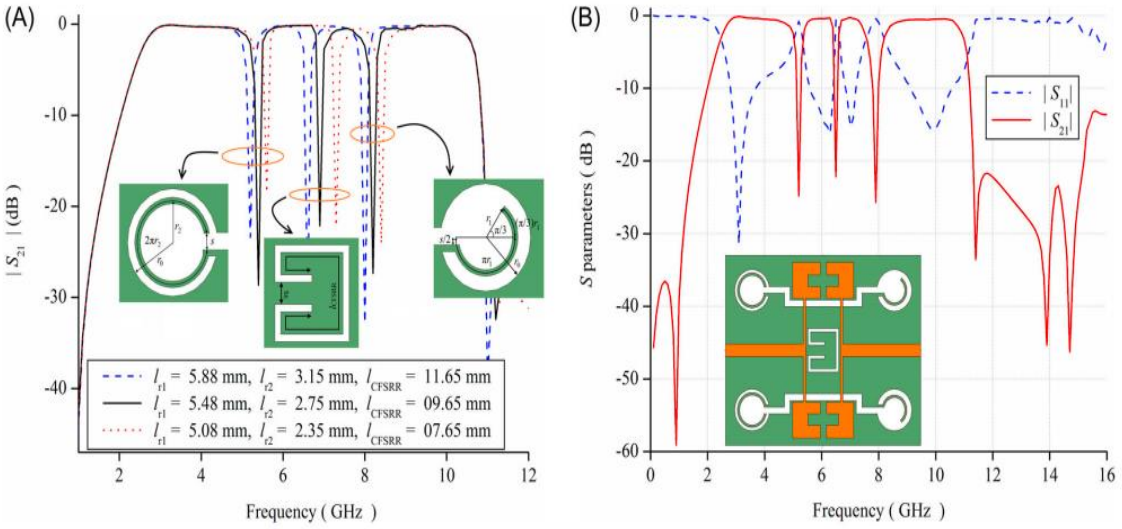


**Fig.6.3:** (A) The length of each of the triple notches gets adjusted to accommodate varied resonator/DGS sizes. (B) Simulated spectrum response of suggested filter.

Figure 3B depicts the optimized performance of the suggested triple notched band UWB-BPF, demonstrating its excellent frequency response. Figure 6.4 depicts the current distribution within the BPF, exhibiting considerable current densities in the CRs, CFSRR, and CRs at 5.2, 6.5, and 7.9 GHz, respectively. This highlights their critical function as the most energetic elements at notched frequencies.

## 6.3. Measurement of the Suggested design:

After fabricating the suggested UWB-BPF layout, experimental testing is performed, and the acquired findings are thoroughly verified and validated against the initial modelling data. Figure 6.5 depicts the observed spectrum characteristics obtained with the Vector Network Analyzer (VNA), verifying the filter's outstanding performance and alignment with the projected results.

(A)

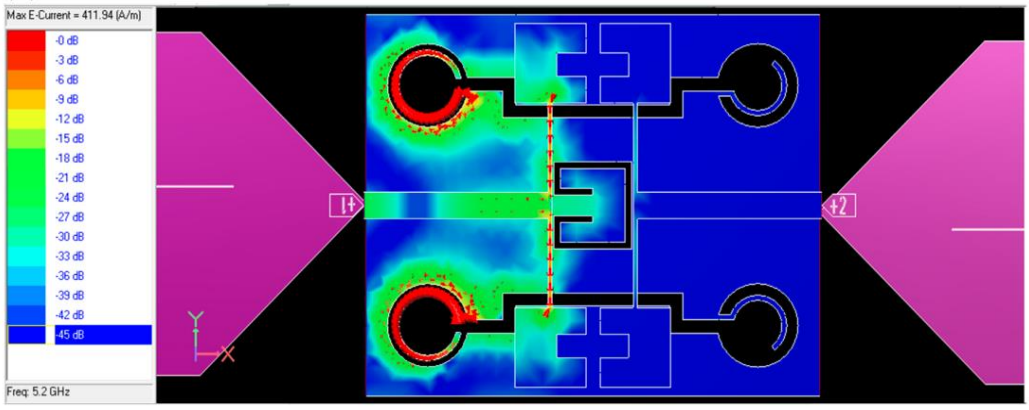


(B)

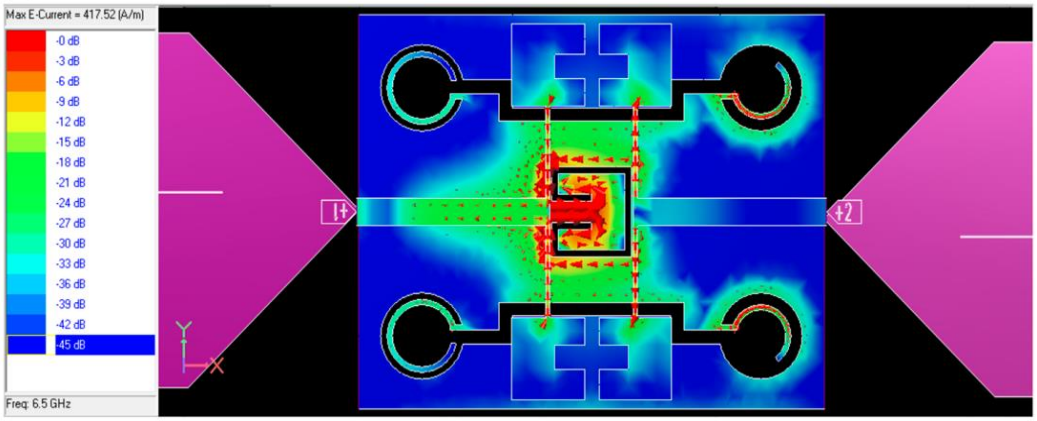

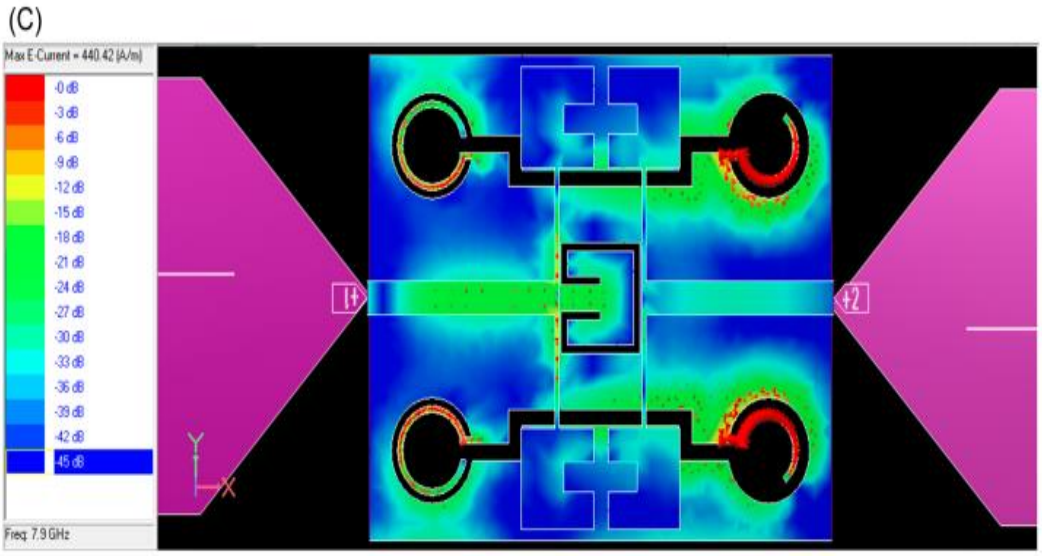


**Fig.6.4:** (A) The distribution of current throughout the BPF at (A) 5.2 GHz, (B) 6.5 GHz, (C) 7.9 GHz.

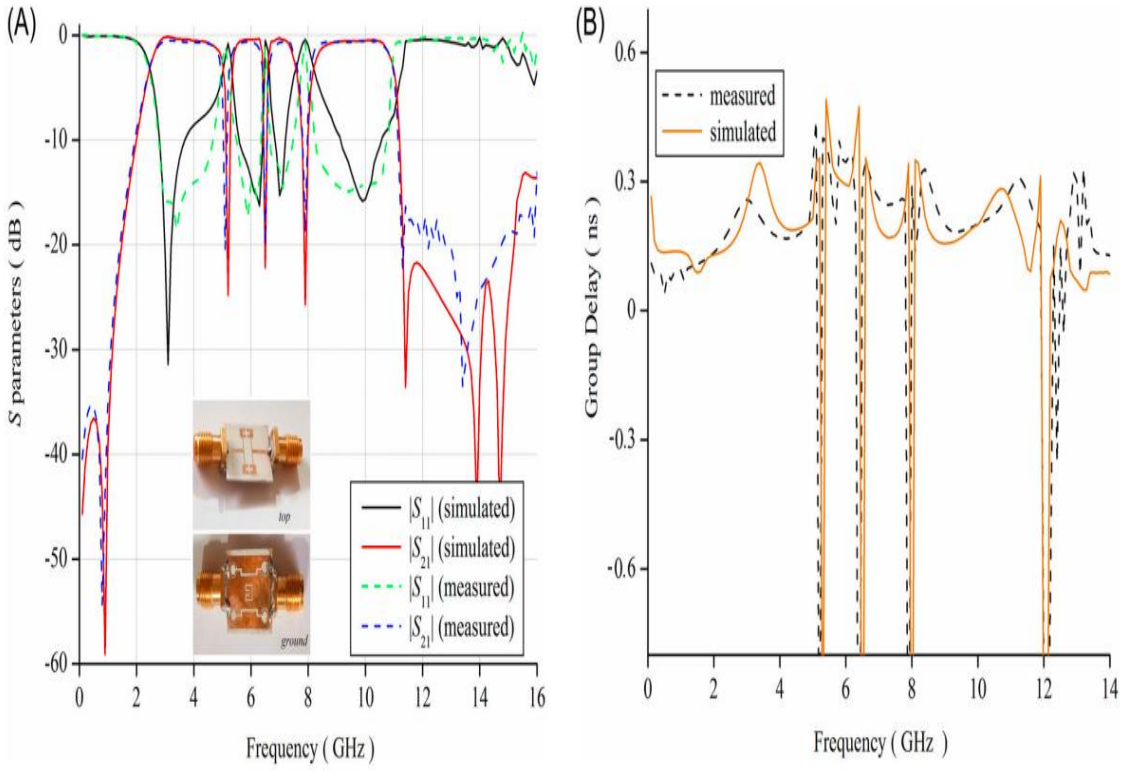


**Fig.6.5:** Observed and simulated frequency frequencies are compared. S parameters (A) and group delay (B).

Figure 6.5A compares the S parameter characteristics, with a recorded passband width of 2.5-10.96 GHz. Significant attenuation over 15 dB is detected in each of the triple TZs operating at frequencies of 5.1, 6.45, and 7.9 GHz. Throughout the passband, the insertion losses maintain consistently low levels, measuring below 0.54 dB before the first notch, 0.44 dB between the first and second notches, and 0.43 dB between the second and third notches. After inserting the 3rd notch, the signal remains robust with a small post-notch insertion loss of 0.52 dB.

Although the attenuation is below 16 dB, the observed stopband is 16 GHz. Apart from the three notches, the observed group delay remains below 0.45 ns across the passband. The difference between what was observed and what the simulation predicted is due to human error during production and measurement. Table 6.1 compares our suggested BPF to those from the literature.

**Table.6.1:** Performance comparisons of reported UWB-BPF

| Reference | Passband (GHz) | Notches (GHz)/ attenuation (dB) | Electrical size (λg × λg) | Physical size (mm × mm) | Stopband (GHz)/ attenuation (dB) | TZs at either passband edges |
|---|---|---|---|---|---|---|
| [93] | 3–10.2 | 5.2, 5.8, 8/>15 | >1.22 × 0.8 | >30 × 30 | 17/>12 | √, √ |
| [94] | 2.7–10.6 | 5.2, 6.1, 8.15/>18 | 1.8 × 0.78 | 25.26 × 11 | 18/>26 | ×, × |
| [95] | 2.1–11.5 | 5.5, 6.2, 8.2/>15 | 1.8 × 0.78 | 25.26 × 11 | 18/>23 | ×, × |
| [60] | 3.25–10.73 | 5.6, 6.42, 8.03 > 19 | 1.04 × 0.66 | 14.6 × 9.2 | 17/>16 | √, √ |
| [69] | 3.3–10.7 | 4.4, 5.5, 7.64/>12 | >1 × 0.65 | >32 × 20 | 20/>20 | √, √ |

| | | | | | | |
|---|---|---|---|---|---|---|
| [96] | 3.5–10.85 | 5.4, 5.8, 8.2/>18 | >1.15 × 0.5 | >38 × 15 | 15/>11 | √, √ |
| [97] | 2.8–11 | 5.2, 5.85, 8/>10 | 1 × 0.66 | 31 × 20 | 20/>10 | ×, × |
| [98] | 2.8–11.8 | 3.6, 5.9, 8/>10 | 1 × 0.66 | 31 × 20 | 20/>10 | ×, × |
| [99] | 3–10.3 | 5.2, 5.8, 6.8/>15 | 0.67 × 0.43 | >18 × 25 | 30/>15 | ×, × |
| [100] | 2.8–10.6 | 3.3, 5.1, 8.3/>12 | >1.67 × 0.67 | >40 × 14 | 11/>10 | ×, × |
| [101] | 3.3–10.4 | 5.2/6.8/9.2 > 15 | >0.74 × 1.02 | >18 × 25 | 28/>15 | ×, × |
| [102] | 1.8–11.8 | 3.7/5.2/7.8 > 11 | 0.68 × 0.486 | 16.6 × 11.8 | 14/>10 | ×, √ |
| [103] | 4.3–10.2 | 5.9, 8, 9/>18 | >0.7 × 0.2 | >30 × 10 | 15/>14 | ×, √ |
| [104] | 3.1–10.6 | 3.6, 5.3, 8.4/>16 | >1.2 × 0.7 | >43 × 30 | 17/>18 | √, √ |
| [105] | 3.1–10.62 | 5.18, 5.86, 7.9/>16 | >1.2 × 0.75 | >37 × 23 | 16/>15 | ×, √ |
| [106] | 2.86–10.72 | 6/6.53, 8.35/15 | >1.23 × 1.02 | >30 × 25 | 16.5/>16 | √, × |
| [107] | 3.1–10.6 | 5.85, 7.12, 8.13 > 21 | >0.93 × 0.37 | >25 × 10 | 18/>17 | ×, × |

| | | | | | | |
|---|---|---|---|---|---|---|
| [108] | 2.6–8.3 | 4.43, 5.2, 6.4 > 11 | 1.22 × 0.53 | 41 × 18 | 11/>19 | √, √ |
| [109] | 3.2–12 | 4.1, 6.6, 9/>13 | >1.24 × 0.32 | >60 × 10 | 14/>10 | √, × |
| This work | 2.5–10.96 | 5.1, 6.45, 7.9/>18 | 0.95 × 0.78 | 14 × 11.4 | 16/>16 | √, √ |

## 6.4. Summary:

The addition of two TZs strategically located at the lower and upper sides of the passband resulted in the effective implementation of the basic BPF response. Iteratively adding numerous CRs and CSRRs to the basic design resulted in triple passband notches at specified required frequencies. The BPF displayed extremely acceptable and desired frequency characteristics as a result of these improvements. Following that, a real prototype was carefully built, and testing was carried out to ensure the accuracy of what was predicted. The resulting BPF design is astonishingly compact and well-suited for usage in current UWB communication systems, offering improved performance and efficiency in practice.

# CHAPTER 7

# UWB-BPF WITH MULTIPLE PASSBAND TRANSMISSION ZEROS

## 7.1. Introduction:

The COVID-19 epidemic imposed severe restrictions, forcing people all across the world to depend primarily on the internet for amusement. Due to restricted data rate capacity, a sudden increase in internet users, reaching billions at the same time, frequently results in bandwidth shortages. at such cases, the actual potential of UWB communication systems is shown, with astounding data speeds of 10 Gb/s at small ranges, such as homes [9]. Despite the benefits of rapid communication rates and low power emissions, UWB systems suffer problems when interrupted by within-band high-power Radio signals. To solve this issue, a cascaded system comprised of a UWB BPF and several BSF to reduce and attenuate interferences is a viable option. However, when merging several BSFs with the current BPF, this technique poses a new challenge of increasing circuit size. As a result, researchers have investigated novel approaches for integrating the BSF into the BPF, assuring compactness and optimizing performance. This integration enables efficient filtering of unwanted signals, enabling the smooth operation of ultra wide band communication systems in the face of high-power RF sources, resulting in improved user experiences and continuous connectivity.

Several ways have been proposed to build triple passband TZs, with one prominent approach including the use of triple stepped impedance (TSIR) in several modified variants, based on a simple premise [97,98,111]. Another approach is to use three defective microstrip structures (DMS) [112, 113], DGS such as three CSRR [114], or three spiral DGS to accomplish triple TZ implementation. Furthermore, the concept of wave cancellation is used to create triple notches in the context of linked MMRs and modified MMR-based BPFs [70] [115]. These novel methodologies enable the development of triple passband TZs with improved performance and efficiency. Stubs, each a quarter wavelength long, are used to create multiple notches at certain notch frequencies [116,117]. These

strategies are combined in [107,118], where a hybrid method is employed to generate triple notched bands in [118], Wave cancellation methods are used with CSRR, whereas in [107], multi-mode SIR function in conjunction with asymmetric coupling structures to attenuate triple passbands using the wave cancellation concept. These various techniques provide with a variety of alternatives for designing and optimizing triple TZs in BPF to meet specific application needs and limits, thereby improving the performance and adaptability of communication systems and wireless technologies.

As displayed in Fig. 7.1, we provide a small and planar UWB-BPF with triple notched bands in this chapter. The filter's basic design comprises of a transition from microstrip to CPW. [63,119], which is accomplished by EM coupling via the substrate. The Multiple Mode Resonator's impedance ratio is changed to position the initial three resonant frequencies into the UWB to get the appropriate frequency response. Due to the meticulous tuning of the MSL above, the transition is tightly coupled, resulting in an FCC-compliant UWB spectrum with numerous TZs.

Multiple DGS are carefully included to introduce notches inside the passband for interference reduction, further enhancing its performance. The complete structure was developed and built on RT/Duriod 6010. using IE3D software. A physical model of the UWB-BPF was built and thoroughly measured to confirm the expected frequency characteristics. The testing findings validate the filter's excellent performance, emphasizing its potential for usage in a variety of UWB communication systems and applications.

## 7.2. Filter Configuration & working Mechanism:

The modelling of the SCCPW begins with the initial design of the basic BPF. Fig. 7.2 depicts the TL analogue of the CPW design. The CPW is an MMR with a central high-impedance (thin) segment and two identical low-impedance (thick) portions on both ends. The analysis is focused on the MMR's frequency characteristics for BPF formation, with insignificant consideration for the CPW step discontinuities at the endpoints because their influence on the BPF features is small [25].

The next step is to determine the impedance conditions required to achieve the appropriate passband and stopband characteristics. The needed physical dimensions of the MMR, such as its length and breadth, are computed using these impedance criteria (7.1)

$$\text{Zin} = \text{jZ2}\frac{2(K tan\theta 1 + tan\theta 2)(K - tan\theta 1 tan\theta 2)}{K(1 - tan^2\theta 1)(1 - tan^2\theta 2) - 2(1 + K^2)tan\theta 1 tan\theta 2} \quad (7.1)$$

The impedance ratio (K) between the MMR's central and end sections, suggested as ZCPW1/ZCPW2, is critical in the design process, along with other pertinent factors. When the MMR is in resonance, the input impedance (Zin) is zero, as a result, a number of equations are needed to be solved to determine the resonant frequencies (f1, f2, f3).The core CPW dimensions are carefully adjusted based on our special design to match the appropriate performance parameters for the BPF, providing efficient signal filtering and transmission within the prescribed frequency range. The impedance ratio (K) between the MMR's central and end sections, indicated as ZCPW1/ZCPW2, is critical in the design process, along with other pertinent factors. The core CPW dimensions are carefully adjusted based on our specific design to match the appropriate performance parameters for the BPF.

**Table.7.1:** The optimized dimensions (in mm) of the suggested structure:

| Parameter | Size | Parameter | Size |
|---|---|---|---|
| l1 | 5.83 | s1=s2=s | 0.4 |
| l2 | 3.185 | s2 | 0.4 |
| L | 14.6 | g0 | 0.9 |
| W | 9.2 | g1 | 5.15 |
| w0 | 0.76 | p | 3.165 |
| w1 | 0.98 | q | 2.5 |

| | | | |
|---|---|---|---|
| w2 | 3.28 | r | 1.6 |
| u | 1.08 | t | 1.5 |

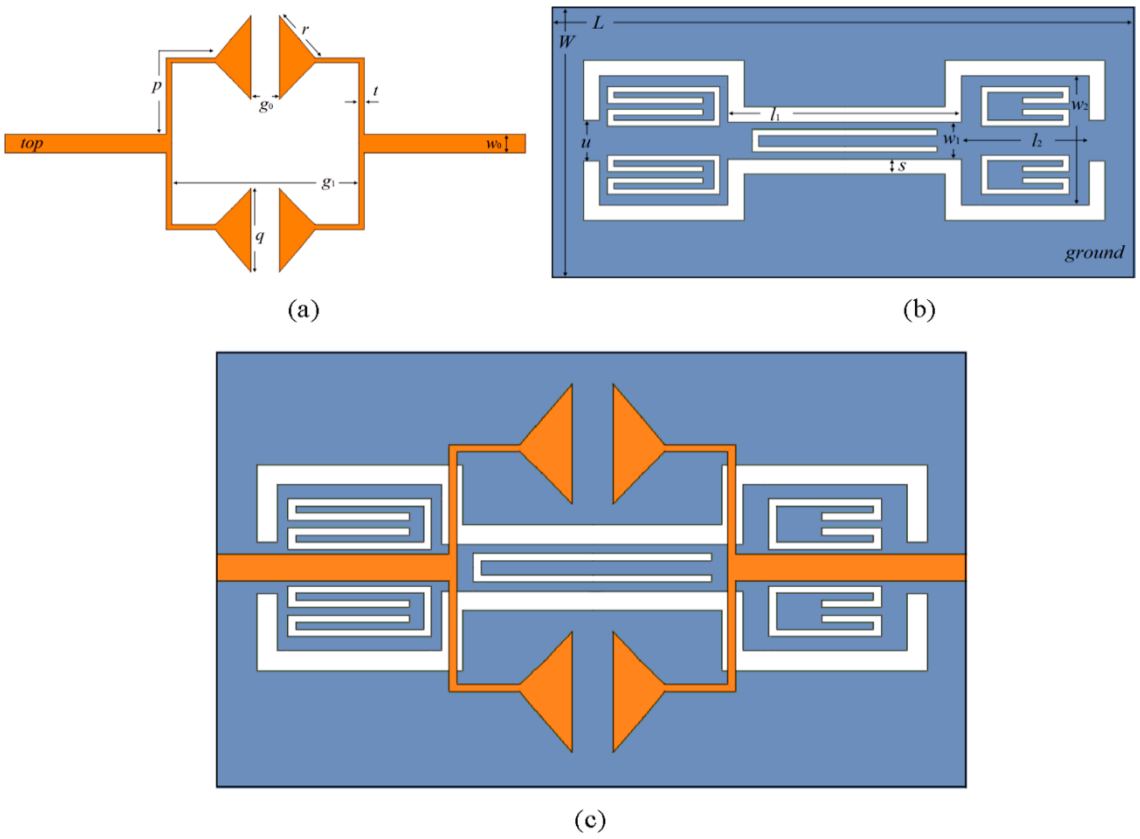


**Fig.7.1.** (a) Top-plane layout (b) Ground plane (c) A complete image of the suggested layout.

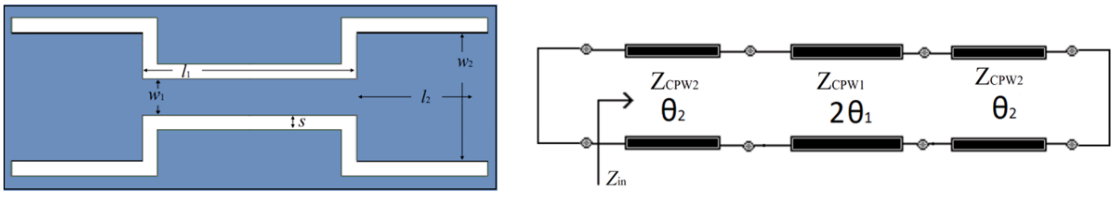


**Fig.7.2.** (a) The layout of the suggested CPW. (b) Model of corresponding TL.

The weak coupling behavior of this MMR is display in Fig.7.3 for various values of K. When K is reduced, the lowest resonant mode (f1) shifts somewhat to the right, but the modes with higher frequencies move substantially to the left. For our design, we assume K = 1.2, which allows us to build the UWB spectrum using (f1, f2) and dragging f3 for over 15 GHz.

The simulated S-parameters are displayed in Fig.7.4,revealing that the filter has a BW range of 3.15-10.62 GHz.

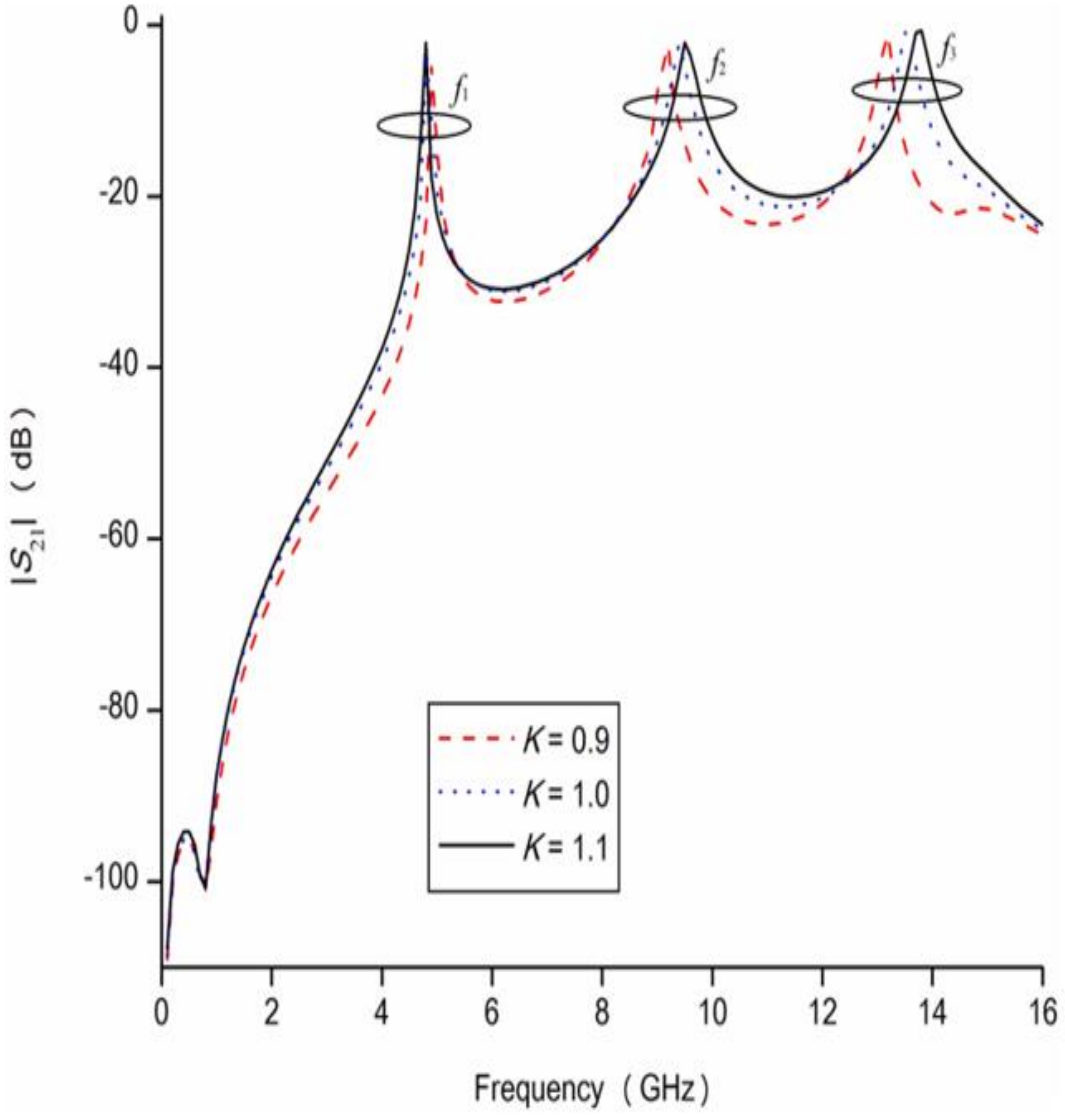


**Fig.7.3.** Weak coupling behavior for varying impedance ratio

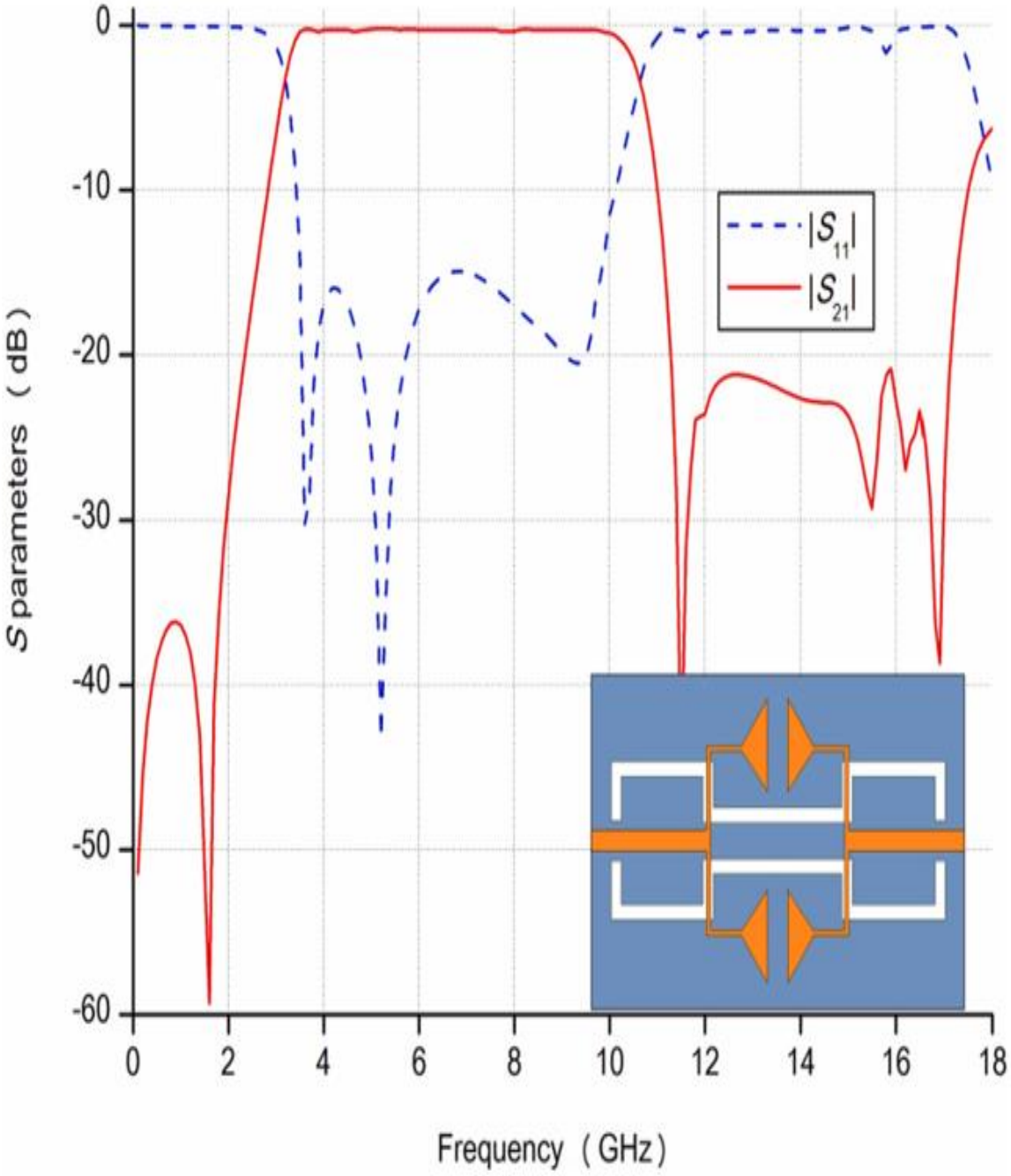


**Fig.7.4.** The simulated $S_{21}$ and $S_{11}$ response without notched bands.

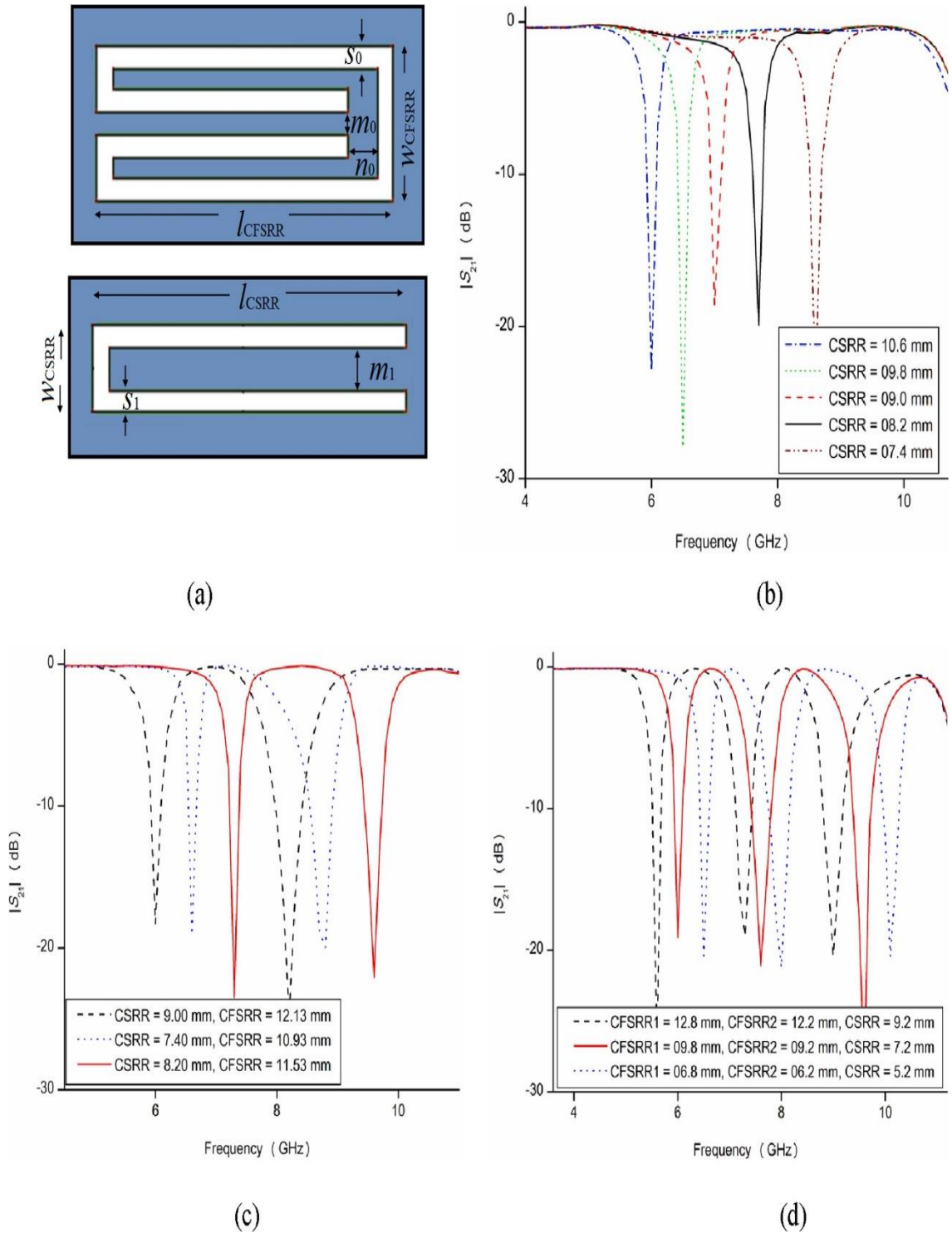


**Fig.7.5.** (a) Architecture of CSRR and CFSRR. (b) Single notch optimization for different length of the CSRR. (c) Dual passband TZs for different length of CSRR and CFSRR. (d) Varying CFSRR1, CFSRR2, and CSRR lengths result in triple passband notches inside the passband.

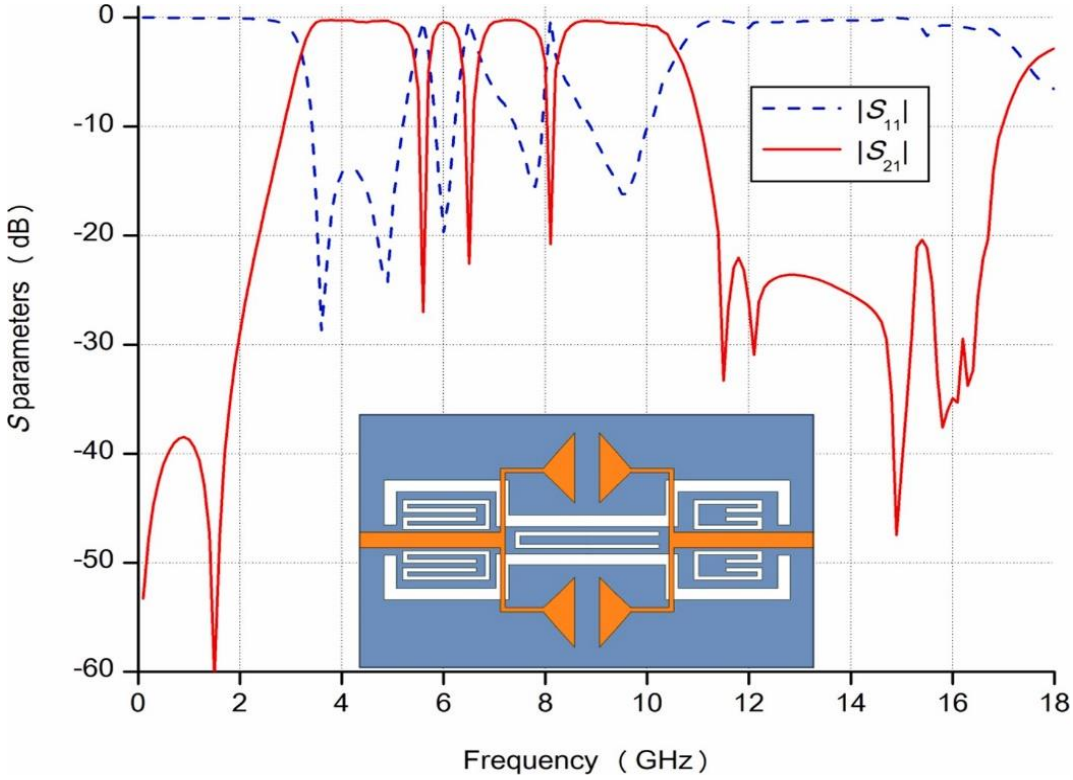


**Fig.7.6.** Simulated frequency characteristics of the suggested structure.

After modelling the CPW, the next step is to improve its transition, an optimization procedure employing a microstrip on the upper layer was used. To achieve optimal transition coupling at around 6.85 GHz, the characteristic impedance of the MSL is tuned to double the value of the CPW [110]. With Z0 (CPW1) at 51.58, a characteristic impedance of Z0(microstrip) = 102 is sought in our suggested BPF structure, requiring a thickness (t) of 0.065 mm. However, because of manufacturing constraints, reaching a thickness of 0.065 mm is difficult. However, because of production restrictions, achieving a width of 0.065 mm is challenging, thus, t = 1.5 mm of thickness is used, resulting in $Z_0$ (microstrip) = 81. The length of this 81 line is 4.165 mm, which corresponds to $\lambda$gmicrostrip/4. Regardless of the impedance difference, the frequency characteristics are only marginally changed.

To mitigate such interference, we incorporate a BSF into UWB systems. As shown in Fig. 7.5(a), the BSF is smoothly incorporated inside the BPF utilizing two DGSs, the CSRR [120] and the CFSRR [121]. Depending on whether they work alone or together, the CFSRR and CSRR can generate a single or several TZs. These TZs are positioned

deliberately within the passband at precise positions that correlate to the sites of interfering RF services. The notches exhibit adjustable characteristics, as displayed in Fig. 7.5 (b, c, d), enables for fine modification to match the conflicting frequencies. Because of its longer length, the CFSRR may locate TZs deeper into the passband than the CSRR, enabling versatile interference mitigation choices for improved UWB system performance. The suggested triple band-notched BPF's optimized frequency characteristics is depicted in Fig. 7.6, and Fig. 7.7 which displays the current distribution at the three corresponding notches. The current distribution clearly identifies the DGS in charge of creating the passband TZs. Each DGS displays a significant concentration of current surrounding it at its allocated notch frequency, demonstrating a clear connection with the notch frequency and a significant linkage to the UWB-BPF. These findings provide important insights into how the DGS structures shape the frequency characteristics of the BPF and provide the required triple notched response. The strong coupling and accurate current distribution at the relevant notched bands justify the suggested design's efficiency and appropriateness for eliminating interference and advanced UWB communication systems.

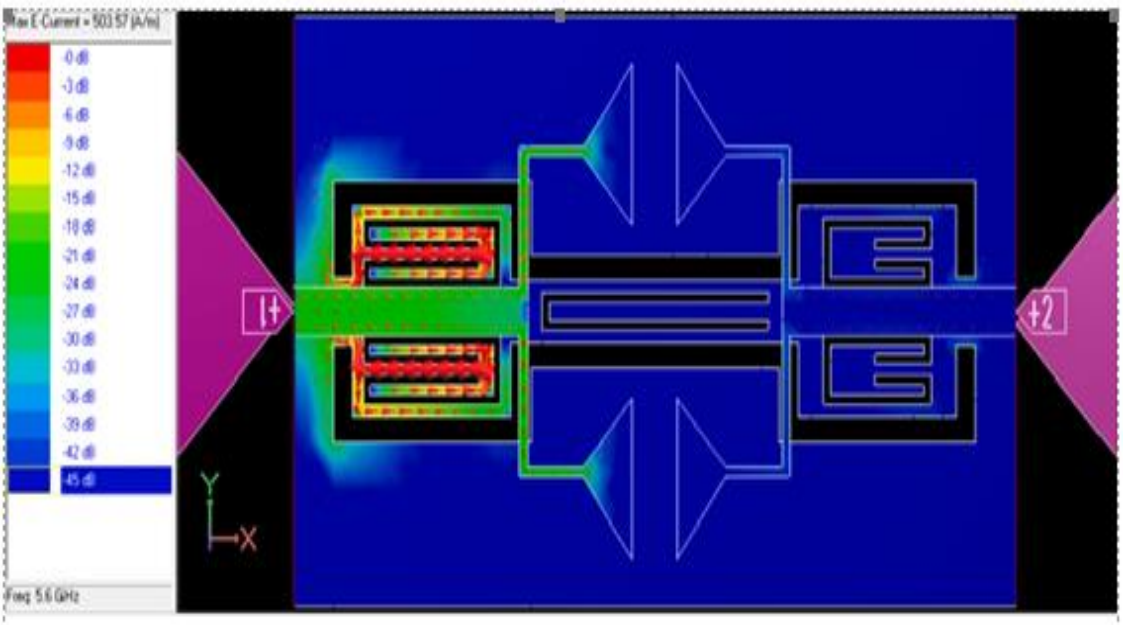


(a)

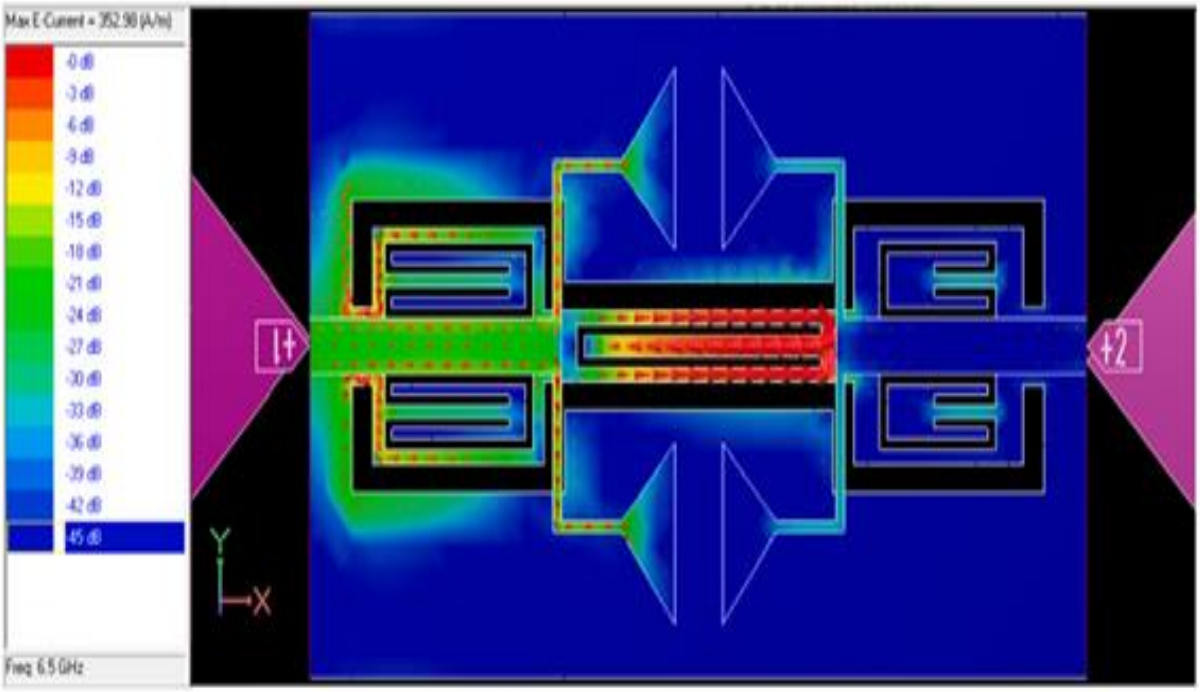


(b)

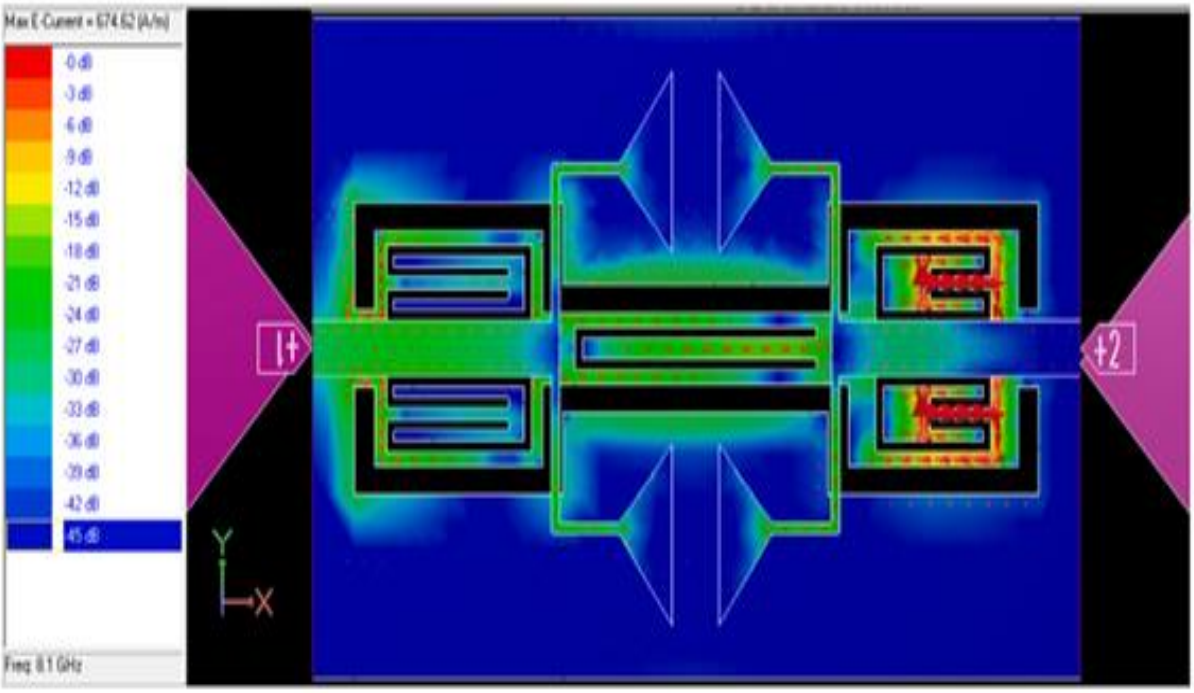


(c)

**Fig.7.7.** Current distribution at different notches.

## 7.3. Measurements:

The suggested structure prototype has been meticulously observed for validation, and the relevant frequency responses are given in Fig. 7.8

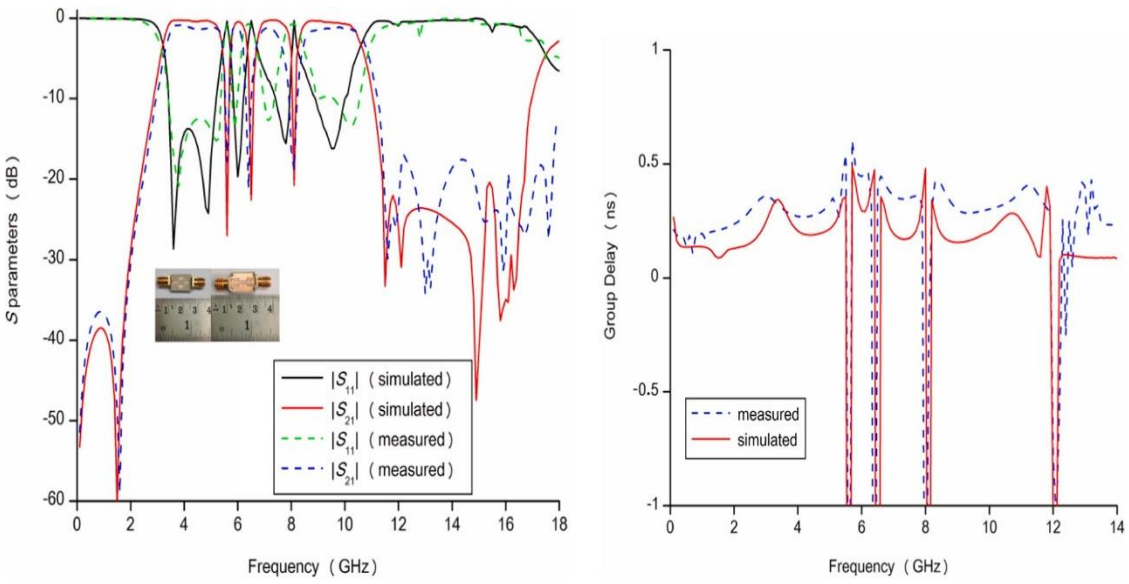


(a) (b)

**Fig.7.8.** Comparing the frequency characteristics of observed and simulated data. (a) $s_{21}/s_{11}$(observed and simulated). (b) Group delay (observed and simulated).

The reported 3-dB BW spans 3.25 to 10.73 GHz, with upper stopband attenuation reaching as high as 17 GHz. Outstanding s21/s11 performance observed during triple notches testing, measuring less than 1.4/13 dB between 3.25 and 5.4 GHz, 1.6/13 dB between 5.8 and 6.1 GHz, 1.1/12 dB between 6.7 and 7.55 GHz, and 1.2/10.2 dB between 8.4 and 10.73 GHz. The triple notches center frequencies are accurately positioned at 5.6, 6.42, and 8.03 GHz, with superior attenuation surpassing 19 dB.

The measured group delay is amazingly less than 0.63 ns, suggesting superb linearity over the passband (excluding the triple notches). However, considerable discrepancy between observed and simulated data is because of human error during manufacture, reflections from connections, and the substrate's limited size. To evaluate the proposed filter's performance, Table 7.2 compares it to reported multiple notches UWB-BPF structures from the literature. In terms of frequency characteristics and dimensions, the results show

that the suggested BPF outperforms or is equivalent to most current structures, indicating its potential for advanced UWB communication applications.

**Table.7.2:** Performance comparisons of reported UWB-BPF

| **Ref.** | **BW (GHz)** | **Notched band frequency (GHz) / Attenuation (dB)** | **Wide Stopband (GHz) / Attenuation (dB)** | **Size ($\lambda_g \times \lambda_g$)** |
|---|---|---|---|---|
| 97 | 2.8–11 | 5.2, 5.85, 8 / > 10 | 20 / > 10 | 1 × 0.66 |
| 98 | 2.8–11.8 | 3.6, 5.9, 8 / > 10 | 20 / > 10 | 1 × 0.66 |
| 111 | 3–10.3 | 5.2, 5.8, 6.8 / > 15 | 30 / > 15 | 0.67 × 0.43 |
| 112 | 3–10.2 | 5.2, 5.8, 8 / > 15 | 17 / > 12 | > 1.22 × 0.8 |
| 113 | 2.1–11.5 | 5.5, 6.2, 8.2 / > 15 | 18 / > 23 | 1.8 × 0.78 |
| 114 | 2.7–10.6 | 5.2, 6.1, 8.15 / > 18 | 18 / > 26 | 1.8 × 0.78 |
| 70 | 3.3–10.7 | 4.4, 5.5, 7.64 / > 12 | 20 / > 20 | > 1 × 0.65 |

| | | | | |
|---|---|---|---|---|
| 115 | 3.5–10.85 | 5.4, 5.8, 8.2 / > 18 | 15 / > 11 | > 1.15 × 0.5 |
| 116 | 3.1–10.6 | 3.6, 5.3, 8.4 / > 16 | 17 / > 18 | > 1.2 × 0.7 |
| 117 | 4.3–10.2 | 5.9, 8, 9 / > 18 | 15 / > 14 | > 0.7 × 0.2 |
| 118 | 3.2–12 | 4.1, 6.6, 9 / > 13 | 14 / > 10 | > 1.24 × 0.32 |
| 107 | 3.1–10.6 | 5.85, 7.12, 8.13 > 21 | 18 / > 17 | > 0.93 × 0.37 |
| This work | 3.25–10.73 | 5.6, 6.42, 8.03 > 19 | 17 / 16 | 1.04 × 0.66 |

## 7.4. Summary:

This chapter describes a planar UWB-BPF with several TZs in its passband, with the essential design relying on two microstrip-to-CPW transitions on opposite side of the dielectric. Multiple Defected Ground Structures (DGS) are interconnected to produce three passband TZs, deliberately located at frequencies of relevance, to improve performance and prevent possible interferences. These TZs effectively remove unwanted disturbances from inside the passband, ensuring constant and efficient signal transmission. Notably, the suggested structure is compact in size, allowing it to be readily integrated with various UWB systems. This capability, together with the BPF's superior frequency management and interference avoidance capabilities, establishes the BPF as an important component in current communication technologies, offering improved performance and smooth integration with UWB communication system.

# CHAPTER 8

# QUAD NOTCHED BAND UWB-BPF

## 8.1. Introduction:

The FCC introduced a spectrum of UWB in 2002 for unlicensed commercial use, providing substantial scope for researchers in UWB technology [9] The utilization of UWB technology is diverse, with applications ranging from imaging systems to radar and communication systems. A crucial aspect of UWB communication systems is the ultra-wide bandpass filter. Due to the rise in spectrum demand and concerns regarding traffic issues, researchers have introduced a notched band that focuses on frequencies of other operational radios to mitigate spurious signals. The objective of this approach is to tackle the problem of signal interference frequency spectrum.

Several strategies have been developed to boost performance parameters of UWB-BPF, such as insertion loss(S21), roll-off, selectivity of filter return loss (S11), and group delay. Some of these methods involve using a MMR [69], employing the broadside-coupled approach [122], open-circuited stub [123], hybrid designs, where elements of both low-pass and highpass filter are integrated into a single topology [124], MSL integrated with coplanar waveguide [125], asymmetric coupled line [126], CMOS based UWB Filter [127], Multilayer filter [128].

This chapter describes a unique UWB-BPF with four passband notches intentionally constructed on opposing sides of the substrate utilizing modified SRR and CSRR. The formation of notched bands into the BW of the suggested UWB-BPF is enabled by this unique arrangement of resonators, and the notched frequency can be tuned by tailoring the dimension of the resonators. To evaluate the design's efficacy, a real prototype of the filter is built and thoroughly tested, validating the correctness of the simulation findings. The UWB-BPF's small size and strong performance features make it an ideal match for current UWB communication systems, enabling increased signal filtering and efficient transmission.

## 8.2. Filter Configuration & working mechanism:

The suggested UWB filter employs a basic geometry that is based on broadside coupling. The filter's top plane is made up of modified ring resonators, while the ground plane is made up of CSRR. This arrangement allows the UWB filter to develop a quad notched band. The complete filter is built on a Roger 6010 substrate. Figure 8.1 depicts the architecture and placement of the modified split ring resonators and CSRR on the substrate of the quad notched band UWB filter.

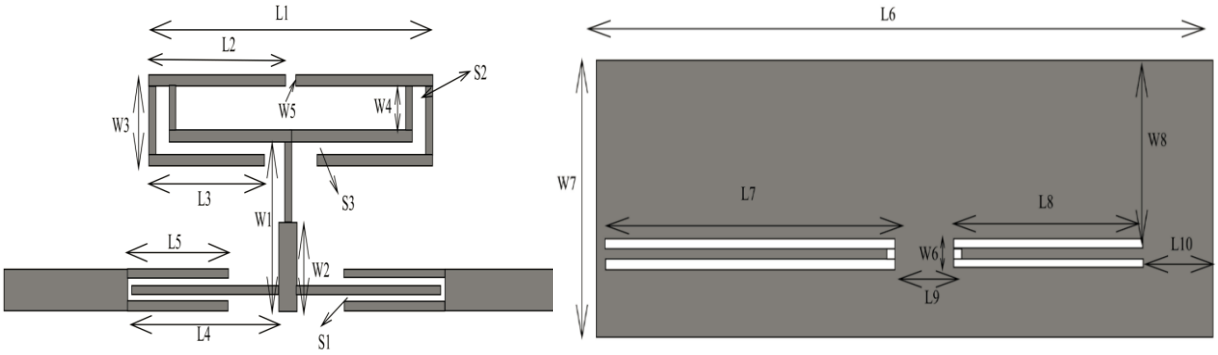


**Fig.8.1:** Schematic of suggested structure:(a) Top plane (b) ground plane,

The UWB BPF proposed in this study was designed with optimize dimension as shown in table-1 and simulated using commercial IE3D EM simulation software.

**Table.8.1:** The optimized dimensions (in mm) of suggested design:

| Dimension | Size | Dimension | Size | Dimension | Size |
|---|---|---|---|---|---|
| L1 | 8.1 | L8 | 5.7 | W5 | 0.2 |
| L2 | 3.95 | L9 | 1.5 | W6 | 0.8 |
| L3 | 3.2 | L10 | 1.95 | W7 | 6.65 |

| | | | | | |
|---|---|---|---|---|---|
| L4 | 5.25 | W1 | 4.4 | W8 | 4.6 |
| L5 | 3.8 | W2 | 2.35 | S1 | 0.10 |
| L6 | 17.6 | W3 | 1.25 | S2=S4 | 0.25 |
| L7 | 8.1 | W4 | 0.5 | S3 | 0.15 |

Figure 8.2 depicts the suggested structure's S-parameters response in the absence of a Complementary modified Split Ring Resonator (CMSRR). This response displays the frequency characteristics and performance of the filter without the CMSRR, allowing for a clear comparison with the succeeding figures that include the CMSRR. The lack of the CMSRR gives vital insights on the filter's initial behavior and functionality, establishing a foundation for assessing the CMSRR's influence on the filter's overall performance and passband notching capabilities.

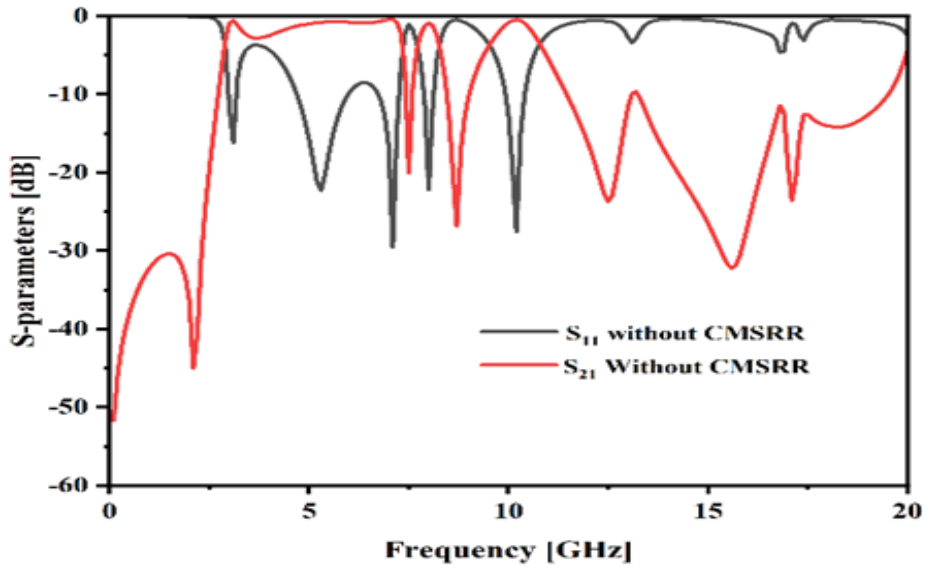


**Fig.8.2:** S-parameters of the filter without CMSRR.

Figure 8.3 depicts the response of the suggested structure using the Complementary Modified Split Ring Resonator (CMSRR). The graph depicts the effect of the CMSRR on

filter performance and the formation of notched bands inside the passband. This comparison demonstrates how the CMSRR adds to the filter's functioning and capacity to efficiently suppress undesirable frequencies. The CMSRR analysis provides vital insights into the filter's improved performance and possible uses in interference avoidance for current UWB communication systems.

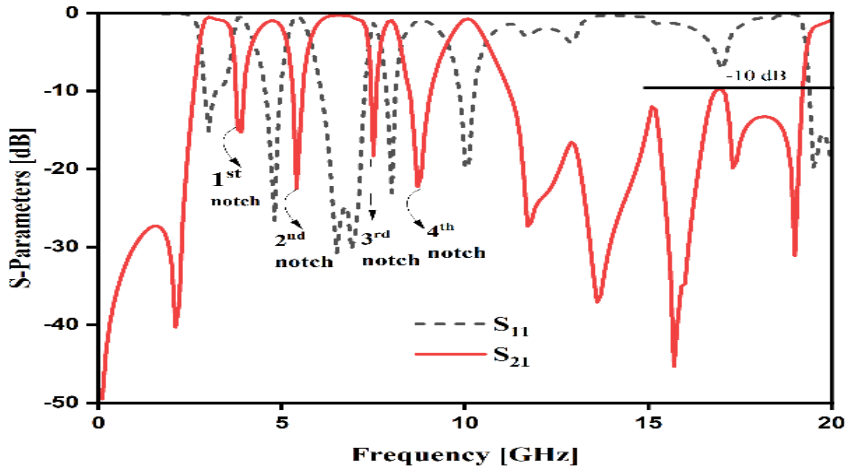


**Fig.8.3:** Simulated response of the suggested filter.

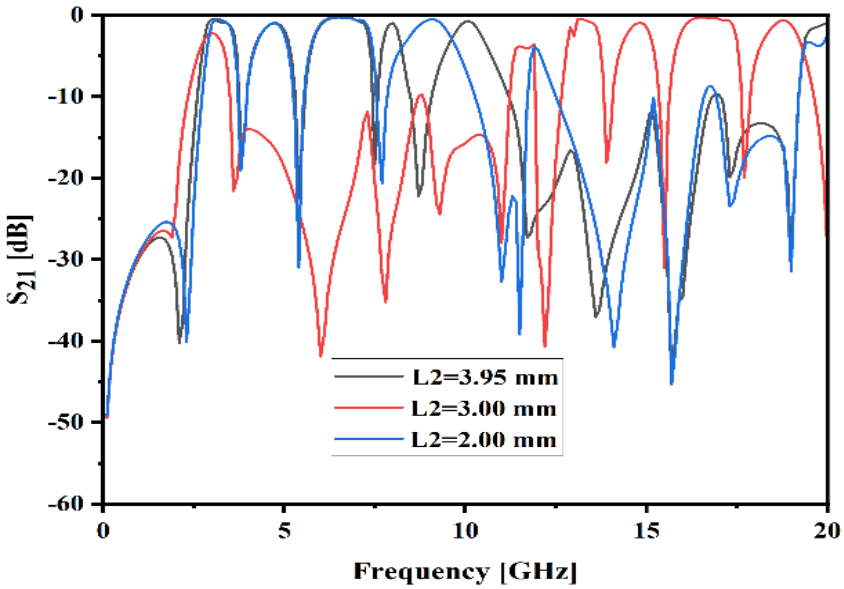


**Fig.8.4:** Parametric study of Second notch $S_{21}$

Modifications in the value of L2 have a major impact on the filter's functionality. As L2 decreases from 3.95 mm to 2 mm, the insertion loss (S21) and upper stopband performance degrade noticeably, as seen in Fig. 8.4. The examination of Fig.8.4 shows that setting L2 to 3.95 mm results in an ideal notch configuration inside the passband, guaranteeing enhanced filter performance and effective suppression of undesirable frequencies.

## 8.3. Measurement and experimental verification of the proposed design:

The suggested structure was constructed on a substrate of Roger 6010. The fabricated circuit was tested using VNA. After comparing the simulated data with the measured data, it was determined that they were in good agreement. Therefore, there was a high degree of similarity between the two data sets. The results displayed a minor deviation, which was linked to a misalignment of the circuit's top and ground layers. Despite this, the quad-notched UWB filter showcased outstanding performance in both the passband and extended stopband band regions, without impacting other frequencies in the passband. Furthermore, it demonstrated a linear phase response throughout the entire passband, with the exception of the band-notched frequencies. The measured $S_{21}$ was less than 1 dB, and the $S_{11}$ was greater than 15 dB. The first notch displayed a rejection of 15.1 dB at 3.6 GHz, whereas the second notch showed a rejection of 20.84 dB at 5.4 GHz. Similarly, the third notch exhibited a rejection of 17.9 dB at 7.5 GHz, and the fourth notch displayed a rejection of 21 dB at 8.7 GHz.

## 8.4. Summary:

In this chapter, a novel compact UWB-BPF with four notches is introduced. The filter incorporates notched bands as a new feature, with the basic design utilizing hybrid technology that combines microstrip and CPW. The basic BPF design is based on the hybrid multimode mode resonator and broadside coupled technology, which facilitates the creation of the necessary UWB with sharp TZs at both passband edges, along with significant $S_{21}$ and $S_{11}$.The integration of composite split ring resonators (CSMRRs) into the ground enables the realization of an improved stopband and the creation of four notches in a filter. To confirm the accuracy of the simulation results, a VNA was used to observed the response of the filter prototype, which validated the results. Owing to its small size and

favorable frequency characteristics, the newly proposed UWB-BPF is a promising component for integration into a variety of UWB communication systems.

# CHAPTER 9

# CONCLUSIONS AND FUTURE WORK

## 9.1. Conclusions:

Compact UWB) BPF are crucial components in UWB systems because they meet the stringent FCC emission mask criteria. Because of their low radiated power, which remains below the noise level, these filters are critical components for enabling efficient communication inside UWB networks without interfering with other wireless services. However, dealing with other wireless services that operate as high-energy radiators and can potentially cause interference to UWB systems presents a substantial challenge. To successfully solve this issue, a UWB filter with integrated passband notch features must be designed. This capability mitigates undesired frequencies from other wireless services, increasing overall system performance. Furthermore, an extended stopband is required to improve isolation and prevent unwanted crosstalk. As a result, the creation of a tiny UWB filter with these vital qualities becomes critical for the operation of a seamless and interference-free UWB system.

This research work presents a novel architecture of an UWB-BPF with multiple passband notches and an extended stopband, which was successfully implemented. Initially, Multimode Resonators (MMR) were utilized in the creation of the UWB filter. The bottom layer was constructed using a DGS linked to the microstrip on the top, sharing a common dielectric. By optimizing the modeling of the MMR, the resonant modes were efficiently excited, leading to the desired UWB passband. To augment the filter's performance, the common overlap area between the MSL on top and the narrow arms of the MMR at the bottom was fine-tuned to increase the capacitance. This adjustment, in turn, significantly improved the coupling strength of the filter, ensuring its effective operation in achieving the specified passband characteristics and extended stopband.

This study investigates the use of various Defected Ground Structures (DGS) within the Multimode Resonator (MMR) to achieve adjustable passband notches. Different DGS types were used, including rectangular, dumbbell, CSRR, CFSRR, CMFSRR, spiral, meander, and so on. DGS disrupts ground current distribution, resulting in passband

notches at their respective resonance frequencies (f). The effective permeability of the material becomes negative in this limited frequency range (f), leading propagating waves to become evanescent and establishing stopband features. The dimension of the DGS profile determines the centre frequency of the notches. Similar DGS structures were cascaded at equidistant spots on the MMR to extend the notch bandwidth, as their near proximity promotes EM coupling.

On the other hand, Widening the gap between the DGS structures, reduces the notch BW due to decreased EM coupling. Dual/triple passband notches were built on the MMR by cascading numerous DGS structures to solve various passband interferences. Dual notches were created by using two non-equidimensional DGS structures spaced apart on the MMR, with their bandwidth shifting according on the distance between them. Similarly, triple passband notches were created by cascading three non-equidimensional DGS structures on the MMR, with the potential for either narrow or wide bandwidth depending on how the DGSs were positioned. Furthermore, quadruple notches were obtained by employing split ring resonators and cascading two non-equidimensional complementary split ring resonators.

A wide and deep stopband is critical for the UWB filter in the context of the UWB system because it offers the essential isolation. This is accomplished by extending and reducing false harmonic frequency points. The harmonics are effectively suppressed by integrating DGS beneath the input/output feeding lines within the ground plane. While standard DGSs normally generate single attenuation poles, this strategy is inadequate for our design, which involves many spurious stopband harmonics. To properly suppress these many harmonics, our suggested filter architectures need the use of a DGS with multiple attenuation poles.

A roughly lumped equivalent circuit model for the UWB-BPF was developed in this study, along with numerous notch configurations. The first priority was to create a lumped equivalent circuit for the UWB-BPF structure. Following that, lumped equivalent circuit models for the multiple notch structures were built, with interconnections established among the multi-notch resonant circuits. The circuit was carefully tuned to provide a matched frequency response of the constructed circuit architectures correlated strongly with the results of EM simulations. These promising outcomes validate the

efficacy of the proposed models in accurately representing the behavior of the UWB-BPF and multiple notch structures.

Finally, all of the proposed structures were built on Rogers RT/Duroid 6010 substrate. However, the flexible and transparent UWB-BPF was designed using silver nanowires printed on a flexible polyethylene terephthalate (PET) substrate with a relative permittivity of 3. The fabricated structures were then observed using an VNA. The frequency graphs obtained were compared to full-wave EM simulations and circuit simulations, and there was remarkable agreement. All of the proposed filter's measured findings showed excellent consistency with the EM simulation results, thus supporting the efficacy and accuracy of the developed filter designs.

## 9.2. Limitations:

Multimode Resonator (MMR) UWB filters are planar structures with a MSL on the upper and a DGS on the bottom layer. With this setup, exact mask alignment becomes critical to avoid misalignment and inaccurate results. Because of the limits imposed by the proposed MMR on the DGS dimension, the center frequency of the lowest passband notch has limited tunability. To attain a lower notch center frequency, the MMR must be increased in size, resulting in an increase in overall filter size. To achieve optimal performance, maintaining a balance between notch frequency tunability and the physical dimensions of the MMR becomes a vital factor in the design process.

## 9.3. Future work:

There are various potential areas of investigation and development for multiple notched band filters in future work. To begin, more research can be done to optimize the design of the various notch structures, with an emphasis on improving their performance in terms of notch depth, bandwidth, and tunability. This could involve experimenting with different Defected Ground Structures (DGS) shapes and configurations in order to get more accurate and controllable notch characteristics.

Furthermore, the incorporation of adaptive tuning processes could be investigated for improvement in the flexibility and reconfigurability of the multiple notched band filters.

This could involve integrating varactors or other tunable elements into the filter structure that allow for dynamic adjustment of the notch frequencies in response to changing system requirements or interference sources. Manufacturing procedures can be improved to increase the overall efficiency and manufacturability of the multiple notched band filters. Exploring alternate substrate materials, sophisticated fabrication processes, and integration approaches to reduce losses, improve signal integrity, and reduce manufacturing difficulties could be part of this. Finally, novel applications for multiple notched band filters can be investigated. This could involve incorporating them into certain wireless communication systems, such as IoT devices, radar systems, or wireless sensor networks, in order to address interference issues and increase spectral efficiency.

To fulfill the expanding requirements of wireless systems, future study on multiple notched band filters should focus on improving their design, tunability, fabrication procedures, performance evaluation, and exploring new applications.

# REFERENCES


[1] G. Mahttei, L. Young, and E. M. T. Jones, *Microwave Filters, Impedance-Matching Networks, and Coupling Structures*, Norwood, MA: Artech House, 1980.

[2] L. Zhu, "Microwave Filters", *Encyclopedia of RF and Microwave Engineering*, John Wiley & Sons, Inc., volume 1, pp.821-833, 2005.

[3] P. I. Richards, "Resistor-transmission-line circuits," *Proc. IRE., 36,* 217–220, Feb. 1948.

[4] H. Ozaki and J. Ishii, "Synthesis of a class of strip-line filters," *IRE Trans. Circuit Theory, CT-5,* 104–109, June 1958.

[5] H. A. Wheeler, "Transmission-line properties of parallel wide strips by a conformal mapping approximation," *IEEE Trans. Microwave Theory Tech.*, vol. 12, no. 3, pp. 172-185, May 1964.

[6] K. C. Gupta, R. Garg, I. Bahl, and P. Bhartia, *Microstrip Lines and Slotlines,* Second Edition, Artech House, Boston, 1996.

[7] R. A. Pucel, D. J. Masse, and C. P. Hartwig, "Losses in microstrip," *IEEE Transactions on Microwave Theory and Techniques,* vol. 16*,* pp. 1064, December 1968.

[8] E. J. Denlinger, "Losses of microstrip lines," *IEEE Transactions on Microwave Theory and Techniques, vol. 28,* pp. 513–522, June 1980.

[9] "Revision of part 15 of the commission's rules regarding ultra-wideband transmission systems," First Note and Order, Federal Communications Commission, ET-Docket 98-153, February 14, 2002.

[10] R. Gomez-Garcia and J. I. Alonso, "Systematic Method for the Exact Synthesis of Ultra-Wideband Filtering Responses Using High-Pass and Low-Pass Sections," in IEEE Transactions on Microwave Theory and Techniques, vol. 54, no. 10, pp. 3751-3764, Oct. 2006..

[11] C.-W. Tang and M.-G. Chen, "A microstrip ultra-wideband bandpass filter with cascaded broadband bandpass and bandstop filters," *IEEE Transactions on Microwave Theory Techniques,* vol. 55, no. 11, pp. 2412-2418, 2007.

[12] K. Li, D. Kurita, and T. Matsui, "An ultra-wideband bandpass filter using broadside-coupled microstrip-coplanar waveguide structure," *IEEE MTT-S Int. Dig*., pp.675-678, June 2005.

[13] K. Li and J.-S. Hong, "Modeling of an Ultra-Wideband Bandpass Filtering Structure," *Proceeding of AMPC,* vol. 1, pp. 41-44, 2006.

[14] K. Li, Y. Yamamoto, T.Matsui and O.Hashimoto, "An ultra-wideband(UWB) bandpass filter using broadside-coupled structure and shunt stub with chip capacitor," *Proceeding of AMPC,* vol. 1, pp. 41-44, 2006.

[15] H. Wang, L. Zhu and W. Menzel, "Ultra-wideband bandpass filter with hybrid microstrip/CPW structure," *IEEE Microwave and Wireless Component Letters, vol.* 15, no. 12, pp. 844-846, 2005.

[16] T. Kuo, S. Lin, and C. H. Chen, "Compact ultra-wideband bandpass filters using composite microstrip-coplanar-waveguide structure," *IEEE Transactions on Microwave Theory Techniques*, vol. 54, no. 10, pp. 3772–3778, Oct. 2006.

[17] T. Kuo, C. H. Wang, and C. H. Chen, "A Compact ultra-wideband bandpass filter based on split mode resonator," *IEEE Microwave and Wireless Component Letters, vol.* 17, no. 12, pp. 852-854, December 2007.

[18] N. Thomson and J.-S. Hong, "Compact Ultra-Wideband Microstrip/Coplanar Waveguide Bandpass Filter," *IEEE Microwave and Wireless Component Letters, vol.* 17, no. 3, pp. 184-186, March 2007.

[19] J.-W. Baik, T. H. Lee, and Y.-S. Kim, "UWB Bandpass Filter Using Microstrip-to-CPW Transition With Broadband Balun," *IEEE Microwave and Wireless Component Letters,* vol. 17, no. 12, pp. 846-848, December 2007.

[20] W. Menzel, L. Zhu, K. Wu, and F. Bogelsack, “On the design of novel compact broad-band planar filters,” *IEEE Transactions on Microwave Theory Techniques*, vol. 51, no. 2, 364-370, 2003.

[21] L. Zhu, H.Bu, and K.Wu, “Broadband and compact multi-mode microstrip bandpass filters using ground plane aperture technique,” *IEE Proc. Microw. Antennas Propag*., vol. 149, no. 1, 71-77, 2002.

[22] L. Zhu, H. Bu, K. Wu, and M. S. Leong, “Miniaturized multi-pole broadband microstrip bandpass filter: Concept and verification,” *30th European Microwave Conf. Proc*., vol. 3, pp. 334-337, Paris, October 2000.

[23] L. Zhu, S. Sun, and W. Menzel, "Ultra-wideband (UWB) Bandpass Filters Using Multiple-Mode Resonator", *IEEE Microwave and Wireless Component Letters, Vol. 15, No.11,* pp.796-798, November 2005.

[24] L. Zhu, and H. Wang, “Ultra-wideband bandpass filter on aperture-backed microstrip line,” *Electronics Letters*, Vol. 41, No. 18, September 2005.

[25] J. Gao, L. Zhu, W. Menzel and F. Bogelsack, “Short-circuited CPW multiple-mode resonator for ultra-wideband (UWB) bandpass filter,” *IEEE Microwave and Wireless Component Letters*, vol. 16, no. 3, pp. 104-106, March 2006.

[26] Wang H., and L. Zhu, “Ultra-wideband bandpass filter using back-to-back microstrip-to-CPW transition structure”, *Electronics Letters*, Vol. 41, No. 24, November 2005.

[27] Z. Zhang and F. Xiao, “An UWB Bandpass Filter Based on a Novel Type of Multi-Mode Resonator,” *IEEE Microwave and Wireless Component Letters*, vol. 22, No. 10, pp. 506-508, October 2012.

[28] S. Sun and L. Zhu, “Capacitive-ended interdigital coupled lines for UWB bandpass filters with improved out-of-band performance,” *IEEE Microwave and Wireless Component Letters*, vol. 16, no.8, pp. 440-442, 2006.

[29] R. Li and L. Zhu, “Compact UWB bandpass filter using stub-loaded multiple-mode resonator,” *IEEE Microwave and Wireless Component Letters*, vol. 17, No. 1, pp. 40-42, January 2007.

[30] S. W. Wong and L. Zhu, “EBG-embedded multiple-mode resonator for UWB bandpass filter with improved upper-stopband performance,” *IEEE Microwave and Wireless Component Letters,* vol. 17, No. 6, pp. 421-423, June 2007.

[31] S. W. Wong and L. Zhu, “Ultra- wideband bandpass filters with improved out-of-band behavior via embedded electromagnetic-bandgap multimode resonators,” *IET Microwaves Antennas and Propagation,* vol. 2, no. 8, pp. 854-862, July 2008.

[32] Q.-X. Chu, X.-H. Wu, and X.-K. Tian, “Novel UWB Bandpass Filter Using Stub-Loaded Multiple-Mode Resonator”, *IEEE Microwave and Wireless Component Letters*, vol. 21, No. 8, pp. 403-405, August 2011.

[33] X.-H. Wu, Q.-X. Chu, X.-K. Tian, and X. Ouyang, “Novel UWB Bandpass Filter Using Stub-Loaded Multiple-Mode Resonator”, *IEEE Microwave and Wireless Component Letters*, vol. 21, No. 12, pp. 661-663, December 2011.

[34] B. Yao, Y. Zhou, Q. Cao, and Y. Chen, “Compact UWB Bandpass Filter With Improved Upper-Stopband Performance,” *IEEE Microwave and Wireless Component Letters*, vol. 19, No. 01, pp. 27-29, January 2009.

[35] Z. Long, M. Tian, T. Zhang, M. Qiao, T. Wu and Y. Lan, "High-Temperature Superconducting Multimode Dual-Ring UWB Bandpass Filter," in IEEE Transactions on Applied Superconductivity, vol. 30, no. 2, pp. 1-4, March 2020.

[36] R. Li and L. Zhu, “Ultra-wideband (UWB) bandpass filters with hybrid microstrip/slotline structures,” *IEEE Microwave and Wireless Component Letters,* vol. 17, no. 11, 778-780, 2007.

[37] J.-K. Lee and Y.-S. Kim, “Ultra-Wideband Bandpass Filter With Improved Upper Stopband Performance Using Defected Ground Structure,” *IEEE Microwave and Wireless Component Letters,* vol. 20, no. 06, 316-318, June 2010.

[38] H. Shaman and J.-S. Hong, "Ultra-Wideband (UWB) bandpass filter with embedded band notch structures," *IEEE Microwave and Wireless Components Letters,* vol. 17, no. 3, pp. 193-195, 2007.

[39] H. Shaman and J.-S. Hong, "Asymmetric parallel-coupled lines for notch implementation in UWB filters," *IEEE Microwave and Wireless Components Letters*, vol. 17, no. 3, 516-518, 2007.

[40] S. W. Wong and L. Zhu, "Implementation of compact UWB bandpass filter with a notch-band," *IEEE Microwave and Wireless Components Letters,* vol. 18, no. 1, pp. 10-12, 2008.

[41] X. Luo, J. –G. Ma, K. Ma, and K. S. Yeo, "Compact UWB Bandpass Filter With Ultra Narrow Notched Band," *IEEE Microwave and Wireless Components Letters*, Vol. 20, No. 3, March 2010.

[42] W. –J. Lin, J. –Y. Li, L. –S. Chen, D. –B. Lin, and M. –P. Houng," Investigation in Open Circuited Metal Lines Embedded in Defected Ground Structure and Its Applications to UWB Filters" *IEEE Microwave and Wireless Components Letters*, Vol. 20, No. 3, March 2010.

[43] Q. Li, Z. J. Li, C. H. Liang and B. Wu, "UWB bandpass filter with notched band using DSRR", *Electronics Letters*, Vol. 46, no. 10, 13th May 2010.

[44] S. Pirani, J. Nourinia, and C. Ghobadi, "Band-Notched UWB BPF design using parasitic coupled lines," *IEEE Microwave and Wireless Components Letters*, vol. 20, no. 8, pp. 444–456, August 2010.

[45] V. Sekar, and K. Entesari, "Miniaturized UWB Bandpass Filters With Notch Using Slow-Wave CPW Multiple-Mode Resonators," *IEEE Microwave and Wireless Components Letters*, Vol. 21, No. 2, February 2011.

[46] C. H. Kim, and K. Chang, "Ultra-Wideband (UWB) Ring Resonator Bandpass Filter with a Notched Band," *IEEE Microwave and Wireless Components Letters*, Vol. 21, No. 4, April 2011.

[47] P. Sarkar, R. Ghatak, M. Pal and D. R. Poddar, "Compact UWB Bandpass Filter With Dual Notch Bands Using Open Circuited Stubs," in IEEE Microwave and Wireless Components Letters, vol. 22, no. 9, pp. 453-455, Sept. 2012.

[48] Y. Song, G. -M. Yang and W. Geyi, "Compact UWB Bandpass Filter With Dual Notched Bands Using Defected Ground Structures," in IEEE Microwave and Wireless Components Letters, vol. 24, no. 4, pp. 230-232, April 2014.

[49] A. N. Ghazali and S. Pal, "A compact UWB filter with notched band and suppressed stopband using DGS," Accepted by *IETE Journal of Research*, 2012.

[50] K. Li, D. Kutrita, and T. Matsui, "Dual-band ultra–wideband bandpass filter," *IEEE MTT-S Int. Dig*., pp. 1193-1196, June 2007.

[51] S. Kumar, R. D. Gupta and M. S. Parihar, "Multiple Band Notched Filter Using C-Shaped and E-Shaped Resonator for UWB Applications," in IEEE Microwave and Wireless Components Letters, vol. 26, no. 5, pp. 340-342, May 2016.

[52] Lihua Wu Pengli Hu Changhao Li Luetao Li Chengpei Tang , "A Novel Compact Microstrip UWB BPF with Quad Notched Bands Using Quad-Mode Stepped Impedance Resonator," Progress In Electromagnetics Research Letters, Vol. 83, 51-57, 2019.

[53] Q. X. Chu and X. K. Tian, "Design of UWB bandpass filter using stepped-impedance stub-loaded resonator," IEEE Microw. Wireless Compon. Lett., vol. 20, no. 9, pp. 501–503, Sep. 2010.

[54] X. Wu, Q. Chu, X. Tian and X. Ouyang, "Quintuple-Mode UWB Bandpass Filter With Sharp Roll-Off and Super-Wide Upper Stopband," in IEEE Microwave and Wireless Components Letters, vol. 21, no. 12, pp. 661-663, Dec. 2011, doi:

[55] Mirzaee, M., Virdee, B.S. and Noghanian, S. (2014), Compact ultra-wideband bandpass filter with variable notch characteristics based on transversal signal-interaction concepts. Int J RF and Microwave Comp Aid Eng, 24: 549-559.

[56] L. C. Lin, S. Yang, S. J. Sun, B. Wu, and C. H. Liang, ``Ultra-wideband bandpass filter using multi-stub-loaded ring resonator," Electron. Lett., vol. 50, no. 17, pp. 1218_1220, Aug. 2014.

[57] S. Kumar, R. D. Gupta and M. S. Parihar, "Multiple Band Notched Filter Using C-Shaped and E-Shaped Resonator for UWB Applications," in IEEE Microwave and Wireless Components Letters, vol. 26, no. 5, pp. 340-342, May 2016.

[58] S. Lan, M. Weng, C. Hung and S. Chang, "Design of a Compact Ultra-Wideband Bandpass Filter With an Extremely Broad Stopband Region," in IEEE Microwave and Wireless Components Letters, vol. 26, no. 6, pp. 392-394, June 2016.

[59] Abu Nasar Ghazali, Mohd Sazid, Srikanta Pal, “A compact broadside coupled dual notched band UWB- BPF with extended stopband”, AEU - International Journal of Electronics and Communications, Volume 82, 2017, Pages 502-507.

[60] Mohd Sazid, N S Raghava "Planar UWB-Bandpass filter with Multiple Passband Transmission Zeros”, AEU - International Journal of Electronics and Communications. Volume 134,2021,153711.

[61] Hua C, Lu Y. Compact UWB bandpass filter with a reconfigurable notched band. Int J RF Microw Comput Aided Eng. 2017;e21212.

[62] Guo, Z. and Yang, T. (2017), Novel compact ultra-wideband bandpass filter based on vialess vertical CPW/microstrip transitions. Electron. Lett., 53: 1258-1260.

[63] Jagadish Baburao Jadhav, Pramod Jagan Deore, A compact planar ultra-wideband bandpass filter with multiple resonant and defected ground structure, AEU - International Journal of Electronics and Communications, Volume 81, 2017, 31-36.

[64] Sun J, Li GR. A balanced ultra-wideband bandpass filter based on H-type s andwich slotline. Int J RF Microw Comput Aided Eng. 2021;31:e22611.

[65] Bhardwaj, P, Deivalakshmi, S, Pandeeswari, R. Compact wideband substrate integrated waveguide bandpass filter for X/Ku-band application. Int J RF Microw Comput Aided Eng. 2021; 31:e22634.

[66] Sharifi A. Optimum design of 6-18 GHz ultra-wideband microstrip filters with arbitrary source and load impedances by the least mean squares Method. Int J RF Microw Comput Aided Eng. 2020;30:e22041.

[67] Lu J., Wang J., Gu H.: 'Design of compact balanced ultra-wideband bandpass filter with half mode dumbbell DGS', Electron. Lett., 2016, 52, (9), pp. 731–732.

[68] C. Zhou, P. Guo, K. Zhou and W. Wu, "Design of a Compact UWB Filter With High Selectivity and Superwide Stopband," in IEEE Microwave and Wireless Components Letters, vol. 27, no. 7, pp. 636-638, July 2017.

[69] A. Kamma, R. Das, D. Bhatt and J. Mukherjee, "Multi Mode Resonators Based Triple Band Notch UWB Filter," in IEEE Microwave and Wireless Components Letters, vol. 27, no. 2, pp. 120-122, Feb. 2017.

[70] Saxena, G., Jain, P., & Awasthi, Y. (2021). Design and analysis of a planar UWB bandpass filter with stopband characteristics using MMR technique. International Journal of Microwave and Wireless Technologies, 13(10), 999-1006.

[71] Li, C., Tong, C., Qi, L., Zou, X. and Ji, M. (2015), Multimode resonator based on composite right-/left-handed transmission line for UWB bandpass filter application. Int J RF and Microwave Comp Aid Eng, 25: 815-824.

[72] R. K. Mongia, I. J. Bahl, P. Bhartia, and S. J. Hong, RF and Microwave Coupled-Line Circuits, 2nd ed. Boston, MA, USA: Artech House, 1999

[73] Sun S, Zhu L, Tan H-H. A compact wideband bandpass filter using transversal resonator and asymmetrical interdigital coupled lines. IEEE Microw Wirel Compon Lett 2008;18(3):173–5.

[74] Chen D, Bu H, Zhu L, Cheng C. A differential-mode wideband bandpass filter on slotline multi-mode resonator with controllable bandwidth. IEEE Microw Wirel Compon Lett 2015;25(1):28–30.

[75] Shang Z, Guo X, Cao B, Wei B, Zhang X, Heng Y, Suo G, Song X. Design of a superconducting ultra-wideband (UWB) bandpass filter with sharp rejection skirts and miniaturized size. IEEE Microw Wirel Compon Lett 2013;23(2):72–4.

[76] Seok S, Kim J. Design, fabrication, and characterization of a wideband 60 GHz bandpass filter based on a flexible perMX polymer substrate. IEEE Trans Compon Packag Manuf Technol 2013;3(8):1384–9.

[77] Pan L, Wu Y, Wang W, Wei Y, Yang Y. A flexible high-selectivity single-layer coplanar waveguide bandpass filter using interdigital spoof surface plasmon polaritons of bow-tie cells. IEEE Trans Plasma Sci 2020;48(10):3582–8.

[78] Koskinen S, Pykäri L, Mäntysalo M. Electrical performance characterization of an inkjet-printed flexible circuit in a mobile application. IEEE Trans Compon Packag Manuf Technol 2013;3(9):1604–10.

[79] Ye L, Chen Y, Xu KD, Li W, Liu QH, Zhang Y. Substrate integrated plasmonic waveguide for microwave bandpass filter applications. IEEE Access 2019;7:75957–64.

[80] Chen Z-M, Liu Y, Liang X, Wang J, Li Y, Zhu J, Jiang W, Shen X, Zhao L, Cui TJ. A high efficiency band-pass filter based on CPW and quasi-spoof surface plasmon polaritons. IEEE Access 2020;8:4311–7.

[81] Krzeminski J, Kanthamneni A, Wagner D, Detert M, Schmidt B, Jakubowska M. Microscale hybrid flexible circuit printed with aerosol jet technique. IEEE Trans Nanotechnology 2018;17(5):979–84.

[82] Cheng S, Yousef H, Kratz H. 79 GHz slot antennas based on substrate integrated waveguides (SIW) in a flexible printed circuit board. IEEE Trans Antennas and Propagation 2009;57(1):64–71.

[83] Courreges S, Donado C, Bhattacharya MS, Papapolymerou J. Reduced-size multilayer X-band filters with stacked resonators on a flexible organic substrate. IET Microw Antennas Propag 2010;4(2): 277–85.

[84] Zhao M, Zhang Y. Compact wearable 5-GHz flexible filter. Electron Lett 2017;53(10):661–3.

[85] Nair NM, Pakkathillam JK, Kumar K, Arunachalam K, Ray D, Swami- nathan P. Printable silver nanowire and PEDOT:PSS nanocomposite ink for f lexible transparent conducting applications. ACS Appl Electron Mater 2020;2(4):1000–10.

[86] A. M. Abbosh, “Design method for ultra-wideband bandpass filter with wide stopband using parallel-coupled microstrip lines,” IEEE Trans. Microw. Theory Techn., vol. 60, no. 1, pp. 31–38, Jan. 2012.

[87] Wu HW and Chen YF. New compact ultra wideband bandpass filter using modified multi mode resonator. Int. J. Electron. Commun. (AEÜ). 2012; 66: 1021-1025.

[88] Deng HW, Zhao Y, He Y, Jia SL and Wang M, Compact dual-notched balanced UWB BPF with folded triple-mode slotline resonator. Electron Lett. 2014; 50: 447-449.

[89] H. Zhu, X. Zhu, Y. Yang and Q. Xue, "Design of Wideband Third-Order Bandpass Filters Using Broadside-Coupled Resonators in 0.13- μ m (Bi)- CMOS Technology," in IEEE Transactions on Microwave Theory and Techniques, vol. 66, no. 12, pp. 5593-5604, Dec. 2018.

[90] A. Taibi, M. Trabelsi, A. Slimane, M. T. Belaroussi, and J.-P. Raskin, “A novel design method for compact UWB bandpass filters,” IEEE Microw. Wireless Compon. Lett., vol. 25, no. 1, pp. 4–6, Jan. 2015.

[91] Q. -X. Chu and X. -K. Tian, "Design of UWB Bandpass Filter Using Stepped-Impedance Stub-Loaded Resonator," in IEEE Microwave and Wireless Components Letters, vol. 20, no. 9, pp. 501-503, Sept. 2010.

[92] Song Y, Yang GM and Geyi W. Compact UWB Bandpass Filter with Dual Notched Bands Using Defected Ground Structures. IEEE Microw Wireless Compon Lett. 2014; 24: 230– 232.

[93] Wang J, Zhao J, Li JL. Compact UWB bandpass filter with triple notched bands using parallel U shaped defected microstrip structure. Electron Lett. 2014;50:89-91.

[94] Ghazali AN, Pal S. Planar UWB filter with multiple notched band and stopband with improved rejection level. Frequenz. 2015;69:207-218.

[95] Ghazali AN, Pal S. Microstrip based UWB filter with controllable multiple notches and extended upper stopband. International Conference on Emerging Trends in Communication, Control, Signal Processing and Computing Applications (C2SPCA). IEEE;2013:1-5.

[96] Gholipoor M, Amin Honarvar M, Virdee BS. UWB bandpass filters with triple notched band characteristics implemented using wave cancellation technique. Microw Opt Technol Lett. 2016;58:1875-1879.

[97] Wei F, Li WT, Shi XW, Huang QL. Compact UWB bandpass filter with triple-notched bands using triple-mode stepped impedance resonator. IEEE Microw Wireless Compon Lett. 2012;22:512-514.

[98] Wei F, Wang ZD, Yang F, Shi XW. Compact UWB BPF with triple-notched bands based on stub loaded resonator. Electron Lett. 2013;49:124-126.

[99] Peng H, Zhao J, Wang B. Compact microstrip UWB bandpass filter with triple-notched bands and wide upper stopband. Prog Electromagn Res. 2014;144:185-191.

[100] Basit A, Khattak MI, Alhassan M. Design and analysis of a microstrip planar UWB bandpass filter with triple notch bands for WIMAX, WLAN, and X-BAND satellite communication systems. Prog Electromagn Res M. 2020;93: 155-164.

[101] Liu X, Zhong C, Song H, Chen Y, Luo T. A new compact microstrip UWB bandpass filter with triple-notched bands and good stopband performance. Prog Electromagn Res Lett. 2018;72:29-37.

[102] Liu J, Lu J, He Z, Luo T, Ying X, Zhao J. Super compact microstrip UWB BPF with triple-notched bands. Prog Electromagn Res Lett. 2018;73:61-67.

[103] Shi XM, Xi XL, Zhao YC, Yang HL. A novel compact ultra- wideband (UWB) bandpass filter with triple-notched bands. J Electromagn Waves Appl. 2015;29(9):1174-1180.

[104] Kumar S, Gupta RD, Parihar MS. Multiple band notched filter using C-shaped and E-shaped resonator for UWB applications. IEEE Microw Wireless Compon Lett. 2016;26:340-342.

[105] Taibi A, Trabelsi M, Saadi A. Efficient design approach of triple notched UWB filter. Int J Electron Commun (AEÜ). 2021;131:153619.

[106] Chakraborty P, Shome PP, Panda JR, Deb A. Highly selective UWB bandpass filter with multi-notch characteristics using comb shaped resonator. Prog Electromagn Res M. 2022;108: 89-101.

[107] Liu JQ, Song KJ, Fan Y. UWB BPF with triple notched bands using novel dual-mode SIR and asymmetrical coupling structure. J Electromagn Waves Appl. 2012;26(16):2112-2120.

[108] Chiang CT, Xu JC, Liu JC. Compact ultrawideband bandpass filter with triple notched-bands and sharp transmission zeros based on CSRR, DGS, and FMRR configurations. Microw Opt Technol Lett. 2014;56:2324-2330

[109] Borazjani O, Nosrati M, Daneshmand M. A novel triple notch- bands ultra wide-band band-pass filters using parallel multi- mode resonators and CSRRs. Int J RF Microw Comput-Aided Eng. 2014;24:375-381.

[110] Baik JW, Lee TH, Kim YS. Novel broadband microstrip-to- CPW transition with easy transmission band control. IEICE Electron Express. 2008;5(2):48-52

[111] Peng H, Zhao J, Wang B. Compact microstrip UWB bandpass filter with triple-notched bands and wide upper stopband. Prog In Electromag Res 2014;144: 185–91.

[112] Wang J, Zhao J, Li JL. Compact UWB bandpass filter with triple notched bands using parallel U shaped defected microstrip structure. Electron Lett 2014;50:89–91.

[113] Ghazali AN, Pal S. Microstrip based UWB filter with controllable multiple notches and extended upper stopband. Int Conf on Emerging Trends in Comm, Control, Signal Process & Computing Appl (C2SPCA), 2013;1–5.

[114] Ghazali AN, Pal S. Planar UWB filter with multiple notched band and stopband with improved rejection level. Frequenz 2015;69:207–18.

[115] Gholipoor M, Honarvar MA, Virdee BS. UWB bandpass filters with triple notched band characteristics implemented using wave cancellation technique. Microw Opt Tech Lett 2016;58:1875–9.

[116] Kumar S, Gupta RD, Parihar MS. Multiple band notched filter using C-shaped and E-shaped resonator for UWB applications. IEEE Microw Wireless Compon Lett. 2016;26:340–2.

[117] Shi XM, Xi XL, Zhao YC, Yang HL. A novel compact ultra-wideband (UWB) bandpass filter with triple-notched bands. J Electromag Waves Appl 2015;29(9): 1174–80.

[118] Borazjani O, Nosrati M, Daneshmand M. A novel triple notch-bands ultra wide-band band-pass filters using parallel multi-mode resonators and CSRRs. Int J RF Microw Comp-Aided Eng 2014;24:375–81.

[119] Ghazali AN, Sazid M, Pal S. Dual band notched UWB-BPF based on hybrid microstrip-to-CPW transition. Int J Electron Commun (AEÜ) 2018;86:55–62.

[120] Choudhury A, Maity S. Design and fabrication of CSRR based tunable mechanically and electrically efficient band pass filter for K-band application. Int J Electron Commun (AEÜ). 2017;72:134–48.

[121] Choudhary DK, Chaudhary RK. A compact CPW-based dual-band filter using modified complimentary split ring resonator. Int J Electron Commun (AEÜ). 2018; 89:110–5.

[122] Ghazali, A.N., Sazid, M. and Pal, S. (2015), Compact broadband balunbased UWB-BPF with minimum insertion loss and sharp selectivity. Electron. Lett., 51: 1174-1175.

[123] Chakraborty, P., P. P. Shome, A. Deb, A. Neogi, and J. R. Panda, "Compact configuration of open ended stub loaded multi-mode resonator based UWB bandpass filter with high selectivity," IEEE 8th International Conference on Signal Processing and Integrated Networks (SPIN), 2021.

[124] Shome, P. P., T. Khan, S. K. Koul, and Y. M. M. Antar, "Two decades of UWB filter technology: From elementary designs-to-recent developments," IEEE Microwave Magazine, Vol. 22, No. 8, 1–20, Aug. 2021.

[125] Kuo, T. N., S. C. Lin, and C. H. Chen, "Compact ultra-wideband bandpass filter using composite microstrip-coplanar-waveguide structure," IEEE Trans. Microwave Theory Tech., Vol. 54, 3772– 3778, Oct. 2006.

[126] Shaman, H. and J.-S. Hong, “Asymmetric parallel-coupled lines for notch implementation in UWB filters,” IEEE Microw. Wireless Compon. Lett., Vol. 17, No. 7, 516–518, Jul. 2007.

[127] J. Xu, F. Liu, S. -Y. Ji, Y. -W. Duan and H. Zhang, "An On-Chip Ultra Wideband Bandpass Filter in 0.18-μm SiGe BiCMOS Technology," in IEEE Electron Device Letters, vol. 43, no. 7, pp. 1009-1012, July 2022.

[128] Z. -C. Hao and J. -S. Hong, "Compact UWB Filter With Double NotchBands Using Multilayer LCP Technology," in IEEE Microwave and Wireless Components Letters, vol. 19, no. 8, pp. 500-502, Aug. 2009.

# List of Publications

**In SCIE Listed Journals**

1. **Mohd Sazid,** N.S. Raghava, Planar "UWB-bandpass filter with multiple passband transmission zeros", AEU - International Journal of Electronics and Communications, Volume 134, 2021,153711, https://doi.org/10.1016/j.aeue.2021.153711.
2. **Mohd Sazid**, Raghava NS, Ghazali AN. "UWB-BPF based on broadside coupled technology with triple-notched passband". Microw Opt Technol Lett. 2023;1-7. https://doi:10.1002/mop.33651.
3. **Mohd. Sazid**, Niraj Agrawal, Mangey Ram Nagar, N.S. Raghava, Anil Kumar Gautam, A.N. Ghazali, "A compact, flexible and transparent UWB bandpass filter with silver nanowires", AEU InternationalJournal of Electronics and Communications,2023,154673, https://doi.org/10.1016/j.aeue.2023.154673

**Communicated:**

**[1] Mohd Sazid,** N S Raghava, Asok De "MMR Based Eight Pole UWB-Bandpass Filter with Multiple Transmission Zeros" International Journal of Microwave and Wireless Technologies**.**

**In International conference**

1. **Mohd Sazid,** N S Raghava, Asok De "Design a Dual Notched Band BPF for Ultra wide band application". International Conference on "Interdisciplinary Research in Technology & Management" delhi 2023 (Taylor & Francis).
2. **Mohd Sazid,** N S Raghava, Asok De "Design a Quad Notched Band BPF for Ultra wide band application." International Conference on "Interdisciplinary Research in Technology & Management" Delhi 2023 (Taylor & Francis).